

THIS REPORT HAS BEEN DELIM.TED
AND CLEARED FOR PUBLIC RELEASE
UNDER DOD DIRECTIVE 5200.20 AND
NO RESTRICTIONS ARE IMPOSED UPON
ITS USE AND DISCLOSURE.

DISTRIBUTION STATEMENT A

APPROVED FOR PUBLIC RELEASE;
DISTRIBUTION UNLIMITED.

UNCLASSIFIED

AD 400 253

*Reproduced
by the*

ARMED SERVICES TECHNICAL INFORMATION AGENCY
ARLINGTON HALL STATION
ARLINGTON 12, VIRGINIA



UNCLASSIFIED

NOTICE: When government or other drawings, specifications or other data are used for any purpose other than in connection with a definitely related government procurement operation, the U. S. Government thereby incurs no responsibility, nor any obligation whatsoever; and the fact that the Government may have formulated, furnished, or in any way supplied the said drawings, specifications, or other data is not to be regarded by implication or otherwise as in any manner licensing the holder or any other person or corporation, or conveying any rights or permission to manufacture, use or sell any patented invention that may in any way be related thereto.

N-63-3-1

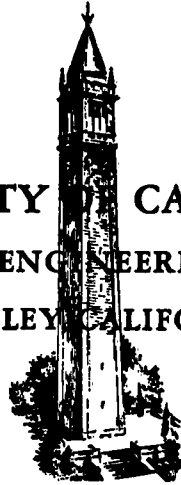
400 253

400 253

CATALOG OF ASTIA
AS AERONAUTICAL SCIENCES

HE-150-210
TECHNICAL REPORT

UNIVERSITY OF CALIFORNIA
INSTITUTE OF ENGINEERING RESEARCH
BERKELEY, CALIFORNIA



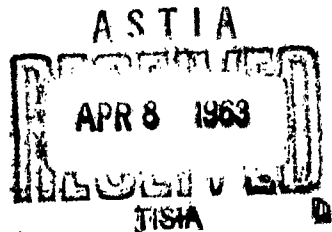
TRANSIENT STRESS DISTRIBUTION IN A RAPIDLY HEATED ROD

by

A. L. Austin

FACULTY INVESTIGATORS:

W. H. GIEDT, Professor of Aeronautical Sciences
J. FRISCH, Associate Professor of Mechanical Engineering



SERIES NO. 128
ISSUE NO. 11
DATE FEBRUARY 14, 1963

PURCHASE ORDER 1243500
UCX-2285
REPORT NO. HE-150-210
SERIES NO. 128-11
FEBRUARY 14, 1963

SPONSORED BY THE
LAWRENCE RADIATION LABORATORY
UNIVERSITY OF CALIFORNIA
LIVERMORE, CALIFORNIA

TRANSIENT STRESS DISTRIBUTION IN A RAPIDLY HEATED ROD

by

A. L. Austin

A portion of a Doctoral Thesis in Engineering

Reproduction in whole or in part is permitted
for any purpose of the United States Government

FACULTY INVESTIGATORS:

W. H. GIEDT, Professor of Aeronautical Sciences
J. FRISCH, Associate Professor of Mechanical Engineering

ABSTRACT

An analytical and experimental investigation of the inertial stresses resulting from very high internal heat generation rates is described. The results show that the amplitude of the thermally induced elastic vibrations in an unrestrained thin rod are dependent upon the ratio of heating time to the fundamental period of oscillation, and that the most severe stress amplitude results from a constant heating rate as compared to an exponential type of input.

In the experimental investigation, rapid heating was accomplished by the discharge of a low-inductance capacitor bank (0.1 uh, 2800 Joules) through the rod. A modified birefringent-coating method was used for observation of the thermally induced oscillations. Utilizing the frozen stress technique of three-dimensional photoelasticity, an initial pattern of interference fringes was introduced into thin strips of birefringent material which were securely bonded to each side of the rod. Strain oscillations were measured by direct observation of the movement of the fringe pattern with a high intensity incident light source, a crossed-circular polariscope, and a high speed framing camera. Interpretation of these measurements required a dynamic calibration and a correction factor for the reinforcing effect of the coating. Oscillations with periods from 35 to 250 microseconds and amplitudes of 9000 psi were measured. The results were in good agreement with the uncoupled thermo-elastic theory, and it is concluded that this technique is suitable for transient measurements in the presence of large magnetic fields which normally restrict the use of electronic methods.

TABLE OF CONTENTS

	<u>Page</u>
ABSTRACT	i
NOMENCLATURE	iv
LIST OF FIGURES	vii
1. INTRODUCTION	1
2. THEORETICAL ANALYSIS OF THE TRANSIENT ELASTIC STRESS DISTRIBUTION IN A ROD SUBJECTED TO RAPID INTERNAL HEAT GENERATION	8
(a) Case I - Constant Internal Heat Generation Rate	14
(b) Case II - The Response of an Unrestrained Rod to an Exponential Temperature Rise	19
(c) Case III - The Response of an Unrestrained Rod to an Exponential Temperature Rise Modified for Zero Initial Stress Rate	22
(d) Summary of Theoretical Calculations	24
3. EXPERIMENTAL EQUIPMENT AND PROCEDURES	26
(a) General	26
(b) Specimen Geometry and Heating Method	27
(c) Electrical Heating Measurements	28
(d) Measurement of Axial Strain in the Heated Rod	31
(e) Operating and Data Reduction Procedure	35
(f) Calculation of Stress from Experimental Data	37
4. EXPERIMENTAL RESULTS	44
5. DISCUSSION OF RESULTS	46
(a) Theoretical Results	46
(b) Experimental Results	48

	<u>Page</u>
6. CONCLUSIONS	56
REFERENCES	57
FIGURES	61
APPENDIX	94
1. Sample Data and Calculations	95
2. Temperature Distribution in the Heated Specimen	103
3. Temperature History of the Photoelastic Coating	105
4. Evaluation of the Secondary Principal Stress	109
5. Reinforcing Effect of the Photoelastic Coating	111
6. Calibration of the Photoelastic Coating	116

NOMENCLATURE

A	cross-sectional area of bar
a	sonic velocity
c	specific heat
C	capacitance
D	thermal diffusivity
E	elastic modulus
f_{ϵ}	strain-optic coefficient of coating
f_{σ}	stress-optic coefficient of coating
G	shear modulus of elasticity
h	width of coating
i	current
J	conversion factor for BTU/Joule
k	thermal conductivity
K	bulk modulus
l	half-length of bar
L	inductance
m	correction factor for reinforcing effect of coating
N	fringe order
q	heating rate
R	resistance
s	Laplace transform parameter
t	time
t_1	characteristic heating time
T	temperature
V	voltage
W	total weight of bar

u, v, w displacement components
 x, y, z rectangular Cartesian coordinates

Greek Letters

α thermal coefficient of expansion
 β arbitrary parameter for Case III heating
 γ specific weight
 δ thickness of coating
 Δ dilatation
 ϵ strain
 η specific electrical resistivity
 θ hydrostatic stress
 λ Lamé' constant of elasticity
 ν Poisson's ratio
 π Pi
 ρ mass density
 σ stress
 τ fundamental mechanical period of oscillation
 ω frequency of oscillation

Subscripts

x, y, z in the x, y, z direction
 o initial
 v at constant volume
 p at constant pressure
 St static
 Dyn dynamic
 s specimen, or steel

c	coating
m	maximum
max	maximum
Avg	average

LIST OF FIGURES

Fig. No.

1. Specimen Geometry
2. Selected Types of Heating
3. Variation of Stress Amplitudes with Ratio of Heating Period
to Fundamental Period
4. Stress Distribution Sequence in a Rapidly Heated Rod (Case I)
5. Stress Histories at a Point in a Rapidly Heated Rod (Case I)
6. Displacement of the End of a Rapidly Heated Rod (Case I)
7. Stress Histories in a Rapidly Heated Rod (Case II)
8. Variation of Stress Amplitudes with Ratio of Heating Period
to Fundamental Periods (Case II)
9. Comparison of Induced Temperature Variations
10. Comparison of Stress Histories Produced by Case II and
Case III Heating
11. Variation of Stress Amplitudes with Ratio of Heating Period
to Fundamental Period (Case III)
12. The Effect of Type of Heating on Stress Amplitude Variation
13. Heating Jig
14. Inductive Probe Circuitry
15. Comparison of Exact Temperature Variation with Case II
16. Fringe Pattern in Prestressed Beam
17. Specimen Preparation
18. Light Source Circuitry
19. Experimental Apparatus
20. Block Diagram

Fig. No.

21. Function Diagram of Sequence of Events
22. Heating Jig Assembly
23. Specimens
24. Stress History at a Point
- 25a. Stress History at a Point
- 25b. Stress History at a Point - Corrected for Damping
26. Stress History at a Point
27. Stress History at a Point
28. Stress History at a Point
29. Stress History at a Point
30. Stress History at a Point
31. Variation of Initial Compression Amplitude with the
Ratio of Heating Period to Fundamental Period
32. Strain Gage Signals

APPENDIX

- 1A Output of the Inductive Probe
- 2A Camera Rotor Signal
- 3A Observed Fringe Movements
- 4A Observed Fringe Movements
- 5A Graphical Procedure for Calculation of Fringe Order
- 6A Longitudinal Motion of the Coated Bar
- 7A Dynamic Calibration of Photoelastic Coating
- 8A Comparison of Photoelastic Coating Data with Strain
Gage Data

1. INTRODUCTION

The effect of high heating rates on the behavior of mechanical systems is becoming a problem of greater and greater engineering importance. For example, the increased use of nuclear reactors for power generation and for studies of intense radiation damage to materials has resulted in a need for an understanding of the effects of rapid internal heat generation on the mechanical response of reactor components. In a fast burst reactor the sudden criticality results in a very high fission rate accompanied by a rapid increase in temperature of the reactive components. As a result of the inertia of these components rapid thermal expansion cannot take place and large transient inertial stresses are produced. Hence, the designer is faced not only with the problems of temperature gradients upon cooling and the resulting quasi-static thermal and contact stresses, but also with initial inertia effects which govern the structural response during the rapid temperature change.

In order for significant inertial stresses to be developed, it has been found that the imposed heating rates must cause a substantial temperature change in a structure in times short compared to the mechanical response time of the system. For large thermal fluxes incident on a surface or for rapid internal heat generation rates, these temperature changes can occur in times which are short relative to the mechanical response time of the heated structure. Hence, the ratio of the time of heat input to a characteristic mechanical time will be indicative of the severity of the inertial stresses caused by rapid heating.

The mechanical response times, or periods of free vibration, for structural members such as beams, plates, rods and shells usually vary anywhere from 10^{-4} to 10^{-1} seconds; consequently, inertial stress effects become important for heating times which may vary from less than 10^{-6} seconds to as high as 10^{-2} seconds. It is evident, then, that even though the heating time may be long in an absolute sense, inertial effects may still create serious design problems. In addition, the problem of coupling effects (i.e., when the temperature field is significantly affected by the state of deformation of a body) between the elastic and thermal field equations may exist when the rate of strain becomes high. However, both the inertia and coupling effects may, within the bounds of practicality, be treated separately, and for the present study it will be shown that coupling effects are negligible and attention can be restricted to inertial effects.

A literature review indicates that only within about the last ten years has considerable attention been given to these problems. Actually, as early as 1837, in the very beginning of the development of thermoelasticity, Duhamel¹ considered inertial effects by noting that if the temperature rate is slow enough, inertia terms in the field equations of thermoelasticity can safely be neglected. However, as far as can be determined, the first extended investigation of inertial effects was carried out in 1950 by Danilovskaya² for the case of an elastic half-space suddenly heated at the boundary. Further work was done in 1952 by Mura³ who determined the transient stress distributions in an elastic half-space and an infinitely long solid cylinder subjected to a sudden temperature change at the surface. The results show that in addition to the thermal expansion wave, an elastic stress

wave arising from the inertial effect is propagated through the half-space at the sonic velocity, while for the cylinder, radial vibrations occur but are of extremely small amplitude even for the most severe type of heating - a step change in surface temperature. Additional work on the inertia effects for the elastic half-space was later performed by Nowacki⁴ and Ignaczak⁵ in 1957 and by Sternberg and Chakravorty⁶ in 1958. All of this work, however, had no direct practical application, but it did serve as a valuable aid to the understanding of the inertia effects associated with rapid heating of an elastic body.

Space exploration activities directed attention to the serious heating problems encountered in the design of high-speed propulsion units, particularly aerodynamic heating of reentry vehicles. In 1955 Boley⁷ analyzed the behavior of a simply supported rectangular beam of depth, h , and thermal diffusivity, D , subjected to a sudden application of heat to the upper edge. He used the elementary Bernoulli-Euler theory of bending with the assumption that the temperature remains constant along the beam and varies only through the depth. Both these assumptions gave good practical approximations to the aerodynamic heating of the leading edge of wing sections. His calculations show that the inertial effects become important when a characteristic heating time defined by h^2/D is less than half the period of free lateral vibration. As the heating time approaches zero, the maximum dynamic deflection approaches twice the static deflection which would result if the beam were heated slowly along the upper edge, and as the heating time approaches infinity, the inertia forces disappear and the static solution alone remains. A year later Boley and

Barber⁸ extended this work to include the analysis of thermally induced vibrations of rectangular plates and beams for several typical heat applications encountered in spacecraft design.

Recent developments in reactor technology have resulted in considerable thermal stress analysis of components subjected to internal heat generation. The most significant quasi-static problems investigated include the work of Kammash, Murch and Naghdi⁹ (1959), who worked out the complete elastic-plastic solution for the cylinder subjected to a radially distributed heat source, and the work of Weil¹⁰ (1962), who determined the thermal stresses in cylinders subjected to internal heat generation due to γ -ray radiation. The only investigation known to the author of inertia effects associated with rapid internal heat generation has been performed by Burgreen¹¹ (1962), who has determined the dynamic elastic response of fuel elements having geometries of thin rods, thin spherical shells, and solid spheres. His calculations reveal the nature of the inertial stress wave propagation, and he concludes that the maximum amplitude of these waves is governed by the ratio of the heating time to the fundamental period of free vibration of the element. These results agree in principle with those obtained by Boley.^{7,8}

In all of the above work mentioned thus far, the thermo-mechanical coupling between the elastic and thermal energy equation derived originally by Jeffreys¹² there is an additional energy term which accounts for the work done by the volume change and manifests itself as a thermo-elastic dissipation which is an important cause of internal damping. Because of the heating or cooling associated with a change of volume, the temperature distribution is dependent upon the state of deformation, and hence, the exact solution to a dynamic thermoelastic problem is

complicated by this coupling between the dynamical equilibrium equations and the general energy equation, or heat conduction equation.

Recently, much attention has been given to the determination of such rigorous solutions. Fundamental to this effort has been the work of Biot¹³ who has presented a unified treatment of thermoelasticity by application and extended development of the methods of irreversible thermodynamics. This work shows that for time dependent problems, the effects of the thermal state and the deformation of an elastic solid cannot logically be treated separately. Thus far, only one partial rigorous solution of this nature has been published, but some effort has been directed toward solution of the coupled equations which are harmonic in the time variable and one spatial coordinate. In 1957 investigations of plane waves in a thermoelastic solid were carried out by Deresiewicz,¹⁴ Lessen,¹⁵ and Chadwick and Sneddon.¹⁶ These authors agree that even for metals at reasonably high temperatures the effect of coupling between elastic and thermal motions can be neglected. Lockett¹⁷ (1957) has also worked out the two-dimensional solution of the propagation of Rayleigh waves and found that coupling effects introduce a difference of less than one percent in the velocity and amplitude of these waves. Finally, in 1960 Chadwick¹⁸ has provided an excellent survey of the present dynamical theory of thermoelasticity in which he discusses the irreversible thermodynamics of an elastic solid, provides a derivation of the general thermoelastic equations, and examines the characteristics of the general thermoelastic boundary value problem. He applies his results to some specific problems which nicely illustrate the nature of thermoelastic dynamics. In their text, Boley and Weiner¹⁹ have summarized much of the above work which took

place before 1959, and have worked out numerical results to specific problems in order to illustrate the effects of inertia, coupling and thermoelastic damping. They have demonstrated that for most engineering design purposes the elastic and thermal field equations may be uncoupled, which will allow considerable simplification of solutions to dynamic problems in thermoelasticity.

All of the aforementioned work has been analytical, but experimental verification of the results is noticeably absent. Despite the considerable number of studies which have indicated that rapid heating of structures is accompanied by serious inertial stresses, to this author's knowledge, there have been only two experimental investigations to verify these results. In 1961, Michaels²⁰ investigated the effect of incident thermal radiation on one face of a cylindrical rod and successfully demonstrated the existence of the resulting elastic wave. Lindholm²¹ (1962) designed an arc image furnace which was used to produce an extremely high, short-duration thermal flux on the surface of a thin spherical cap. His results consisted primarily of subjective observations of the gross effects of the rapid heating, and were inconclusive. In view of this situation, it was concluded that additional experimental work was highly desirable. Realizing that serious practical problems surround the design and operation of suitable experimental techniques, considerable thought was given to the approach to be taken. This led to the decision to conduct a study of the behavior of a long, thin rod subjected to high internal heat generation rates. Uniform heating was accomplished electrically by the discharge of a low-inductance capacitor bank through the rod. The movement of the isochromatic fringe pattern in a photoelastic coating on the bar was observed with a high speed

framing camera. The significant feature of this optical method is that the transient axial strain can be observed during the heating pulse. Semiconductor strain gages on the bar were also used to observe the steady state oscillations which occurred after the electrical heating pulse and to provide a dynamic calibration of the photoelastic coating. In preparation for these experimental techniques a one-dimensional analysis of the elastic behavior of the bar was carried out to provide a theoretical comparison for the experimental measurements. The results of these activities are shown and discussed in the following sections.

2. THEORETICAL ANALYSIS OF THE TRANSIENT ELASTIC STRESS DISTRIBUTION IN A ROD SUBJECTED TO RAPID INTERNAL HEAT GENERATION

The system selected for study consisted of a long, completely unrestrained elastic bar of length $2l$ and constant cross-sectional area A (see Fig. 1) subjected to a uniform internal heat generation rate per unit volume, q . If the heating is rapid, the inertia of the bar will oppose thermal expansion and stresses will develop. Also, if the heating time is short relative to the time required for heat transfer away from the bar, the temperature will be uniform and independent of position along the bar. It will be assumed that only simple tension or compression exists and that the axial stress is accompanied only by lateral strains $- \nu \epsilon_x$. This assumption is valid provided the wavelength of axial waves is large compared to the lateral dimensions of the bar.^{22,23,24,25} Hence, inertial effects corresponding to lateral motion will be neglected so that the following analysis is restricted to a one-dimensional problem which further implies that plane sections remain plane during deformation.

Let the origin of a set of rectangular Cartesian coordinates (x, y, z) coincide with the center of a bar such that the x -axis lies along the axis of the bar. For one-dimensional motion of the bar, only the axial stress σ_x remains, and the stress equations of equilibrium²⁶

$$\begin{aligned}
 \frac{\partial \sigma_{xx}}{\partial x} + \frac{\partial \sigma_{xy}}{\partial y} + \frac{\partial \sigma_{xz}}{\partial z} &= \rho \frac{\partial^2 u}{\partial t^2} \\
 \frac{\partial \sigma_{xy}}{\partial x} + \frac{\partial \sigma_{yy}}{\partial y} + \frac{\partial \sigma_{yz}}{\partial z} &= \rho \frac{\partial^2 v}{\partial t^2} \\
 \frac{\partial \sigma_{xz}}{\partial x} + \frac{\partial \sigma_{yz}}{\partial y} + \frac{\partial \sigma_{zz}}{\partial z} &= \rho \frac{\partial^2 w}{\partial t^2}
 \end{aligned}
 \tag{2.1}$$

reduce to

$$\frac{\partial \sigma_x}{\partial x} = \rho \frac{\partial^2 u}{\partial t^2} \quad (2.2)$$

Since this work will consider only elastic deformation, the behavior of the bar is governed by the linear thermoelastic stress-strain relations²⁷

$$\begin{aligned} \sigma_x &= \lambda(\epsilon_x + \epsilon_y + \epsilon_z) + 2G \epsilon_x - (3\lambda + 2G) \alpha (T - T_0) \\ \sigma_y &= \lambda(\epsilon_x + \epsilon_y + \epsilon_z) + 2G \epsilon_y - (3\lambda + 2G) \alpha (T - T_0) = 0 \\ \sigma_z &= \lambda(\epsilon_x + \epsilon_y + \epsilon_z) + 2G \epsilon_z - (3\lambda + 2G) \alpha (T - T_0) = 0. \end{aligned} \quad (2.3)$$

where the temperature T_0 corresponding to the stress-free state has been added, and all shear components of stress and strain are zero.

Eliminating ϵ_x and ϵ_y , Eqs. (2.3) reduce to

$$\sigma_x = E [\epsilon_x - \alpha(T - T_0)] \quad ; \quad (2.4)$$

also,

$$\epsilon_y = \epsilon_z = -\nu \epsilon_x + (1 + \nu) \alpha (T - T_0) \quad . \quad (2.5)$$

From the strain-displacement relations²⁸ for small strains,

$$\epsilon_x = \frac{\partial u}{\partial x} \quad (2.6)$$

$$\epsilon_y = \frac{\partial v}{\partial y} \quad ; \quad \epsilon_z = \frac{\partial w}{\partial z} \quad . \quad (2.7)$$

Since the surface tractions are specified ($\sigma_x = 0$ at $x = \pm l$), it will be convenient to write the equation of motion (2.2) in terms of the stress. Hence, differentiating (2.2) with respect to x and substituting (2.6) into (2.4) and then combining with the partial derivative of (2.2)

we get the one-dimensional Beltrami-Michell equation of compatibility

$$\frac{\partial^2 \sigma_x}{\partial x^2} - \frac{\rho}{E} \frac{\partial^2 \sigma_x}{\partial t^2} = \rho \alpha \frac{\partial^2 T}{\partial t^2} \quad (2.8)$$

If the temperature history of the bar is known or prescribed, solution of Eq. (2.8) will yield the stress in the bar directly. However, in most problems the heat generation function is usually given and the temperature calculated from the energy equation. For a linear isotropic solid, the complete energy equation is well known. It was obtained originally by Jeffreys¹² and later re-derived and discussed by Biot.¹³ This equation is sometimes referred to as the coupled heat, or diffusion equation, and is

$$k \nabla^2 T + q = \gamma c_v \frac{\partial T}{\partial t} + (3\lambda + 2G) \alpha T_0 \frac{\partial \Delta}{\partial t} \quad (2.9)$$

where $\Delta = \epsilon_x + \epsilon_y + \epsilon_z$ = elastic dilatation. The addition of the last term in the heat equation accounts for the work done by deformation of the solid at temperature T_0 . Since it has been assumed that the temperature is uniform, the first term on the left-hand side is identically zero. From the thermoelastic stress-strain relations

$$\frac{\partial \Delta}{\partial t} = \frac{1}{3\lambda + 2G} \frac{\partial \Theta}{\partial t} + 3\alpha \frac{\partial T}{\partial t} \quad (2.10)$$

$$\Theta = \sigma_x + \sigma_y + \sigma_z$$

and for the one dimensional formulation $\Theta = \sigma_x$. Substituting in (2.9) and differentiating once with respect to time

$$\frac{\partial q}{\partial t} = [\gamma c_v + 3\alpha^2 T_0 (3\lambda + 2G)] \frac{\partial^2 T}{\partial t^2} + \alpha T_0 \frac{\partial^2 \sigma_x}{\partial t^2} \quad (2.11)$$

which when combined with (2.8) yields

$$\frac{\partial^2 \sigma_x}{\partial x^2} - \frac{\rho}{E} \left[1 - \frac{E\alpha^2 T_0}{\gamma c_v + 3(3\lambda + 2G)\alpha^2 T_0} \right] \frac{\partial^2 \sigma}{\partial t^2} = \left[\frac{\rho\alpha}{\rho c_v + 3(3\lambda + 2G)\alpha^2 T_0} \right] \frac{\partial q}{\partial t} \quad (2.12)$$

The problem has obviously been considerably simplified by the assumption that the temperature is independent of x . Otherwise Eqs. (2.8) and (2.11) would be coupled by the last term in (2.11), and would require the simultaneous determination of temperature and stress. This simplifying assumption is, however, justified (see Appendix, Sect. 2). Equation (2.12) can be simplified further by noting that for most metals

$$\frac{JE\alpha^2 T_0}{\gamma c_v + 3(3\lambda + 2G)J\alpha^2 T_0} \ll 1 \quad ,$$

and

$$\rho c_v \gg 3(3\lambda + 2G)J\alpha^2 T_0 \quad ,$$

where $J = 1.07 \times 10^{-4}$ BTU/in-lb has been inserted for dimensional correction where appropriate. For instance, for 304 stainless steel

$$\gamma c_v = (0.28)(0.12) = 0.034 \text{ BTU/in}^3\text{F}$$

$$3(3\lambda + 2G)J\alpha^2 T_0 = 3(73 \times 10^6)(10^{-4})(9 \times 10^{-6})^2 (70) = 0.00016 \text{ BTU/in}^3\text{F}$$

$$\frac{JE\alpha^2 T_0}{\gamma c_v + 3(3\lambda + 2G)J\alpha^2 T_0} = 0.00063$$

Hence, the above inequalities are valid.

It is interesting to note that the bracketed coefficients in the second and last terms of Eq. (2.12) can be interpreted as the corrections for the adiabatic sonic velocity and the specific heat at constant pressure, respectively. These expressions agree with the general three-dimensional derivations given by Jeffreys,²⁹ namely that

$$a_{\text{adiabatic}}^2 = \frac{E}{\rho} \left[\frac{1}{1 - \frac{E\alpha^2 T_0 J}{\gamma c_v + 3(\lambda + 2G)J\alpha^2 T_0}} \right],$$

where

$$a_{\text{isothermal}} = \sqrt{\frac{E}{\rho}} = \text{sonic velocity.} \quad (2.13)$$

Hence for this work

$$a_{\text{ad.}} \approx a_{\text{isoth.}} \quad (2.14)$$

Also, the specific heat at constant pressure C_p is

$$C_p = c_v \left[1 + \frac{3(\lambda + 2G)J\alpha^2 T_0}{\gamma c_v} \right] \approx c_v \frac{\lambda}{\gamma} c. \quad (2.15)$$

As a result of these simplifications Eq. (2.12) can be written simply as

$$\frac{\partial^2 \sigma_x}{\partial x^2} - \frac{1}{a^2} \frac{\partial^2 \sigma_x}{\partial t^2} = \frac{\alpha}{gc} \frac{\partial q}{\partial t}, \quad (2.16)$$

with the heat equation reduced to the familiar result

$$q = \gamma c \frac{\partial T}{\partial t}. \quad (2.17)$$

Hence, Eqs. (2.16) and (2.17) are equivalent to our original equation,

Eq. (2.8), which is sufficient for problems involving uniform internal heat generation in which the temperature is automatically known for any prescribed heating process. The above simplifications are in agreement with Boley and Weiner,³⁰ who performed a similar analysis for the displacement formulation of a similar problem. They considered a more general problem in which the temperature is space dependent as well as time dependent, and show that the coupling term in (2.9) can be neglected if the dilatation rate is of the same order of magnitude as the temperature rate. In all thermoelastic problems there is an additional restriction on the use of the complete energy equation. It is necessary that $|T - T_0| < T_0$. However, this restriction can be relaxed for the linear theory involving small strains since even for high temperatures $|T - T_0|$ is normally less than the strain level ($\sim 10^{-3}$) permitted by the infinitesimal theory. A complete discussion of this is given by Chadwick.³¹

Returning now to the problem of the inertial stresses induced in a rapidly heated rod, the equations to be solved are

$$\frac{\partial^2 \sigma}{\partial x^2} - \frac{1}{a^2} \frac{\partial^2 \sigma}{\partial t^2} = \rho \alpha \frac{\partial^2 T}{\partial t^2} \quad , \quad (2.8)$$

$$q = \gamma c \frac{\partial T}{\partial t} \quad (2.17)$$

and

$$\frac{\partial u}{\partial x} = \frac{\sigma}{E} + \alpha T \quad . \quad (2.18)$$

where the subscript x has been dropped for convenience, and

$$\begin{aligned} \sigma &= \sigma(x, t) & T &= T(t) \\ u &= u(x, t) & q &= q(t) \end{aligned}$$

In this work, the temperature rise will be kept small enough so that variation in material properties can be neglected. However, if it is desired to incorporate temperature dependence of E and α , Eq. (2.8) could be solved by numerical methods. Let us now consider the elastic response of a rapidly heated rod for three special cases of heating functions shown in Fig. 2 which have been chosen for their similarity to experimental heating conditions. These are the cases of constant internal heat generation for a finite time, the exponential temperature rise, and the exponential temperature rise with zero initial conditions, i.e., zero initial stress rate as well as zero initial stress.

(a) Case I - Constant Internal Heat Generation Rate

Let a rod be heated by a constant internal heat generation rate acting for time t_1 . This can be written as

$$q = q_0 [H(t) - H(t-t_1)] \quad (2.19a)$$

where H is the unit step function, i.e.,

$$H(t-t_1) = \begin{cases} 0 & t < t_1 \\ 1 & t > t_1 \end{cases} .$$

The corresponding temperature history is obtained from (2.17), and is

$$T = T_m \left[\frac{t}{t_1} (H(t) + \left(1 - \frac{t}{t_1}\right) H(t-t_1)) \right] \quad (2.19b)$$

where $T_m = q_0/\gamma c$ = maximum steady-state temperature. These functions are shown in Fig. 2a. Since the stress is proportional to the temperature, which has a finite rate at zero time, we cannot specify a zero initial stress rate. Hence, the initial conditions are

$$\sigma(x, 0) = 0$$

(2.20)

$$\dot{\sigma}(x, 0) = \dot{\sigma}_0$$

Also, since the heating is considered to be rapid, the temperature is independent of x . This implies that $\dot{\sigma}_0$ is a constant and that the stress will reach its maximum value, $-E \alpha T_m$, in time t_1 . Hence

$$\dot{\sigma}_0 = -\frac{E \alpha T_m}{t_1} = -\frac{\sigma_{St}}{t_1} \quad (2.21)$$

where σ_{St} is the stress developed if the bar were clamped at both ends and heated slowly to T_m . This initial condition will be verified later from the solution of (2.8). In order to solve (2.8) Laplace transform methods are used, and Eq. (2.8) in the transform $\bar{\sigma}(x, s)$ is

$$\frac{d^2 \bar{\sigma}}{dx^2} - \frac{1}{a^2} (s^2 \bar{\sigma} - s\sigma(0) - \dot{\sigma}(0)) = \rho \alpha [s^2 \bar{T} - sT(0) - \dot{T}(0)] \quad (2.22)$$

where x is the Laplace transform parameter, and

$$\mathcal{L}[\sigma(x, t)] = \bar{\sigma}(x, s) = \int_0^\infty e^{-st} \sigma(x, t) dt,$$

$$\bar{T} = T_m \left[\frac{1}{s^2 t_1} + \frac{e^{-st_1}}{s} - e^{-st_1} \left(\frac{1}{st_1} + \frac{1}{s^2 t_1} \right) \right] = T_m \left[\frac{1 - e^{-st_1}}{s^2 t_1} \right],$$

and

$$T(0) = 0; \quad \dot{T}(0) = \frac{T_m}{t_1}.$$

Substitution into (2.8) yields

$$\frac{d^2 \bar{\sigma}}{dx^2} - \frac{s^2}{a^2} \bar{\sigma} = \frac{\sigma_{St}}{t_1} - \frac{\rho \alpha T_m}{t_1} e^{-st_1}. \quad (2.23)$$

The solution of this non-homogeneous ordinary differential equation is

$$\bar{\sigma}(x, s) = C_1 e^{sx/a} + C_2 e^{-sx/a} - \frac{a^2}{s^2} \left[\frac{\sigma_{St}}{a^2 t_1} - \frac{\rho \alpha T_m e^{-st_1}}{t_1} \right] \quad (2.24)$$

The arbitrary constants C_1 and C_2 can easily be evaluated from the boundary conditions. Since the bar is unrestrained

$$\bar{\sigma}(l, s) = \bar{\sigma}(-l, s) = 0,$$

substitution into (2.24) yields

$$C_1 = C_2 = \left[\frac{1}{2 \cosh sl/a} \right] \left[\frac{\sigma_{St} - \rho \alpha a^2 T_m e^{-st_1}}{s^2 t_1} \right] \quad (2.25)$$

Since $\rho \alpha a^2 T_m = \rho \alpha (E/\rho) T_m = E \alpha T_m = \sigma_{St}$, substitution of (2.25) in (2.24) gives

$$\bar{\sigma}(x, s) = \sigma_{St} \left[\frac{\cosh sx/a}{\cosh sl/a} - 1 \right] \left[\frac{1 - e^{-st_1}}{s^2 t_1} \right] \quad (2.26)$$

In order to invert this solution back to the time domain, we note the following inverse Laplace transforms:³²

$$\mathcal{L}^{-1} \left[\frac{1}{s} \frac{\cosh sx/a}{\cosh sl/a} \right] = t + \frac{2l}{\pi a} \sum_{n=1}^{\infty} \frac{(-1)^n}{(n - \frac{1}{2})^2} \cos(n - \frac{1}{2}) \frac{\pi x}{l} \sin(n - \frac{1}{2}) \frac{\pi a t}{l} \quad (2.27a)$$

$$\mathcal{L}^{-1} \left[e^{-st_1} \bar{f}(s) \right] = [f(t-t_1)] H(t-t_1) \quad (2.27b)$$

Rewriting (2.26),

$$\frac{\bar{\sigma}(x, s)}{\sigma_{St}} = \frac{1}{t_1} \left[\frac{1}{s} \frac{\cosh sx/a}{\cosh sl/a} - \left(\frac{1}{s} \frac{\cosh sx/a}{\cosh sl/a} \right) e^{-st_1} - \frac{1 - e^{-st_1}}{s^2} \right],$$

and making use of (2.27) and (2.28) we obtain

$$\begin{aligned} \frac{\sigma}{\sigma_{St}} = & \frac{2\ell}{\pi^2 a t_1} \sum_{n=1}^{\infty} \frac{(-1)^n}{(n - \frac{1}{2})^2} \cos(n - \frac{1}{2}) \frac{\pi x}{\ell} \sin(n - \frac{1}{2}) \frac{\pi a t}{\ell} \\ & - \frac{2\ell}{\pi^2 a t_1} \left[\sum_{n=1}^{\infty} \frac{(-1)^n}{(n - \frac{1}{2})^2} \cos(n - \frac{1}{2}) \frac{\pi x}{\ell} \sin(n - \frac{1}{2}) \frac{\pi a (t-t_1)}{\ell} \right] H(t-t_1) \end{aligned}$$

Defining the fundamental period of free vibration of the bar as τ ,

where

$$\tau = \frac{4\ell}{a}, \quad (2.28)$$

then we can rewrite this solution in terms of the ratio t_1/τ . Hence,

For $t \leq t_1$

$$\frac{\sigma}{\sigma_{St}} = \frac{1}{2\pi^2} \left(\frac{\tau}{t_1} \right) \sum_{n=1}^{\infty} \frac{(-1)^n}{(n - \frac{1}{2})^2} \cos(n - \frac{1}{2}) \frac{\pi x}{\ell} \sin \omega_n t, \quad (2.29a)$$

and for $t \geq t_1$

$$\frac{\sigma}{\sigma_{St}} = \frac{1}{2\pi^2} \left(\frac{\tau}{t_1} \right) \sum_{n=1}^{\infty} \frac{(-1)^n}{(n - \frac{1}{2})^2} \cos(n - \frac{1}{2}) \frac{\pi x}{\ell} \left[\sin \omega_n t - \sin \omega_n (t-t_1) \right], \quad (2.29b)$$

where $\omega_n = (n - 1/2) \frac{\pi a}{\ell} = 4\pi (n - 1/2) \frac{1}{\tau}$. The displacement $u(x,t)$ can readily be obtained from an integration of Eq. (2.18) with the condition that $u(0,t) = 0$. The result is

$$\begin{aligned} \frac{u}{u_{St}} = & \left[\frac{t}{t_1} H(t) + \left[1 - \frac{t}{t_1} \right] H(t-t_1) \right] \frac{x}{\ell} + \frac{2}{\pi^3} \left(\frac{\tau}{t_1} \right) \sum_{n=1}^{\infty} \frac{(-1)^n}{(n - \frac{1}{2})^3} \sin(n - \frac{1}{2}) \frac{\pi x}{\ell} \\ & \sin \omega_n t - \left[\frac{2}{\pi^3} \left(\frac{\tau}{t_1} \right) \sum_{n=1}^{\infty} \frac{(-1)^n}{(n - \frac{1}{2})^3} \sin(n - \frac{1}{2}) \frac{\pi x}{\ell} \sin \omega_n (t-t_1) \right] H(t-t_1) \end{aligned} \quad (2.30)$$

where $u_{St} = l \alpha T_m$ = maximum static displacement if the bar were heated slowly and allowed to expand freely. Equations (2.29) and (2.30) constitute the complete solution for the axial stress and displacement. They satisfy the boundary and initial conditions and have been verified by substitution back into the original differential equations (2.2) and (2.8).

In order to illustrate the physical significance of the solution (2.29) it is noted that the amplitude is solely a function of the ratio t_1/τ . This is the ratio of the heating time t_1 to the characteristic mechanical response time τ . Hence, it is possible to calculate $\sigma_{\max}/\sigma_{St}$ and u_{\max}/u_{St} as a function of t_1/τ . It should be noted that a cursory glance at (2.29) indicates that as $(t_1/\tau) \rightarrow 0$, $(\sigma/\sigma_{St}) \rightarrow \infty$. This is not the case, however, since a limiting process must be followed. If $t_1 \rightarrow 0$, then for $t \leq t_1$, $\sin(\omega_n t) \rightarrow 0$, and for $t \geq t_1$

$$\frac{\sigma}{\sigma_{St}} = \frac{\tau}{2\pi^2} \sum_{n=1}^{\infty} \frac{(-1)^n}{(n - \frac{1}{2})^2} \cos(n - \frac{1}{2}) \frac{\pi x}{l} \left[\frac{(1 - \cos \omega_n t_1) \sin \omega_n t + \sin \omega_n t_1 \cos \omega_n t}{t_1} \right].$$

Expanding the sine terms in their series form and passing to the limit we obtain

$$\lim_{t_1 \rightarrow 0} \frac{\sigma}{\sigma_{St}} = \frac{2}{\pi} \sum_{n=1}^{\infty} \frac{(-1)^n}{(n - \frac{1}{2})^2} \cos(n - \frac{1}{2}) \frac{\pi x}{l} \cos \omega_n t. \quad (2.31)$$

Hence, $\sigma_{\max}/\sigma_{St} = \pm 1.0$ when $t_1/\tau \rightarrow 0$. $\sigma_{\max}/\sigma_{St}$ has been calculated for various values of t_1/τ and the result is shown in Fig. 3. In order to illustrate the stress-wave propagation phenomena resulting from rapid heating, the solution (2.29) has been evaluated for the special case of

a $0.035 \times 0.500 \times 10$ inch 304 stainless steel rod subjected to a constant internal heat generation rate of 65,000 BTU/sec acting for a time duration of 4 microseconds.

$$\tau = \frac{4l}{a} = \frac{4 \times 5}{0.203 \times 10^6} = 98.5 \text{ } \mu\text{sec.}$$

$$t_1/\tau \approx 0.04$$

$$T_m - T_o = \frac{Q_o t_1}{2Aky_c} = \frac{(65,000)(4 \times 10^{-6})}{2(0.035)(0.5)(5)(0.28)(0.12)} \approx 46^\circ\text{F}$$

$$u_{St} = l \alpha (T_m - T_o) = 5(9 \times 10^{-6})(46) = 0.002 \text{ in.}$$

$$\sigma_{St} = E \alpha (T_m - T_o) = (30 \times 10^6)(9 \times 10^{-6})(46) = 12,500 \text{ psi.}$$

Since $t_1 \ll \tau$, $\sigma_{\max} \approx \sigma_{St}$; hence, for a temperature rise of only 46° , it is evident that a fairly large stress can be developed provided the heating time is short relative to the mechanical response time. The stress distribution over the bar length, $-l \leq x \leq +l$, is shown in Fig. 4 for several successive times, and in Fig. 5 the stress histories are shown at points $x = 0$, $l/4$, $l/2$, and $3l/4$. The displacement history of the end of the rod, $x = l$ is shown in Fig. 6. These results were calculated from Eqs. (2.29) and (2.30).

(b) Case II - The Response of an Unrestrained Rod to an Exponential Temperature Rise

The temperature function given in Case I is physically unrealistic since discontinuities at t_1 are unlikely. Regardless of how a body is heated, the temperature history can normally be approximated by an exponential temperature rise of the form (see Fig. 2b)

$$T = T_m (1 - e^{-t/t_1}) \quad (2.32)$$

Again we specify the initial conditions as

$$\begin{aligned}\sigma(x,0) &= 0 \\ \dot{\sigma}(x,0) &= -\sigma_{St}/t_1\end{aligned}\tag{2.33}$$

Substitution in (2.8)

$$\frac{\partial^2 \sigma}{\partial x^2} - \frac{1}{a^2} \frac{\partial^2 \sigma}{\partial t^2} = -\frac{\rho \alpha T_m e^{-t/t_1}}{t_1^2},$$

and with the above initial conditions this equation in the transform

$\bar{\sigma}(x,s)$ is

$$\frac{d^2 \bar{\sigma}}{dx^2} - \frac{s^2 \bar{\sigma}}{a^2} = \frac{\rho \alpha T_m}{t_1} \left[1 - \frac{1}{t_1} \left(\frac{1}{s+1/t_1} \right) \right].$$

Using the same boundary conditions as before and following the same procedure, the solution for $\bar{\sigma}(x,s)$ is

$$\begin{aligned}\bar{\sigma}(x,s) &= \frac{\rho \alpha T_m}{t_1} \left[\frac{1}{2} \frac{\cosh sx/a}{\cosh sl/a} - \frac{1}{t_1(s+1/t_1)} \frac{\cosh sx/a}{\cosh sl/a} - \frac{1}{t_1 s^2} \right. \\ &\quad \left. + \frac{1}{t_1 s^2 (s+1/t_1)} \right].\end{aligned}$$

The only inversion that poses a problem is the second term on the right-hand side. However, using (2.27) and

$$\mathcal{L}^{-1} \left[\frac{1}{s+1/t_1} \right] = e^{-t/t_1},$$

we can make use of the convolution integral,³³

$$\mathcal{L}^{-1} [g(s) \cdot h(s)] = g(t) * h(t) = \int_0^t g(t-\lambda) h(\lambda) d\lambda.$$

Hence,

$$\mathcal{L}^{-1} \left[\frac{1}{s^2} \frac{\cosh sx/a}{\cosh s\ell/a} \frac{1}{(s+1/t_1)} \right] = \int_0^t e^{-\frac{t-\lambda}{t_1}} \left[\lambda + \frac{2\ell}{\pi^2 a} \sum_{n=1}^{\infty} \frac{(-1)^n}{(n-\frac{1}{2})^2} \cos(n-\frac{1}{2}) \frac{\pi x}{\ell} \sin \omega_n \lambda \right] d\lambda ,$$

and

$$\mathcal{L}^{-1} \left[\frac{1}{s^2} \frac{1}{(s+1/t_1)} \right] = t_1^2 (e^{-t/t_1} + \frac{t}{t_1} - 1) .$$

Noting again that $\rho \omega a^2 T_m = E \sigma T_m = \sigma_{St}$, the inversion is

$$\frac{\sigma}{\sigma_{St}} = \frac{2}{\pi} \sum_{n=1}^{\infty} \frac{(-1)^n \cos(n-\frac{1}{2}) \frac{\pi x}{\ell}}{(n-\frac{1}{2})^2 [1+\omega_n^2 t_1^2]} \left[\cos \omega_n t + (\omega_n t_1) \sin \omega_n t - e^{-t/t_1} \right] \quad (2.34)$$

where again

$$\omega_n = (n - \frac{1}{2}) \frac{\pi a}{\ell} = 4\pi (n - \frac{1}{2}) \frac{1}{\tau} .$$

The displacement can be calculated in the same manner as before, and is

$$\frac{u}{u_{St}} = (1 - e^{-t/\tau_1}) \frac{x}{\ell} + \frac{2}{\pi^2} \sum_{n=1}^{\infty} \frac{(-1)^n \sin(n-\frac{1}{2}) \frac{\pi x}{\ell}}{(n-\frac{1}{2})^2 [1+\omega_n^2 t_1^2]} \left[\dots \right. \\ \left. \left[\cos \omega_n t + \omega_n t_1 \sin \omega_n t - e^{-t/t_1} \right] \right] . \quad (2.35)$$

Equations (2.34) and (2.35) represent the complete solution for Case II, and have been verified by substitution back into the original differential equations (2.2) and (2.8). The nature of this solution is shown in Figs. 7 and 8, where the stress histories are plotted at $x/\ell = 0$ and $x/\ell = 1/2$ and the maximum amplitudes are plotted as a function of the ratio t_1/τ ,

respectively. It should also be noted that as $t_1 \rightarrow 0$, Eq. (2.34) agrees with the corresponding solution (2.31) for Case I when $t_1 \rightarrow 0$.

(c) Case III - The Response of an Unrestrained Rod to an Exponential Temperature Rise Modified for Zero Initial Stress Rate

Both the temperature functions chosen for the previous two cases are perhaps unrealistic since they assume non-zero initial stress rates or particle velocities, and this implies an infinite initial acceleration. The exponential temperature history, which is reasonable for $t > 0$, requires some modification to incorporate zero initial conditions while retaining the exponential character during the temperature rise. This can be accomplished by the function (see Fig. 2c)

$$T - T_0 = T_m [1 - (1 + t/\beta t_1) e^{-t/\beta t_1}] \quad (2.36)$$

in which β is selected arbitrarily on the basis of the degree of approximation to the simple exponential function given by Eq. (2.32). A comparison of (2.36) with (2.32) and the Case I temperature rise (2.19b) is shown in Fig. 9 for various values of the parameter β . It is apparent that if $\beta = 1/3$ good agreement with (2.19b) is obtained, and if $\beta = 1/2$ or $3/4$, good agreement with (2.32) is obtained for $t > 0$.

Assuming Eq. (2.36) as the temperature function, the initial conditions are given by

$$T(0) = \dot{T}(0) = \sigma(x,0) = \delta(x,0) = 0$$

so that the transformed Eq. (2.8) is

$$\frac{d^2 \bar{\sigma}}{dx^2} - \frac{s^2}{a^2} \bar{\sigma} = \frac{\rho \alpha T_m}{\beta^2 t_1^2} \left[\frac{s}{(s+1/\beta t_1^2)} \right]$$

Following the same procedure as before, we find

$$\bar{\sigma}(x, s) = \frac{\sigma_{St}}{\beta^2 t_1^2} \left[\frac{\cosh sx/a}{\cosh s\ell/a} - 1 \right] \left[\frac{1}{s(s+1/\beta t_1)^2} \right]$$

and again using the convolution integral

$$\begin{aligned} \mathcal{L}^{-1} \left[\frac{1}{s} \frac{\cosh sx/a}{\cosh s\ell/a} \cdot \frac{1}{(s+1/\beta t_1)^2} \right] \\ = \int_0^t (t-\lambda) e^{-\frac{t-\lambda}{\beta t_1}} \left[1 + \frac{2}{\pi} \sum_{n=1}^{\infty} \frac{(-1)^n}{(n-\frac{1}{2})} \cos(n-\frac{1}{2}) \frac{\pi x}{\ell} \cos \omega_n \lambda \right] d\lambda \end{aligned}$$

we obtain the solution for the stress as

$$\begin{aligned} \frac{\sigma}{\sigma_{St}} = \frac{2}{\pi} \sum_{n=1}^{\infty} \frac{(-1)^n \cos(n-\frac{1}{2}) \frac{\pi x}{\ell}}{(n-\frac{1}{2}) [1+\beta^2 t_1^2 \omega_n^2]} \left[\dots \right. \\ \left. \frac{t}{\beta t_1} e^{-t/\beta t_1} - \frac{2\beta t_1 \omega_n \sin \omega_n t + (1-\beta^2 t_1^2 \omega_n^2) (\cos \omega_n t - e^{-\frac{t}{\beta t_1}})}{1 + \beta^2 t_1^2 \omega_n^2} \right] \end{aligned} \quad (2.37)$$

The displacement is, therefore, given by

$$\begin{aligned} \frac{u}{u_{St}} = \left[1 - \left(1 + \frac{t}{\beta t_1} \right) e^{-\frac{t}{\beta t_1}} \right] \frac{x}{\ell} \dots \\ + \frac{2}{\pi^2} \sum_{n=1}^{\infty} \frac{(-1)^n \sin(n-\frac{1}{2}) \frac{\pi x}{\ell}}{(n-\frac{1}{2})^2 [1+\beta^2 t_1^2 \omega_n^2]} \left[\dots \right. \\ \left. \frac{t}{\beta t_1} e^{-\frac{t}{\beta t_1}} - \frac{2\beta t_1 \omega_n \sin \omega_n t + (1-\beta^2 t_1^2 \omega_n^2) (\cos \omega_n t - e^{-\frac{t}{\beta t_1}})}{1 + \beta^2 t_1^2 \omega_n^2} \right] \end{aligned} \quad (2.38)$$

where, as shown before,

$$\omega_n = (n - \frac{1}{2}) \frac{\pi a}{\ell} = 4\pi(n - \frac{1}{2}) \frac{1}{\tau}$$

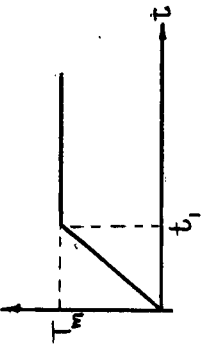
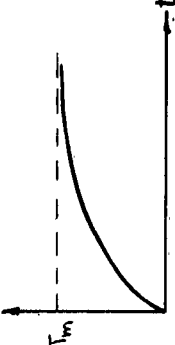
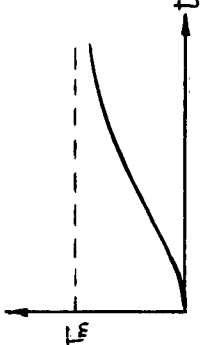
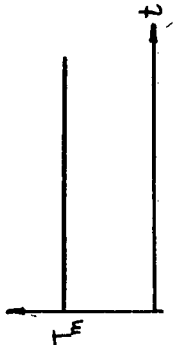
The Eqs. (2.37) and (2.38) represent the complete solution for Case III type heating, and have been verified by substitution back into the original differential equations (2.2) and (2.8). This solution also agrees with (2.31) for an instantaneous temperature rise, i.e., $t_1 = 0$ or $\beta = 0$. Equation (2.37) is compared with (2.34) in Fig. 10 for the special case of $t_1/\tau = 0.1$, and $\beta = 3/4$. Since the two are significantly different only during the initial compression pulse, or transient part of the solution, but agree reasonably well during the steady-state oscillation, the stress histories at a point, as shown in Fig. 7, need not be constructed.

The significant feature of all of these solutions is the amplitude dependence upon the ratio t_1/τ . For Case III heating, this is shown in Fig. 11 for $\beta = 1/2$ and $\beta = 3/4$. It should be mentioned that all of the plots of the theoretical solutions in this work were obtained from calculations performed on the IBM 650 Digital Computer at the Lawrence Radiation Laboratory at Livermore, California. The series solutions were evaluated by calculating as many terms in the series as necessary to reduce the partial sums to magnitudes on the order of 10^{-4} . Hence, the theoretical curves shown in this work represent an accuracy of about 0.01%.

(d) Summary of Theoretical Calculations

For the purposes of clarity the following tabular summary is prepared. Associated with this summary, Fig. 12 shows the comparison of the amplitude dependence upon t_1/τ for the three different types of heating functions.

TABLE I - SUMMARY OF THEORETICAL CALCULATIONS

Case	Assumed Temperature History	Solution for the	
		Stress	Displacement
I	Eq. (2.19b): $T_m \left[\frac{t}{t_1} H(t) + \left(1 - \frac{t}{t_1}\right) H(t - t_1) \right]$ 	Eq. (2.29)	Eq. (2.30)
II	Eq. (2.32): $T_m (1 - e^{-t/t_1})$ 	Eq. (2.34)	Eq. (2.35)
III	Eq. (2.36) $T_m \left[1 - \left(1 + \frac{t}{\beta t_1}\right) e^{-\frac{t}{\beta t_1}} \right]$ 	Eq. (2.37)	Eq. (2.38)
	Special Case of Instantaneous Heating: $T_m H(t)$ 	Eq. (2.31)	—

3. EXPERIMENTAL EQUIPMENT AND PROCEDURES

(a) General

Investigations of the inertia effects of rapid heating are extremely difficult to perform experimentally. The primary difficulty is obtaining very high heat generation rates or thermal fluxes which can be applied in a very short time (see Figs. 3, 7, and 11). Heat sources such as solar energy, plasma jets and propellants produce high thermal fluxes, but the heating times are necessarily long (on the order of 10^{-1} sec) demanding excessive natural periods of the heated test specimen. Also, since only one surface is heated, it becomes necessary to determine the instantaneous temperature gradient in order to evaluate the inertial effects separately. Further, any theoretical solution of Eq. (2.8) for which the temperature function is also spatial, as well as time dependent poses analytical difficulties which complicate verification of experimental results. Additional practical difficulties arise in the design and operation of high thermal radiation sources.

It was decided, therefore, to make use of electrical heating methods. Joulean heating will produce a reasonably uniform temperature, and since it is dependent upon the current, can be easily measured. In order to produce short heating times, however, the electrical system must have a low inductance so that the energy deposition time is short. Also, since very high heat generation rates are required, the system must have a "high" capacitance operating at a high voltage. These requirements are similar to those faced in investigations of exploding wire phenomena, plasma physics, and magnetic metal-forming studies. Researchers in these activities at the Lawrence Radiation Laboratory have designed and

built several types of low-inductance, high energy, mobile capacitor banks which have an inductance on the order of 10^{-7} henries and an energy storage capability as high as 50 kilojoules. Depending on the external circuit resistance, discharge times for these systems are on the order of microseconds. These units are compact, simple to operate and maintain, and provide reproducible energy deposition rates. Hence, the loan of one of these units was requested for use in this work.

(b) Specimen Geometry and Heating Method

The experimental problem consisted of determining the dynamic elastic strain in a long, thin unrestrained rod subjected to rapid internal heat generation such that the heating time was short relative to the fundamental natural period of oscillation of the rod. The theoretical solution for the behavior of an unrestrained or "free-free" rod was first worked out as shown previously in Section 2. However, a completely "free-free" rod is difficult to simulate, but due to the spatial symmetry exhibited by the solution (see Eqs. (2.34) and (2.35), for example), the results for a bar of length fixed at one end and free at the other are identical to the results for a "free-free" bar of length 2. Hence, the test specimen was chosen to be a "fixed-free" rod clamped at one end and submerged in a shallow mercury pool at the other for the necessary electrical continuity. Heating was accomplished with a Lawrence Radiation Laboratory "Mosquitoette" capacitor bank with a capacity of 14 μ fd, an inductance of about 0.1 μ h, an internal resistance of 0.02 ohms, and with a voltage control system for charging to any voltage up to 20 kilovolts so that the maximum energy storage capacity is 2800 joules.

The heating jig is shown schematically in Fig. 13. This arrangement was chosen in order to equalize the magnetic forces on the specimen, and to allow control of the circuit inductance, if necessary, by varying the distance between the return conductor rods. This allows some control over the frequency of the current in the bar. The jig can hold specimens up to 15 inches long and 0.5 inches wide.

The specimens were fabricated from Type 304 stainless steel and for reasons discussed later were rectangular in cross-section with dimensions of 0.050 x 0.250 inches or 0.125 x 0.250 inches with lengths from about 1.50 to 12.0 inches. In order to maximize the i^2R heating and the time for heat conduction out the ends, stainless steel was chosen for its high electrical resistivity and low thermal conductivity. Also, all other physical and mechanical properties are well known.

(c) Electrical Heating Measurements

The system described thus far consisted simply of an R-L-C circuit. The current in the bar will be governed by the circuit constants, and for the oscillatory case is given by

$$i = \frac{CV_o}{b} (a^2 + b^2) e^{-at} \sin bt \quad (3.1)$$

where

$$a = \frac{R}{2L} \quad (3.2)$$

$$b = \sqrt{\frac{1}{LC} - \frac{R^2}{4L^2}}$$

Since the initial charge voltage V_o and the capacitance C are known (the capacitance of the jig can be neglected relative to 14 μfd), it was necessary to determine only the inductance L and total resistance

R to evaluate the current and hence the heating time. This was accomplished with an inductive probe consisting of a small coil wound around a glass tube placed next to the specimen. The current induced in the coil was measured with a Type 551 dual-beam Tektronix oscilloscope fitted with Type L preamplifiers. The output of the coil is proportional to the first time derivative of the current in the bar (or the oscillating magnetic field); hence, an RC integrator was placed in series with the probe. The non-integrated signal was also recorded as a precautionary measure. This circuitry is shown in Fig. 14. From Eq. (3.1) the period of oscillation of the current is

$$\tau_i = \frac{2\pi}{b} = \frac{2\pi}{\sqrt{\frac{1}{LC} - \frac{R^2}{4L^2}}} \quad (3.3)$$

and the amplitude decay characteristic can be obtained from

$$\frac{R}{2L} = - \frac{1}{t_1 - t_2} \log i_1/i_2 \quad (3.4)$$

where i_1 and i_2 are two successive maximums of the same sign. Thus, a measurement of the period of oscillation τ_i and the logarithmic decrement of the probe signal allows a calculation of L and R from (3.3) and (3.4).

In order to calculate the characteristic heating time it was assumed that the current was uniform throughout the specimen. Actually, however, due to the skin effect the current must be greater at the surface. This effect was calculated from standard formulae, and the aforementioned specimen dimensions chosen so that the effective increase in resistance was on the order of 1.1 greater than the D-C value (the bar dimensions are roughly twice the skin depth). The temperature history due to the

Joulean heating is then obtained from Eq. (2.17)

$$i^2 R_s = \gamma c \frac{\partial T}{\partial t}$$

where R_s is the resistance of the specimen alone. Substituting Eq. (3.1) and integrating, the temperature history is

$$T - T_o = \frac{CV_o^2}{2} \left(\frac{1}{Wc} \right) \frac{R_s}{R} \left[1 - \left(\frac{2a^2}{b^2} \sin^2 bt + \frac{a}{b} \sin 2bt + 1 \right) e^{-2at} \right] \quad (3.5)$$

This result assumes that no heat is conducted or radiated away, which is a valid assumption relative to the microsecond time scales which occur in this work. This is discussed in detail in Sec. 2 of the Appendix. A comparison of this temperature history with the simple exponential (2.32) and the compound exponential (2.37) is shown in Fig. 15. It is evident that the sine terms in the parenthesis in Eq. (3.5) are small compared to unity which gives the approximation (see Case II, Sec. 2)

$$T - T_o \approx T_m (1 - e^{-t/t_1})$$

Or, to incorporate zero initial temperature rate conditions (Case III, Sec. 2)

$$T - T_o = T_m \left[1 - \left(1 + \frac{t}{\beta t_1} \right) e^{-\frac{t}{\beta t_1}} \right]$$

where

$$T_m = \frac{CV_o^2}{2} \left(\frac{J}{Wc} \right) \frac{R_s}{R} \quad ^\circ F \quad (3.6)$$

$$J = 9.48 \times 10^{-4} \text{ BTU/joule}$$

The electrical method of heating is obviously very convenient since the characteristic heating time t_1 can be controlled by the inductance

and resistance. With the freedom to vary the length of the bar, the mechanical response time τ can be varied (see Eq. [2.28]), which then allows experimentation at any desired ratio of t_1/τ . Also within the energy capability of the capacitor bank and the heat capacity, W_c , of the bar, the maximum temperature can be closely controlled. However, no means of direct instantaneous temperature measurement was provided. This is the major restriction in this work and its significance will be discussed later.

(d) Measurement of Axial Strain in the Heated Rod

The most direct method of strain measurement is to scribe a grid on the specimen surface and observe the resulting movement with a high-speed camera. However, since the present study is restricted to elastic motion, the strains are very small and cannot be measured directly in this manner.

An alternate method is to fasten strain gages directly to the bar, and observe their output electronically. Since electrical discharge provides the only convenient method of heating the bar, any electronic measurement or equipment must be shielded or removed from the high transient magnetic field surrounding the specimen during the high voltage discharge of the capacitor bank. The millivolt output of a strain gage system mounted on the bar could not be adequately shielded to obtain an adequate signal to noise ratio. However, this technique was useful for determining the steady-state oscillations observed after the heating pulse, and was used with reasonable success at low bank voltages. Above bank voltages of about 5 kv, arcing occurred and destroyed gage continuity. It has been suggested that the heated bar itself could be used as a strain gage by measuring the change in resistance over a section. In addition

to the problem of shielding, this method would measure the integrated change in resistance over the bar giving only the integrated strain. Since the instantaneous currents in the bar can be as high as 75,000 amps, it was apparent that optical methods were more likely to be successful for measuring the small elastic strains during, as well as after, the heating pulse, and that electronic methods are rendered unsatisfactory by magnetic shielding difficulties.

Since the elastic strains in the heated rod are very small, some means was sought to amplify their effect. In the technique known as "Photostress"^{34,35,36} the bar is coated with a birefringent material which produces interference fringes as the parent bar is deformed. Using a reflecting polariscope with an intense light source, the fringe pattern could be photographed with a high-speed camera. Since the coating must be necessarily thin to prevent restriction of the bar movement, and since the fringe order and the resultant accuracy are directly proportional to the coating thickness, this method proved to be too insensitive. Hence, this technique was modified in the following manner.

A 0.25 inch thick by 1.0 inch deep beam of a photoelastic material (Bakelite ERL 2774) was loaded in pure bending in the plane of the beam. The resulting fringe pattern was frozen into the loaded beam by raising the temperature, holding it constant at 165°F for four hours, and then allowing it to cool slowly back to room temperature. When viewed through a crossed circular polariscope the residual fringe pattern appeared as shown in Fig. 16. The beam was polished on its lateral surfaces and then cut into 0.050 inch strips which were glued to each side of the rectangular specimen as shown in Fig. 17. An epoxy resin glue commonly used in "Photostress" techniques was found satisfactory for this

application. If careful attention was given to the cutting technique, the fringe pattern remained unaltered. In order to eliminate thermal effects during cutting, it was necessary to perform all cutting and polishing by hand. Polishing of the surface to be glued to the bar was done in successive stages by using emery cloth of decreasing grit size mounted on plate glass since it was important to maintain a plane surface in order to eliminate initial bending.

With the photoelastic coating mounted in the manner shown in Fig. 17d it was possible to use incident rather than reflected light as is normally done in "Photostress" techniques. Also, the initial fringe pattern allows accurate determination of fractional fringe order changes, and by observing the movement of the entire fringe pattern, a complete stress distribution over the one inch coating length can be obtained. This is discussed in some detail by Zandman³⁷ who has recently contributed some interesting variations of the photoelastic stress gage. In order to observe the fringe motion during heating, a Model 601 high-speed framing camera was used with a crossed circular polariscope and white light so that a dark field with integral fringe orders was obtained. A high intensity light source was designed which consisted of an Edgerton, Germeschausen and Grier Type FX-1 Xenon flash tube mounted at the focus of a cylindrical parabolic reflector. A standard Lawrence Radiation Laboratory (IWL-1733A) pulse-line chassis was modified to provide power for the tube as shown in Fig. 18. This system provided approximately 250 μ secs of sufficient light with a 2 μ sec rise-time to expose 35 mm Kodak high speed Ektachrome film with camera speeds of approximately 350,000 frames/sec at f:23.

Since it was considered sufficient to obtain the stress at only one point on the bar (at $x = \ell/2$), white light was used which aided the identification on the film record of the zero and two first order fringes. The zero order is always black and the two first order fringes are always marked by the passage from red to blue. However, higher fringe orders in the initial pattern cannot be observed easily with white light. If the stress distribution over the entire coating length is desired, it is necessary to use a 5461A° green filter with black and white film to clearly mark the higher order fringes, as shown for example by the static photograph in Fig. 16. The reasons for using only white light will be discussed later.

The experimental apparatus used in an actual test run is shown in Fig. 19. The light from an exploded bridge wire mounted next to the specimen marks "zero" time on the photographic record and also by electromagnetic induction causes a pulse to be superposed on the oscilloscope trace of the output of the current probe. In this manner, the photographic record is synchronized with the electronic record of the current. A 535 Tektronix oscilloscope fitted with a Type H pre-amplifier was used to measure the camera rotor speed by recording the output of a reluctance pickup mounted on the rotor shaft. This accurately fixes the interframe time of the camera record. Hence, a synchronized record of the fringe pattern in the coating is obtained simultaneously with the current-time relationship. The schematic block diagram and the function-time diagram for this procedure are shown in Figs. 20 and 21, respectively. A photograph of a specimen mounted in the heating jig is shown in Fig. 22. It should be noted that to compensate for film shrinkage a calibration length was provided. This consisted of two

lines, a known distance apart, scribed on a piece of polaroid mounted next to the coating. This allowed light to pass through the crossed polariscope so that the scribe marks were illuminated. Some sample specimens are shown in Fig. 23.

(e) Operating and Data Reduction Procedure

With the apparatus arranged as shown previously in Figs. 19 and 20, the test was carried out as follows. Since the Model 601 camera was used in the "unsynchronized" mode of operation, no synchronized shuttering facility was available. Hence, the room containing the heating jig was darkened and the camera ran at the desired rotor speed with the mechanical shutter held open manually. Closure of the "fire" switch on the control unit dispatched a 500 volt fiducial pulse which triggered the oscilloscopes, discharged a condenser unit to explode the bridge-wire, discharged the main capacitor bank through the specimen, and triggered the charged pulse-line for the light source. Time delay units were included in this equipment, but were not needed since the inherent delays in the system proved satisfactory.

The oscilloscopes triggered first, at 5 microseconds the light source and bridge-wire discharged, and at 12 to 20 μ sec the bank discharged. Both the light source and the bridge-wire light outputs had rise times of about 2 μ sec; hence, both appeared on the "zero" frame of the film strip. In order to prevent rewriting the light source duration was kept less than the time for one revolution of the camera rotor since no shuttering was used. A 250 μ sec light source was used as the camera had 164 frames and interframe times from 2 to 3 μ second were desired. The oscilloscope traces were recorded permanently with Dumont Oscilloscope Cameras loaded with Type 400 Polaroid Film. Sample oscilloscope traces of the rotor

frequency and the output of the induction probe are shown in Figs. 1A and 2A of Sec. 1, Appendix. The use of this data is also shown in Sec. 1, Appendix, where the complete data reduction procedure is illustrated for two sample runs.

After development, the 35 mm color film was scanned with a 10X Bausch and Lomb binocular microscope fitted with an "x-y" travelling stage graduated to 0.01 mm. The positions of the zero and two first order fringes in the coatings were measured in each frame with respect to the fixed calibration scribe marks. Also, the known distance between these marks was measured to provide a correction for film shrinkage from frame to frame. Hence, the measurements per frame consisted of six fringe positions and a calibration length, giving a total of seven separate measurements. The average movement of the zero and two first order fringes was calculated and plotted as a function of time (or frame number). Sample plots are shown in Figs. 3A and 4A. Since the movements of the fringe patterns in the coatings glued on each side of the bar were averaged, any effect due to lateral bending of the specimen was eliminated automatically, which insured measurement of only the longitudinal motion of the bar.

It should be noted here that theoretically it is possible to obtain the transient stress distribution over the length of the coating. This would require the use of a green filter in the light path which would clearly display all fringe orders from zero to, in this case as shown in Fig. 16, six, but black and white film would be necessary, which requires some means of identification of the zero order fringe. This was attempted, but it was found that with visual microscope scanning it was very difficult to maintain constant reference to the zero order. Hence,

color film was used since the zero order and two first order fringes are always clearly marked by black and the passage from red to blue, respectively. However, the higher order fringes above the first are not clear, but for the purpose of obtaining the stress at a point, observation of only the zero and first orders were sufficiently accurate. In addition to the identification problem with black and white film, it became evident that since visual scanning of only three fringe movements resulted in seven measurements per frame, or a total of about 500 separate measurements for a complete film record, observation of the complete fringe pattern would be extremely time consuming and impractical. This difficulty could have been eliminated, however, if it had been possible to obtain an automatic film densitometer which would plot the fringe movements on a strip chart. Even with this equipment, the ensuing calculation of the fringe orders with time would still exist and would require voluminous computations.

Once the fringe movements recorded on the color film were plotted, the change in fringe order at a point was calculated graphically from the relative positions of the three fringes as shown in Fig. 5A. This was done for as many points in time as desired. With the change in fringe order at the initial position of the zero order fringe determined as a function of time, the stress-optic law was used to calculate the stress as a function of time. The derivation of the relationships used for this purpose are given in the following section.

(f) Calculation of Stress from Experimental Data

The equation governing the relationship between the observed birefringence in the coating and the uniaxial stress in the heated bar is obtained in the following manner. Referring to Fig. 1, consider the parent material, or specimen, to be in a state of biaxial stress such

that the stress σ_y normal to the surface s is zero. If the coating c is securely bonded to the specimen and is of substantially lower stiffness, then the strains in the coating and specimen are equal at the interface, i.e.,

$$\epsilon_s = \epsilon_c \quad \text{or} \quad \frac{\partial u_s}{\partial x} = \frac{\partial u_c}{\partial x} = \frac{\partial u}{\partial x} \quad (3.7)$$

where the subscripts s and c refer to the specimen and coating, respectively. For the biaxial stress condition the linear thermoelastic stress-strain relations (2.3) reduce to

$$\sigma_{x_s} = \frac{E_s}{1-\nu_x^2} [\epsilon_{x_s} + \nu_s \epsilon_z - (1+\nu_s) \alpha_s T(t)] \quad (3.8)$$

and for the coating

$$\sigma_{x_c} = \frac{E_c}{1-\nu_c^2} [\epsilon_{x_c} + \nu_c \epsilon_z - (1+\nu_c) \alpha_s T(t)] \quad (3.9)$$

It is important to recognize that since the coating remains at the initial ambient temperature (see Sec. 3, Appendix) and is securely bonded during the period of measurement, the only thermal strain present is that of the specimen and is denoted by $(1+\nu_s) \alpha_s T$ in both (3.8) and (3.9). Also, since the theory of thermoelasticity is based on the linear superposition of thermal and mechanical strains, ϵ_x and ϵ_z represent only the effect of the loading which in this work is the inertia of the specimen. However, as pointed out (see Sec. 2, p. 8) a uniaxial stress state can safely be assumed so that ϵ_z is zero. Therefore, combining Eqs. (3.7), (3.8) and (3.9) gives

$$\frac{\sigma_{x_s}}{\sigma_{x_c}} = \frac{E_s}{E_c} \cdot \frac{1-\nu_c^2}{1-\nu_s^2} \left[\frac{\epsilon_x - (1+\nu_s) \alpha_s T(t)}{\epsilon_x - (1+\nu_c) \alpha_s T(t)} \right]$$

or

$$\sigma_{x_s} = \frac{E_s}{E_c} \left[\frac{1-\nu_c^2}{1-\nu_s^2} \right] \sigma_{x_c} \quad (3.10)$$

The observed birefringence N in the coating is related to the state of stress by the stress-optic law

$$\sigma_1 - \sigma_2 = \frac{f_\sigma}{h} N \quad (3.11)$$

where σ_1 and σ_2 are the largest and smallest principal stresses acting in the plane of observation. Since it will be shown later in Sec. 4,

Appendix, that $\sigma_2 = \sigma_y \approx 0$,

$$\sigma_{x_c} = \frac{f_\sigma}{h} N \quad (3.12)$$

Since the coating is subjected to the thermal strain $\alpha_s T$ in the specimen, Eq. (3.12) will yield the total stress in the coating. Hence in order to determine the stress due to inertia effects alone, the stress $E_c \alpha_s T(t)$ must be subtracted.

$$\sigma_{x_c} = \left(\frac{f_\sigma}{h} \right) N - E_c \alpha_s T(t) \quad (3.13)$$

Combining (3.13) with (3.10) will give the inertia stress in the bar as

$$\sigma_{x_s} = \left(\frac{E_s}{E_c} \right) \left(\frac{1-\nu_c^2}{1-\nu_s^2} \right) \left[\frac{f_\sigma N}{h} - E_c \alpha_s T(t) \right]$$

This can be non-dimensionalized by dividing through by $E_s \alpha_s T_m$, or σ_{st} . Dropping the subscripts,

$$\frac{\sigma}{\sigma_{st}} = \frac{1-\nu_c^2}{1-\nu_s^2} \left[\frac{1}{\alpha T_m} \left(\frac{f_\sigma N}{E_c h} \right) - \frac{T(t)}{T_m} \right]$$

If the bar were heated slowly to T_m , the average strain would be

$$e_{Avg} = \alpha_s T_m = \left(\frac{f_u}{E_c} \right)_{St} \left(\frac{N_{Avg}}{h} \right) = \left(\frac{1}{1+\nu_c} \right) (f_e)_{St} \frac{N_{Avg}}{h} \quad (3.14)$$

since the interdependence between f_u and f_e is

$$f_e = \frac{1+\nu_c}{E_c} f_u \quad (3.15)$$

Poisson's ratio is not rate dependent; hence, substitution of (3.14) and (3.15) into (3.13) gives

$$\frac{\sigma}{\sigma_{St}} = \frac{1-\nu_c^2}{1-\nu_s^2} \left[\frac{(f_e)_{Dyn}}{(f_e)_{St}} \left(\frac{N}{N_{Avg}} \right) - \frac{T(t)}{T_m} \right] \quad (3.16)$$

Since $\nu_c = 0.35$ and $\nu_s = 0.30$, the quantity in the parentheses is nearly unity and can be dropped, giving the result

$$\frac{\sigma}{\sigma_{St}} = \frac{(f_e)_{Dyn}}{(f_e)_{St}} \left[\frac{N}{N_{Avg}} \right] - \frac{T(t)}{T_m} \quad (3.17)$$

where $T(t)$ is given by (2.19b), (2.32) or (2.36).

Since the presence of a shear stress increases the birefringence, Eq. (3.17) should be corrected for stress gradients in the x direction. In order to account for the effect of a shear stress, Zandman³⁷ has provided the correction factor.

$$\frac{N}{\sqrt{N^2 + 4h^2 (\Delta N/\Delta x)^2}}$$

which will reduce the magnitude of σ/σ_{St} obtained from (3.17). However, in this work, observations of the fringe patterns indicate that $\Delta N/\Delta x$ is very small. This can also be verified theoretically for the positions chosen for measurement of the strain. Hence, Eq. (3.17) is used directly.

In order to evaluate the effect of rate of loading on the optical properties of the coating, a separate calibration experiment was performed (see Sec. 6, Appendix). As pointed out by Goldsmith,³⁹ the strain-optic coefficient may vary appreciably with loading rate, and any interpretation of photoelastically obtained data must rely upon a calibration at substantially the same rates. This was done on specimen No. 2 so that the calibration was carried out at a period of oscillation of approximately 100 μ sec. The results of this experiment showed that the optical properties are essentially unaffected at this rate. Hence, the ratio of the dynamic to the static strain-optic coefficients in (3.17) can be taken as unity which allows (3.17) to be written simply as

$$\frac{\sigma}{\sigma_{St}} = \frac{N}{N_{Avg}} - \frac{T(t)}{T_m} \quad (3.18)$$

Actually, the coating reinforces the steel bar and a correction for this must be determined. Zandman, Redner and Riegner³⁸ have worked out the correction factors for the reinforcing effects, but confined their analysis to quasi-static stress states. However, for dynamic loading, the inertia as well as the stiffness of the coating must be considered. Hence, the analytical procedure of Zandman, et.al. was modified to investigate the reinforcing effect present during dynamic loading. This analysis is performed in Sec. 5 of the Appendix, where it is shown that only the period of oscillation is affected. The corrected period τ' is given by

$$\tau' = \sqrt{m} \tau \quad (3.19)$$

where

$$m = \frac{1 + \frac{A_c}{A_s} \frac{\rho_c}{\rho_s}}{1 - \frac{A_c}{A_s} \frac{E_c}{E_s}} \quad (3.20)$$

The amplitude of the stress is increased slightly since it has been shown to be dependent upon t_1/τ which decreases with the increase to τ' . Hence, the period τ in the theoretical solutions (2.29), (2.34) or (2.37) must be replaced by τ' for comparison of these solutions to the experimental data. It should be noted here that this correction is not exact since its derivation was based on several simplifying assumptions as noted in the analysis. The simplifications however, are not severe, and for engineering purposes this correction factor is sufficiently accurate.

In order to obtain the reported data, then, Eq. (3.18) is used. If some means were available to measure temperature during the heating, the function $T(t)$ could be evaluated directly. However, no accurate method exists and it is necessary to assume a temperature history. It was determined that a simple exponential rise gave a good approximation to Joulean heating. This is shown by the curve in Fig. 16 which was constructed from a measurement of the current with the inductive probe. The maximum temperature as calculated from (3.6) was also verified by mounting a thermocouple on a bar which was rapidly heated at various bank voltages. Observation of the temperature during the first 60 seconds of cooling allowed an extrapolation back to zero by plotting the measured temperatures on semi-log graph paper. It was found that (3.6) was in agreement to within 5% for temperature increases up to 80°F. Hence, despite the fact that no direct means of temperature measurement was provided, it was evident that an assumed temperature history in (3.18) would not seriously affect the validity of the experimental results. Since the maximum temperature, and hence σ_{St} , can be determined accurately from (3.6), the only assumption arises when selecting

an appropriate temperature rise. In order to consider upper and lower bounds, Case II and Case III types of heating were both investigated analytically. Thus, the respective theoretical solutions (2.34) and (2.37) were compared with experimental results obtained from

$$\text{Case II: } \frac{\sigma}{\sigma_{St}} = \frac{N}{N_{Avg}} - (1 - e^{-t/t_1}) \quad (3.21)$$

$$\text{Case III: } \frac{\sigma}{\sigma_{St}} = \frac{N}{N_{Avg}} - \left[1 - \left(1 + \frac{t}{\beta t_1} \right) e^{-t/\beta t_1} \right] \quad (3.22)$$

These equations are used directly to obtain experimental values of σ/σ_{St} as a function of time. The fringe order N and N_{Avg} is obtained from the film records, and t_1 is determined by a measurement of L/R from the probe record. The results are compared with the appropriate theoretical solution modified by the correction factor (3.20). Complete sample calculations are shown in Sec. 1 of the Appendix for two representative tests.

4. EXPERIMENTAL RESULTS

The experimental results were obtained from tests on four bars of differing sizes with two of the bars each having two different coating sizes. All bars were fabricated from the same stock of 304 stainless steel, and all coatings were cut from the same piece of Bakelite (ERL-2774). Coating sizes were varied to evaluate the effect of the coating on the response of the bar. This was accomplished by selecting one specimen with large bar volume and the other with small bar volume relative to coating volume. All specimens were tested under "fixed-free" end conditions with the exception of one specimen tested under an approximate "free-free" condition for the purpose of illustrating the effect of imperfect clamping. The bars were rapidly heated to cause temperature changes of approximately 30°F for different bar lengths selected to provide a range of heating ratios, t_1/τ , varying from 0.05 to 0.28. All test parameters are listed in Table II, and the measurements of the inertial stresses as a function of time are plotted and compared with the appropriate theoretical solutions in Figs. 24 to 31. A comparison of these results to the theoretical prediction for the dependence of the initial compressive stress on the heating ratio t_1/τ is shown in Fig. 31. Sample calculations and data are given in Sec. 1 of the Appendix.

TABLE II - TEST PARAMETERS

Run	Specimen* Size	Coating Size**	t ₁ μsecs	τ' μsecs	x/l	End Conditions	Capacitor Voltage	T _m °F	σ _{St} psi
1	0.125 x 0.25 x 12.0	0.04 x 1.0	13.2	254	0.50	Fixed-Free	14.1 kv.	35	9300
2	0.125 x 0.25 x 5.00	0.03 x 0.56	9.4	105	0.50	Fixed-Free	10.3	23	6100
3	0.050 x 0.25 x 2.47	0.05 x 1.0	7.1	57.7	0.45	Fixed-Free	5.2	35	9450
4	0.050 x 0.25 x 1.46	0.03 x 0.657	7.45	32.6	0.38	Fixed-Free	4.2	27	7400
5	0.050 x 0.25 x 1.46	0.03 x 1.0	9.2	32.6	0.38	Fixed-free	4.7	25	6800
6	0.125 x 0.25 x 10.0	0.035 x 1.0	11.1	105	0	Free-Free	12.6	22	6300
7	0.125 x 0.25 x 5.00	0.05 x 1.0	11.0	106	0.50	Fixed-Free	10.2	26	7000

* All specimens were fabricated from Type 304 stainless steel. Sizes given in inches.

** All coating widths were 0.25 inches.

5. DISCUSSION OF RESULTS

Theoretical Results

The interpretation of the theoretical solutions obtained in Sec. 2 leads to some interesting conclusions concerning the physical nature of thermoelastic dynamics. The steady state portion of the solutions (when $t \gg t_1$) coincide with the solution for the response of a thin rod subjected to initial compression and sudden release.⁴¹ Hence, thermoelastic dynamic problems are exactly analogous to mechanical vibration or shock problems. If an elastic body is heated rapidly enough, the inertia prevents rapid thermal expansion such that a large inertial compressive stress state exists equal to that which would result if the body were restrained and heated slowly. Subsequent unloading takes place as a free periodic oscillation about the initial stress state as shown in Figs. 4, 5 and 7, for example. It is evident, then, that the maximum stress possible will be equal to the static or initial value, and the corresponding maximum displacement is twice the static value. These conditions occur only if the body is heated instantaneously, i.e., $t_1/\tau = 0$, which represents the extreme conditions of heating.

As shown in Figs. 3, 8 and 11, the stress amplitude depends only on the ratio of a characteristic heating time to a characteristic mechanical time which is the fundamental period of free oscillation of the rod. Hence, the meaning of "rapid heating" is made clear since the inertial effect becomes important only when the heating time is significantly less than the mechanical response time. It is also evident from Fig. 12 that variation in the imposed heating function influences the stress amplitude. This is expected, since the time to reach a given temperature will be shortest for a constant heating

rate (Case I) as compared to an exponential heating rate (Case II or III). It should be noted that these curves are plotted for $x/l = 0.5$. Due to the spatial distribution of stress, the maximum amplitude is largest at $x/l = 0$; hence these curves do not represent the maximum stress in the entire rod, but only the maximum stress at the position indicated.

In a real material there will be some damping present which will reduce the subsequent oscillations to zero. The theoretical analysis presented here does not include this effect; however, the solutions given do represent the maximum stress conditions. If damping were considered, its effect would probably be manifested by some type of exponential decay function multiplying the series solutions given in Sec. 2. Since the mechanical and physical properties of 304 stainless steel are nearly constant for small temperature changes, this work was performed by restricting the maximum temperature rise to less than 40°F. For large temperature changes the temperature dependence of the elastic modulus, specific heat and coefficient of thermal expansion can be considered in the solution of Eq. (2.8), but would require numerical solution with machine computation. However, if the temperature rise is large enough, then σ_{St} will exceed the yield stress and plastic flow may occur during the first compressive pulse. If this occurs then the solution is complicated by the deviation from elastic behavior. However, it was shown (Fig. 4) that if no temperature gradients exist, all points are raised to some stress level at the same time during the temperature rise. Hence, yielding would occur only during the initial compression, while subsequent free oscillation would occur elastically after some permanent deformation had taken place upon the first stress reversal.

The physical nature of thermoelastic dynamics has interesting experimental consequences as it would be possible to simulate the effects of rapid heating by mechanical rather than thermal loading. For instance, a long rod could be heated slowly to the desired temperature and then compressed until the stress level reached the value associated with the desired value of t_1/τ . Sudden release of the rod would result in free oscillation. An example of a utilization of this idea is the calibration procedure used in this work and described fully in Sec. 6 of the Appendix. This technique could be useful for testing at high temperatures. However, the photoelastic coating could not be used, but instead high-temperature strain gages would be utilized for dynamic strain measurement. Obviously, a rod is of little practical interest, but this technique would prove useful for studies of the motion of thin shells at high temperatures since the geometry of such structures restricts attempts to experimentally induce rapid uniform internal heat generation by conventional methods. The elastic-plastic response of thin spherical shells has been investigated by the author, and it was found that, as expected, the results are analogous to the thin rod. Hence, the mechanical method is feasible and would require heating a shell slowly, compressing it to an initial stress and observing the subsequent oscillation upon release.

Experimental Results

Generally, agreement between the experimental data and theoretical predictions is comparatively good over the first half cycle of response, but gradually decreases with time. Since this subsequent disagreement appears primarily as a deviation in amplitude but not frequency, it was apparent that some damping effect was present. Calibration of the coating (Sec. 6, Appendix) established that the optical properties were essentially

rate independent, and because the coating temperature remained constant during the period of observation (Sec. 3, Appendix), accurate measurements of the dynamic strain were obtained. Since the internal damping of 304 stainless steel would not be sufficient to significantly affect the first two or three cycles, it was reasoned that either the forced oscillation of the coating introduced sufficient energy loss per cycle or that the damping was caused by imperfect clamping at the fixed end. Experimental investigation of these effects revealed that significant damping was present and was primarily caused by the clamp. Hence, it is concluded that the bar is not behaving exactly as predicted by the theoretical solution which assumes zero damping, and that the photoelastic data provides accurate measurement of the response of the bar. The experimental verification of these conclusions is discussed in the following.

The theoretical solutions were based on idealized boundary conditions, i.e., the displacement at the fixed end of the rod was assumed to be identically zero, and that the free end is stress free. It is unrealistic to expect a clamp to be efficient enough to satisfy the assumed condition of zero rod displacement. If there is relative movement between the rod and the clamp, then certainly structural damping of the oscillations will occur. The clamp used in actual tests consisted of a 0.50 x 0.63 x 0.75 inch copper block used to clamp the specimen to the upper electrode with two 4-40 steel machine bolts, as shown in Fig. 13. It will be demonstrated that depending upon the tension in these bolts, the response of the bar can vary widely. This was investigated experimentally by clamping a specimen in the heating jig and preloading it with a weight suspended by a thin wire fastened at the free end of the specimen. Sudden release of the load was achieved by exploding a section of the wire with the capacitor bank. The

resulting oscillations were observed with strain gages mounted on the bar, as shown in Fig. 23. This procedure is identical to the calibration procedure discussed in Sec. 6, Appendix and illustrated in Fig. 7A. The strain records so obtained are shown in Figs. 32a, 32b and 32c. Test (a) was run with the clamping bolts as tight as possible, test (b) with the bolts under "medium" tension, and test (c) with the bolts under minimum tension, or just "snug". These records were reproducible and many more were obtained for various combinations of bolt tension in the top, bottom, or both bolts.

The results show that as long as the bolts are reasonably tight the strain records were all nearly identical, but for minimum bolt tension the oscillations were completely damped as shown in Fig. 32c. Even for maximum bolt tension (Fig. 32a) damping was present, as indicated by the first two cycles. Apparently, the oscillations after these two cycles are drastically affected by subsequent erratic motion of the wire upon unloading, and are, therefore, not representative of the "fixed-free" condition. Using the first two cycles of test (b), a damping factor, or logarithmic decrement, was calculated and applied to the theoretical solution used for Run 2. The envelope of this exponential decay is shown by the dotted lines superposed over the plots in Fig. 25a. The excellent agreement indicates that the apparent discrepancy is not a result of the coating method, but instead is due to imperfect clamping. Hence, the theoretical solutions derived in Sec. 2 should be modified by the inclusion of a damping factor for purposes of comparison with experimental data. Since only one specimen was large enough to be fitted with strain gages, the experimental damping correction was applied only to the corresponding heating test, namely Run 2. The results of this correction are shown in Fig. 25b, which illustrates the improved agreement with the experimental data.

Further examination of the strain records in Fig. 32 shows that the first two cycles do have the same general wave form as predicted theoretically. However, it was noted that in some tests the peaks of the oscillations were cut off sharply, apparently by some action of the clamp. This effect is particularly pronounced for Run 1 in Fig. 24, and serves to explain the large disagreement between experimental data and non-damped theoretical predictions. Also, since the specimen used for Run 1 was physically the largest, its erratic behavior is expected due to the decrease of clamp efficiency for the larger specimens.

Some thought was given to the redesign of the clamp in order to reduce the damping. An exploratory experiment was performed by clamping the specimen between two large steel plates with a heavy C-clamp. It was expected that excessive clamp mass coupled with extreme tightness would approximate the best clamp that could be designed. The resulting strain records obtained as above indicated that the damping was reduced, but nevertheless, still present. The logarithmic decrement was reduced from 0.0045 to about 0.003. Also, the wave form was slightly improved for the first cycle with the peak appearing as predicted, but the peak of the second cycle was removed. Hence, it was decided that complete redesign of the clamp was not justified.

In order to further verify the effect of clamping, a separate heating test was performed on a "free-free" bar. An attempt was made, with some difficulty, to design end supports that would not restrict specimen motion. This was done by supporting the ends with styrofoam cushions mounted in 5/16 inch grooves cut into suitable copper electrodes. Mercury was used to achieve electrical continuity between the specimen and the electrodes, and the entire assembly was mounted horizontally in the heating jig which

had been rotated 90° in the plane of the return conductors. The specimen was cut from the 12 inch bar (Run 1) such that the coating was at the center ($x/l = 0$) of a 10 inch "free-free" rod which theoretically had an oscillatory period of 100 microseconds. The results of this test are shown in Fig. 29, and much better agreement with theory was obtained. The experimental data indicates that, for at least the duration of observation, no damping was present. As contrasted with Fig. 25, the difference in wave shape is due to the difference in location of strain measurement; i.e., $x/l = 0$ instead of $x/l = 0.5$. This is also shown by Fig. 7.

The results from this test are compared with theory for the two types of heating in Fig. 29 (Case II) and Fig. 30 (Case III, $\beta = 3/4$). A comparison of these two figures shows that best agreement is obtained for Case II heating. This indicates that the simple exponential provides the best approximation to the temperature history, although the actual time constant t_1 may be longer than measured by the inductive probe method. This is likely since the determination of L/R was made by taking the average logarithmic decrement of the current trace which did not always decay in an exact exponential manner but was, nevertheless, sufficiently close to justify this procedure. For rapid heating by capacitor discharge, then, it is evident that the simple exponential is the best assumption for the temperature history since it will be slightly conservative and will give reasonable accuracy with a minimum of calculations.

The only other source of specimen damping was the damping induced by the coating motion. In order to evaluate this effect, specimens of the same size, but with different coating size were tested. Also, a separate

calibration test was performed in which a bar was loaded by a weight, as mentioned previously, once with a coating and once without a coating, but with strain gages mounted on the bar. The results of these tests showed that no significant difference in response occurred. Hence, it was concluded that the coatings used in this work introduced no observable damping.

In view of these additional experiments, and by virtue of the excellent agreement obtained in the calibration test shown in Fig. 8A, it is evident that the photoelastic coating technique can provide accurate measurement of the dynamic strain distribution in rapidly heated specimens. It should be noted, however, that this technique is applicable only for short times since all measurements must be made before heat transfer to the coating can take place. This is not a serious restriction, however, as it was shown in Sec. 3, Appendix that the temperature of the coating at a distance of only 0.005 inches from the heated bar remains unaffected for the first 300 microseconds, the coating is essentially at room temperature during this period.

In this work only the stress at a point was measured, but this technique is directly applicable to measurement of the stress distribution over the coating. This can be done by using monochromatic light and black and white film, and/or by spacing coatings all along the bar. The only major difficulty arises in carrying out the multitude of measurements and calculations involved in using more than three fringes in each coating. An example of the type of data obtained from use of 5461 Å light and black and white film is shown in Fig. 3A of Sec. 1, Appendix. This, however, is not a serious drawback provided such a time-consuming task can be justified.

Since one of the primary concerns was to determine the validity of the theoretical relationship for the dependence of the inertial stress on the heating ratio t_1/τ , several tests were conducted on bars of shorter lengths. These lengths were selected to provide some variation in the heating ratio - from 0.05 to about 0.30. From the results of these additional tests shown in Figs. 26, 27 and 28, the maximum initial compression stress was obtained. This data is plotted in Fig. 31 and compared with the theoretical prediction for Case II heating. Due to the damping effect of the clamp, these results should logically lie below the predicted values. The only large disagreement occurs at $t_1/\tau = 0.05$, and is probably due to the erratic behavior peculiar to the larger specimens as shown by Fig. 24. These results, then, illustrate the validity of the theoretical solution, and from these tests it can be concluded that similar calculations for bodies of other geometries will provide accurate results for engineering design purposes.

The primary restriction in this work is that the measurement of the transient response during the heating actually depends upon an independent measurement of the temperature rise. However, to this author's knowledge, no successful temperature measurement device with microsecond response time has been developed for use in the presence of large magnetic fields. Since it was shown that the temperature rise resulting from capacitor discharge is closely approximated by a simple exponential function, lack of a separate temperature measurement is not a serious restriction. Hence, the determination of stress from Eq. (3.21) will provide accurate results. In fact, a significant result of this work is that the photoelastic coating technique can be used directly to determine the temperature by measuring the fringe order with time and using the strain-optic law. However, the

temperature dependence of the coefficient of thermal expansion of the heated body and the dynamic strain-optic coefficient of the coating must be known. This will require an extended calibration of the coating at the frequencies expected during the measurement. The calibration procedure presented in this work provides an excellent technique since it can be performed at any desired frequency by simply varying the length of the specimen.

Additional experimentation was performed in which the coated specimens were rapidly heated to as high a temperature as possible with the 2800 joule capacitor bank. These tests indicated that for temperatures beyond 350°F, the coatings did not remain bonded. No actual photographs were taken to determine the fringe movement at these high temperatures, but examination of the fringe pattern and glue joint showed no appreciable change. Hence, it is concluded that the coating technique should be useful for transient measurements at elevated temperatures at high as 350°F.

6. CONCLUSIONS

The results of this study lead to the following conclusions:

1. The amplitude of thermally induced stresses in an unrestrained elastic rod are dependent upon the ratio of the heating time to the mechanical period of oscillation. For a given total heat input, the maximum stress amplitude results from a constant heating rate as compared to an exponential type of input.
2. It has been demonstrated that rapid uniform internal heat generation can be accomplished by the discharge of a low-inductance capacitor bank, and that this method provides high heating rates with close control over the ratio of heating time to mechanical response time.
3. An experimental technique utilizing a photoelastic coating has been developed for observing the dynamic stress distribution in a rapidly heated rod. Since this is basically an optical technique, measurements made in short time intervals are independent of environmental conditions, particularly magnetic fields, which normally restrict the use of electronic methods. Hence, this method can be used to obtain accurate measurements of the transient as well as the steady state mechanical response.
4. Experimental measurements verify the results of the analysis which was based on the uncoupled thermoelastic field equations, and also indicate that the heating rate produced by capacitor discharge through an underdamped circuit can be satisfactorily approximated by a simple exponential function. In fact, the photoelastic coating technique can be used to measure transient temperatures provided the temperature dependence of the thermal coefficient of expansion of the parent material is known.

REFERENCES

1. J. M. C. Duhamel, "Second Memoire sur les phenomenes thermo-mecaniques," Journal de l'Ecole Polytechnique, 15, 25, 1837, pp. 1-57.
2. V. I. Danilovskaya, "Thermal Stresses in an Elastic Half-Space Arising after a Sudden Heating of its Boundary," Prikl. Mat. Mekh. 14, May-June 1950, pp. 316-318, and "On a Dynamical Problem of Thermoelasticity," Prikl. Mat. Mekh., 16, May-June 1952, pp. 314-344.
3. T. Mura, "Thermal Strains and Stresses in Transient State," Proc. Sec. Jap. Congress of Appl. Mech., 1952, pp. 9-13, and "Dynamical Thermal Stresses due to Thermal Shocks," Research Reports of the Faculty of Engineering, Meiji Univ., No. 8, Pt. 2, 1956, pp. 63-73.
4. W. Nowacki, "A Dynamical Problem of Thermoelasticity," Nadb. Arch. Mech. Stos., Vol. 9, 1957, p. 325.
5. J. Ignaczak, "Thermal Displacement in an Elastic Semispace Due to a Sudden Heating of the Boundary Plane," Nadb. Arch. Mech. Stos., Vol. 9, 1957, p. 395.
6. E. Sternberg and J. G. Chakravorty, "On Inertia Effects in a Transient Thermoelastic Problem," Tech. Rep. 2, Contract Nonr-562(25), Brown Univ., May, 1958.
7. B. A. Boley, "Thermally Induced Vibrations of Beams," J. Aero. Sci. 23, 2, 179-181, 1956.
8. B. A. Boley and A. D. Barber, "Dynamic Response of Beams and Plates to Rapid Heating, J. Appl. Mech. 24, 3, 413-416, Sept. 1957.

9. T. B. Kammash, S. A. Murch and P. M. Naghdi, "The Elastic-Plastic Cylinder Subjected to Radially Distributed Heat Source, Lateral Pressure and Axial Force with Application to Nuclear Reactor Fuel Elements," J. Mech. Phys. of Solids, 8, 1-25, 1960.
10. N. A. Weil, "On Thermal Stresses in Cylinders Subjected to γ -ray Heating," J. Eng. for Ind., Trans. ASME, pp. 35-41, Feb. 1962.
11. D. Burgreen, "Thermoelastic Dynamics of Rods, Thin Shells, and Solid Spheres," Nuclear Sci. and Eng., 12, 203-217, 1962.
12. H. Jeffreys, "The Thermodynamics of an Elastic Solid," Proc. Cambridge Phil. Soc., 26, 101-106, 1930.
13. M. A. Biot, "Thermoelasticity and Irreversible Thermodynamics," J. Appl. Phys. 27, 3, 240-253, 1955.
14. H. Deresiewicz, "Plane Waves in a Thermoelastic Solid," J. Acoust. Soc. Am., 29, 2, 204-209, 1957.
15. M. Lessen, "The Motion of a Thermoelastic Solid," Quart. Appl. Math., XV, 1, 105-108, 1957.
16. P. Chadwick and I. N. Sneddon, "Plane Waves in an Elastic Solid Conducting Heat," J. Mech. Phys. Solids, 6, 223-230, 1958.
17. F. J. Lockett, "Effect of Thermal Properties of a Solid on the Velocity of Rayleigh Waves," J. Mech. Phys. Solids, 7, 71-75, 1958.
18. P. Chadwick, "Thermoelasticity. The Dynamical Theory," Prog. in Solid Mechanics, I, 265-328, 1960.
19. B. A. Boley and J. H. Weiner, Theory of Thermal Stresses, John Wiley and Sons, New York, 1960, Chap. 1 and 2.
20. J. E. Michaels, "Thermal Impact--The Mechanical Response of Solids to Extreme Electromagnetic Radiation," Planetary and Space Science, Vol. 7, Pergamon Press, New York, July 1961.

21. U. S. Lindholm, "Effects of Thermal Impact on a Thin Spherical Cap,"
Exper. Mech., Proc. of SESA, Vol. 2, No. 10, Oct. 1962, pp. 303-306.
22. A. E. H. Love, A Treatise on the Mathematical Theory of Elasticity,
4th Ed., Dover Publications, New York, 1944, pp. 287-291.
23. L. Pochhammer, J. Math (Crelle's j.) 81, 1876, p. 324.
24. C. Chree, Quart. J. Math., 21, 1886.
25. R. M. Davies, Trans. Roy. Soc., London, A240, 1948, p. 375.
26. I. S. Sokolnikoff, Mathematical Theory of Elasticity, 2nd Ed., McGraw-Hill, New York, 1956, p. 80.
27. Ibid., p. 359.
28. Ibid., p. 22.
29. H. Jeffreys, Cartesian Tensors, Cambridge Univ. Press, 1931, p. 81.
30. Boley and Weiner, Op. Cit., p. 44.
31. Chadwick, Op. Cit., pp. 276-279.
32. A. Erdelyi, W. Magnus, F. Oberhettinger and F. Tricomi, Tables of Integral Transforms, C.I.T. Bateman Manuscript Project, McGraw-Hill, New York, 1950.
33. C. R. Wylie, Jr., Advanced Engineering Mathematics, McGraw-Hill, New York, 1951, p. 188.
34. M. Mesnager, "Sur la Determination Optique des Tensions Interieures dans les Solides A Trois Dimensions," Comptes Rendus, Paris 190, 1930, p. 1249.
35. J. D'Agostino, D. C. Drucker, C. K. Liu, and C. Mylonas, "An Analysis of Plastic Behavior of Metals with Bonded Birefringent Plastic," Proc. of the Soc. for Experimental Stress Analysis XII (2), 1955, pp. 115-122.
36. F. Zandman and M. R. Wood, "Photostress," Product Eng., Sept. 1956, pp. 167-178.

37. F. Zandman, "Concepts of the Photoelastic Stress Gage," *Experimental Mechanics*, 2, 8, 225-233, Aug. 1962.
38. F. Zandman, S. S. Redner, and E. I. Riegner, "Reinforcing Effects of Birefringent Coatings," *Experimental Mechanics*, 2, 2, 55-64, Feb. 1962.
39. W. Goldsmith, "Dynamic Photoelasticity," Colloquium on Experimental Techniques in Shock and Vibration, Appl. Mech. Div. ASME, Nov. 1962, pp. 25-54.
40. J. Duffy, "Effects of the Thickness of Birefringent Coatings," *Proc. SESA*, 18, 1, 74-82, 1962.
41. S. Timoshenko, Vibration Problems in Engineering, D. von Nostrand Co., 3rd Ed., 1955, p. 303.

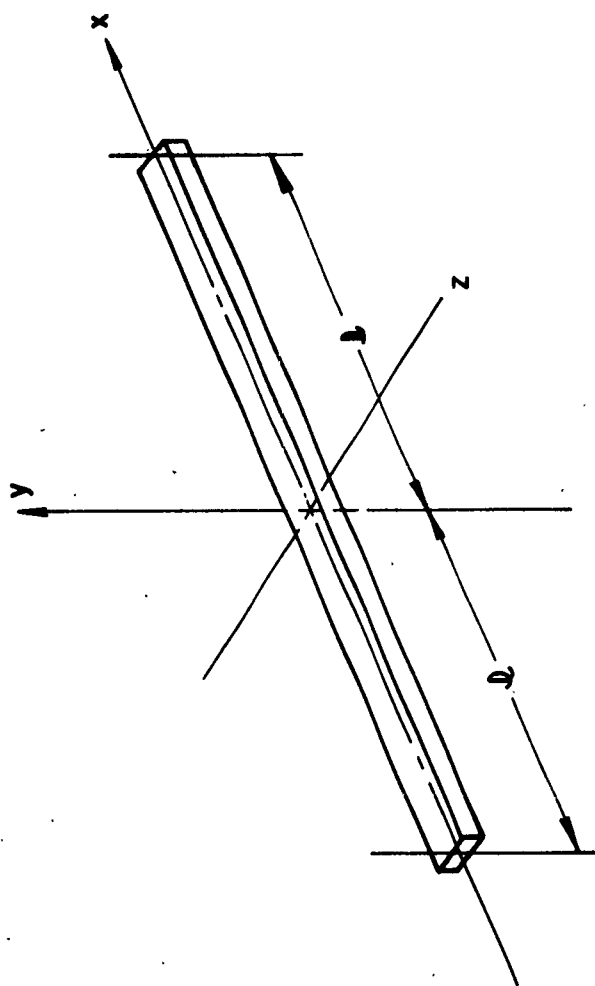


FIG. 1. SPECIMEN GEOMETRY

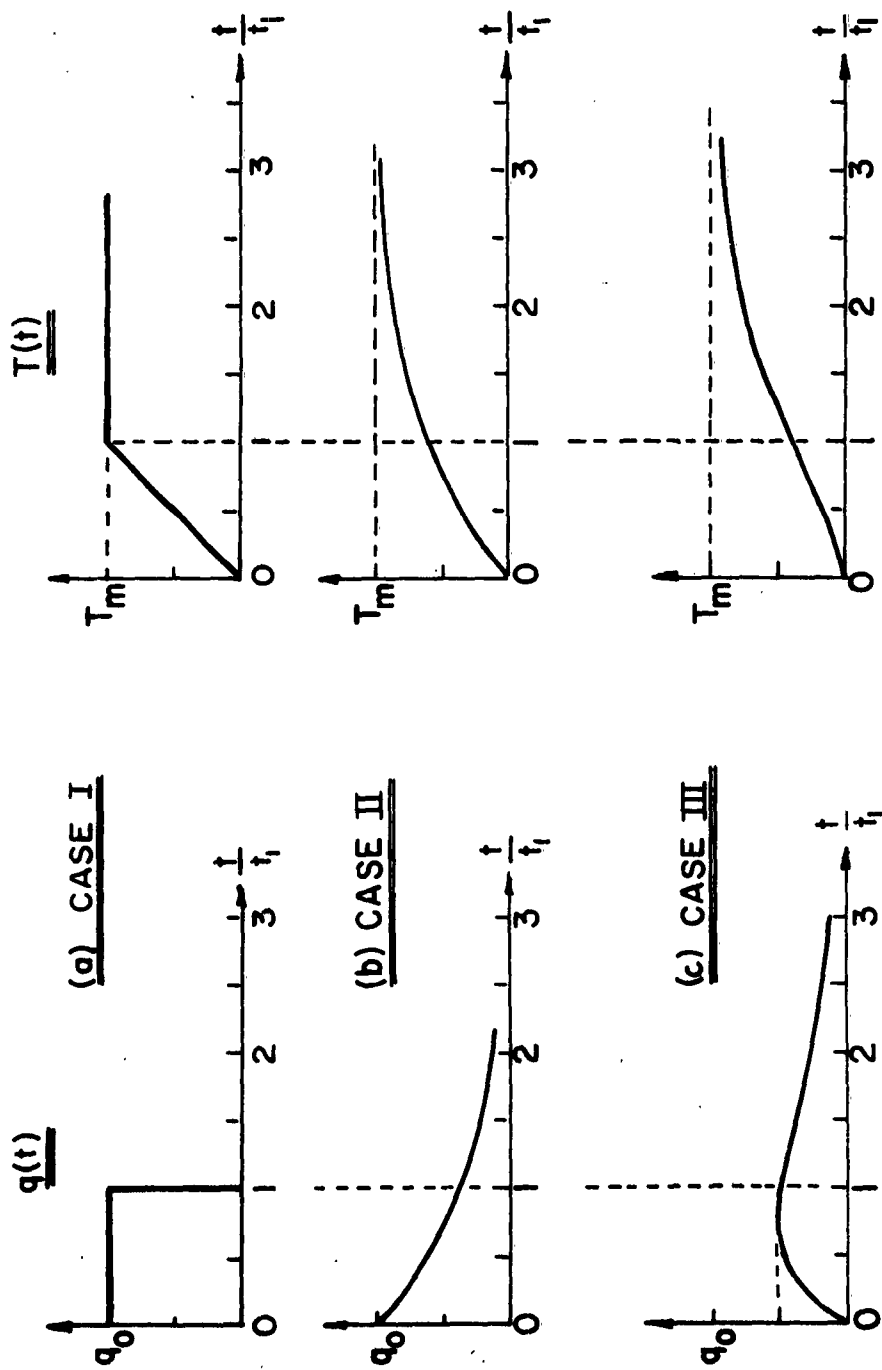


FIG. 2. SELECTED TYPES OF HEATING

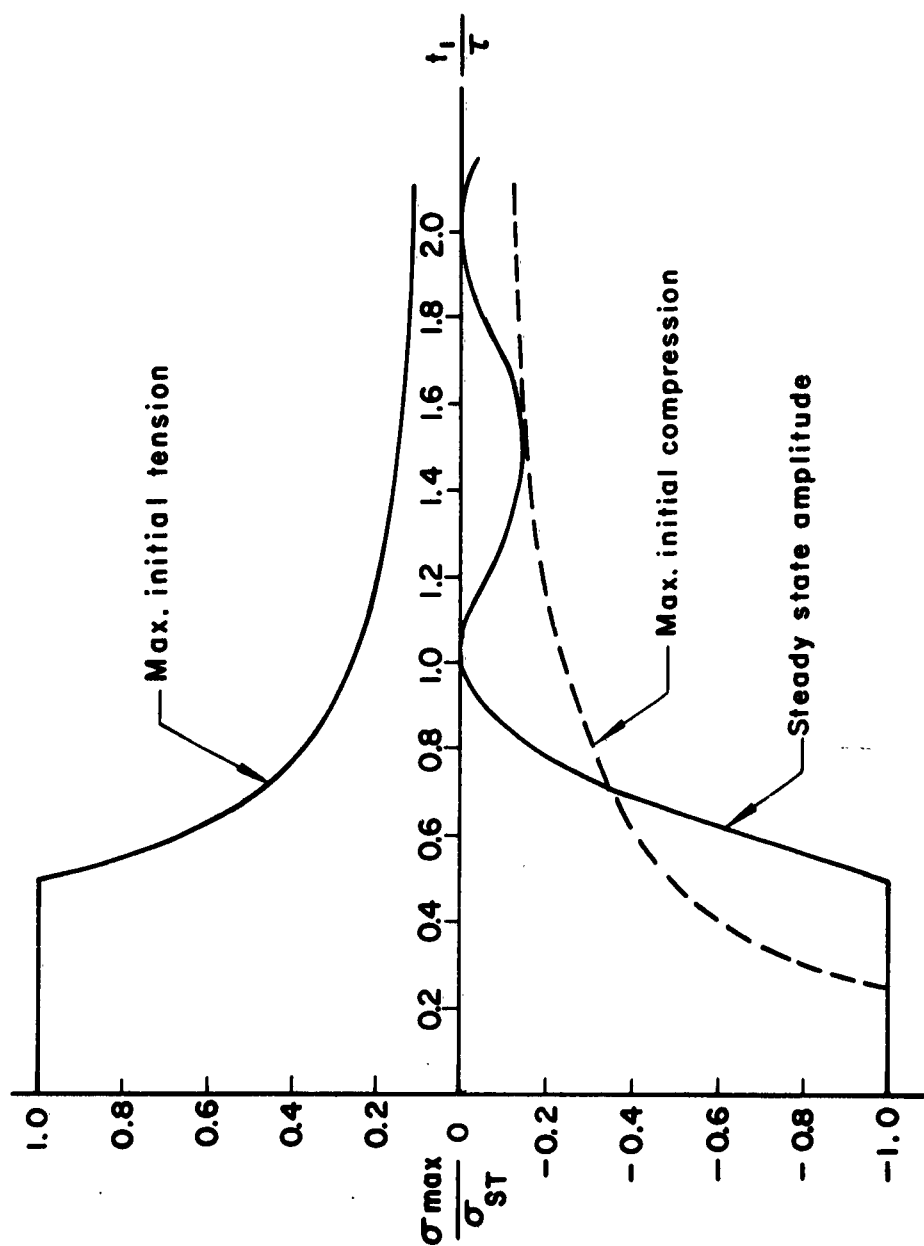


FIG. 3. VARIATION OF STRESS AMPLITUDES WITH RATIO OF HEATING PERIOD TO FUNDAMENTAL PERIOD

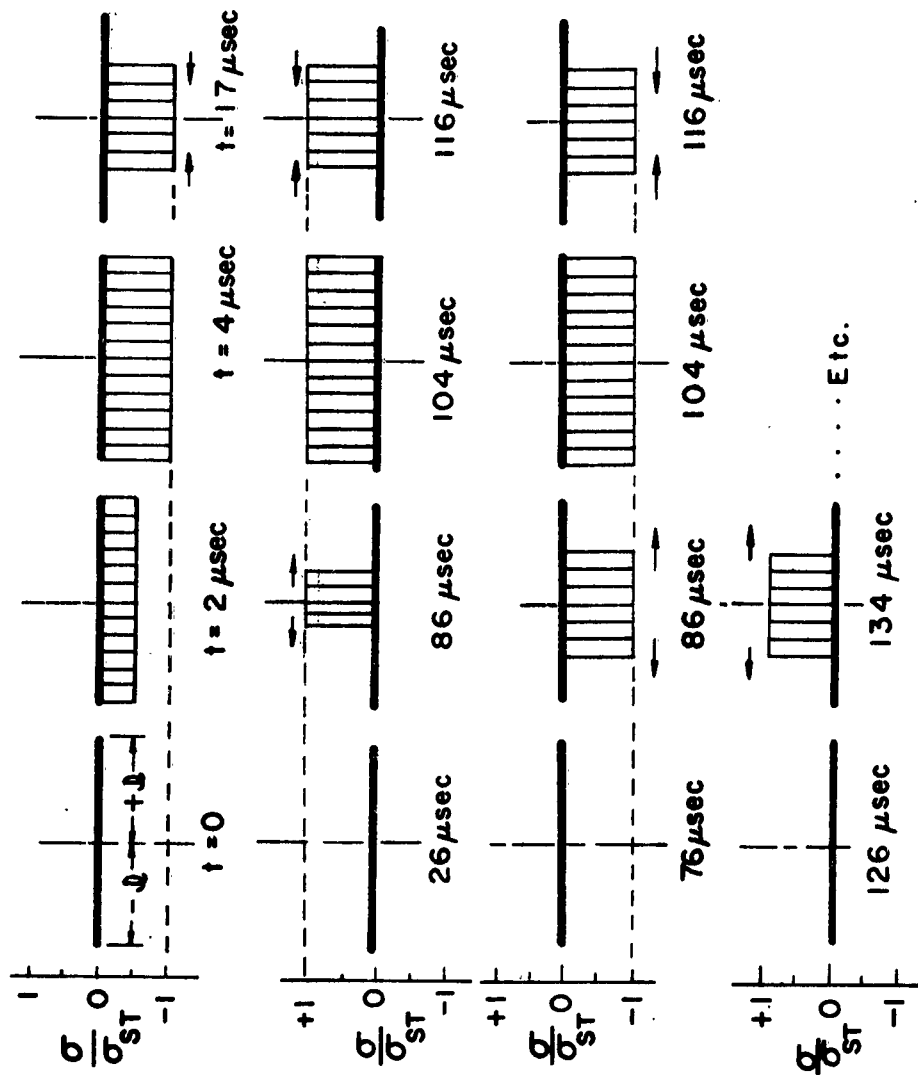


FIG. 4. STRESS DISTRIBUTION SEQUENCE IN A RAPIDLY HEATED ROD (CASE I)

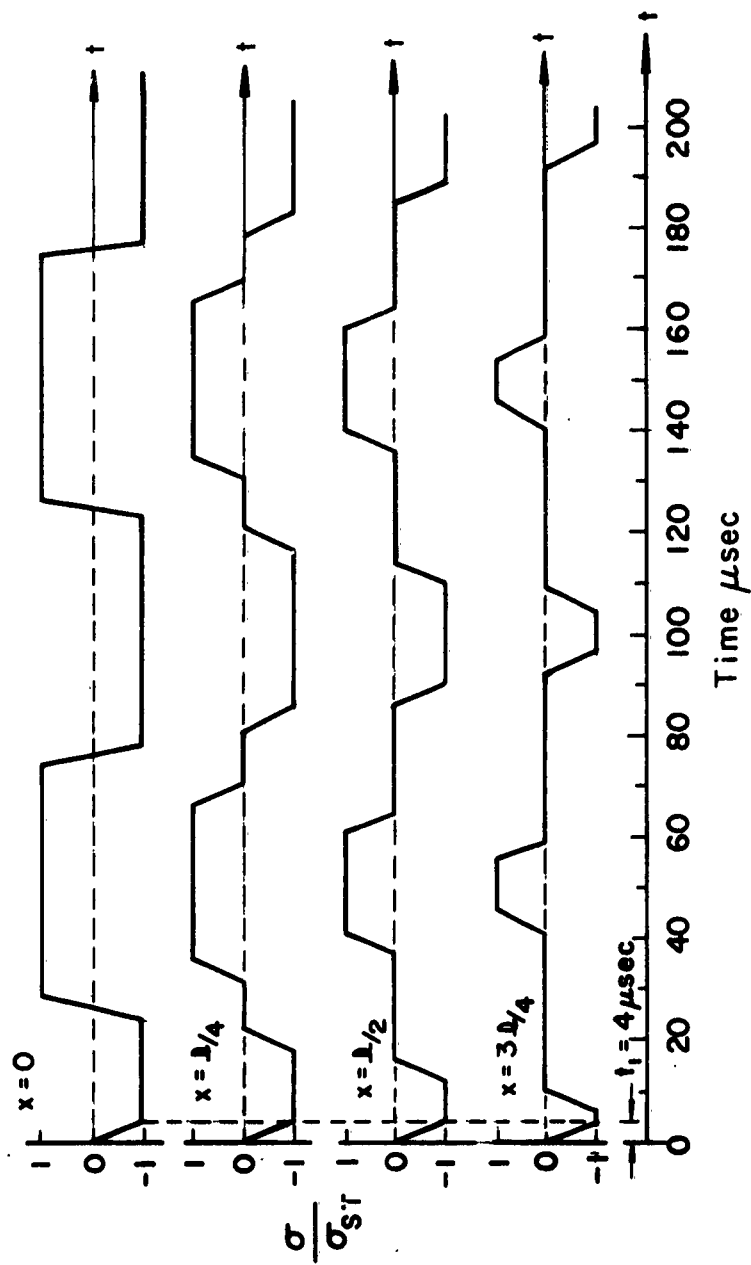


FIG. 5. STRESS HISTORIES IN A RAPIDLY HEATED ROD (CASE II)

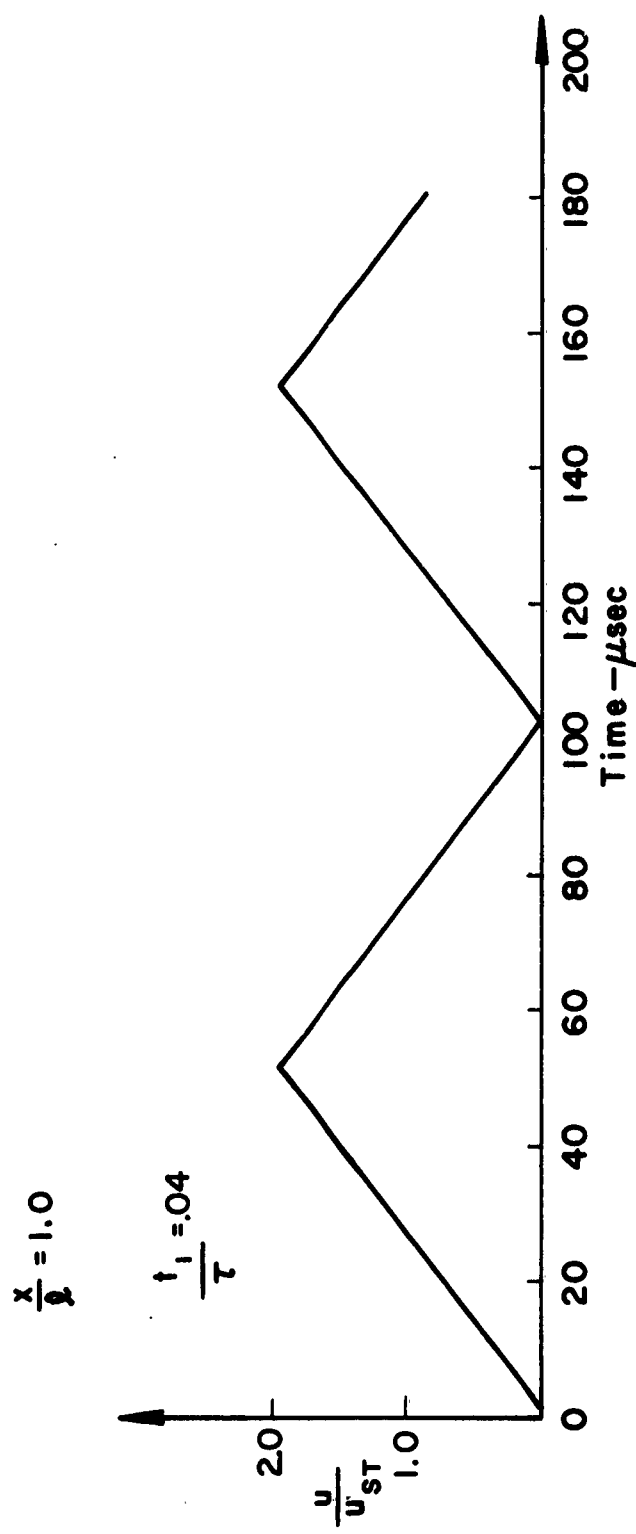


FIG. 6. DISPLACEMENT OF THE END OF A RAPIDLY HEATED ROD (CASE I)

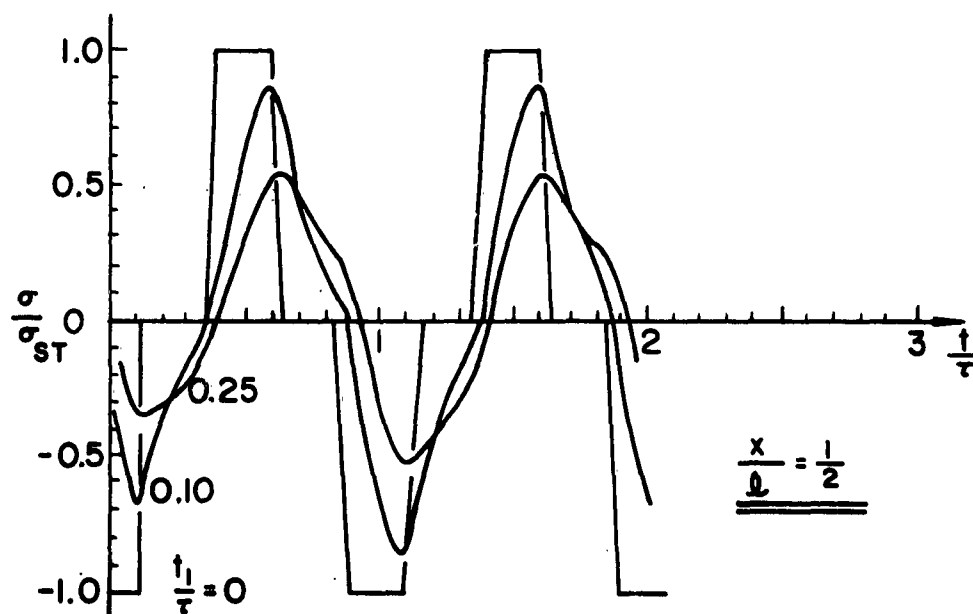
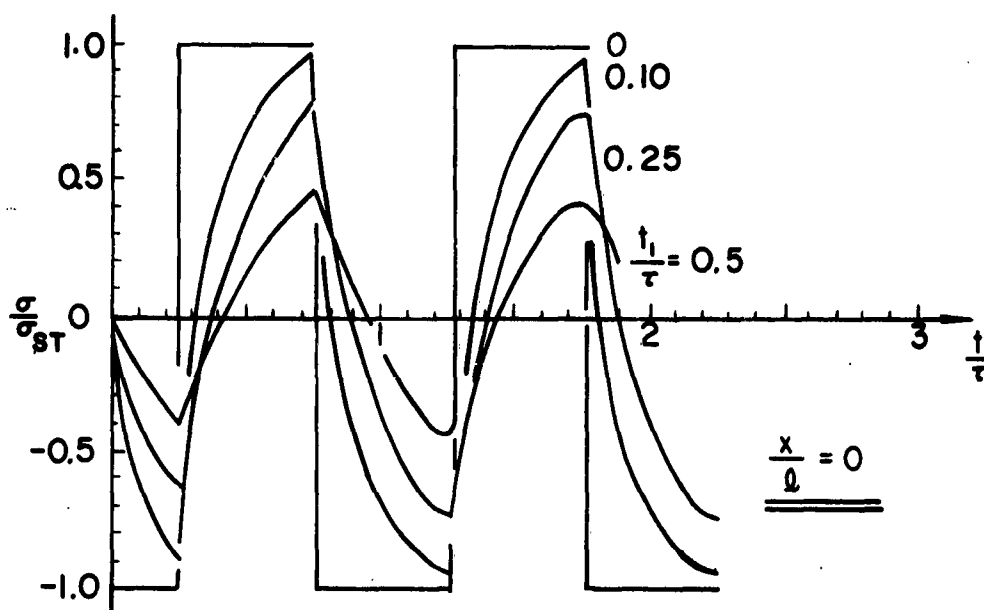


FIG. 7. STRESS HISTORIES IN A RAPIDLY HEATED ROD (CASE II)

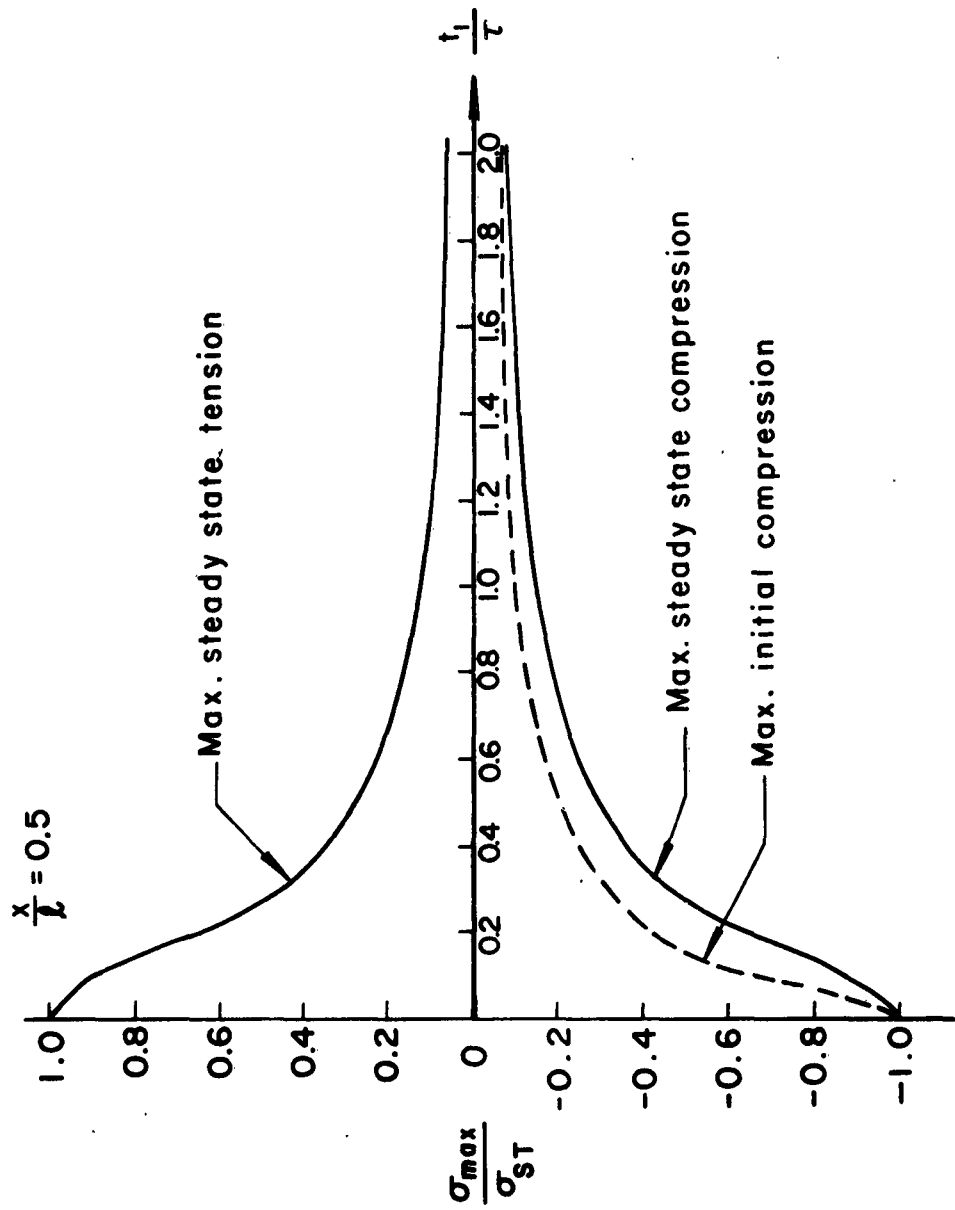


FIG. 8. VARIATION OF STRESS AMPLITUDES WITH RATIO OF HEATING PERIOD TO FUNDAMENTAL PERIOD (CASE II)

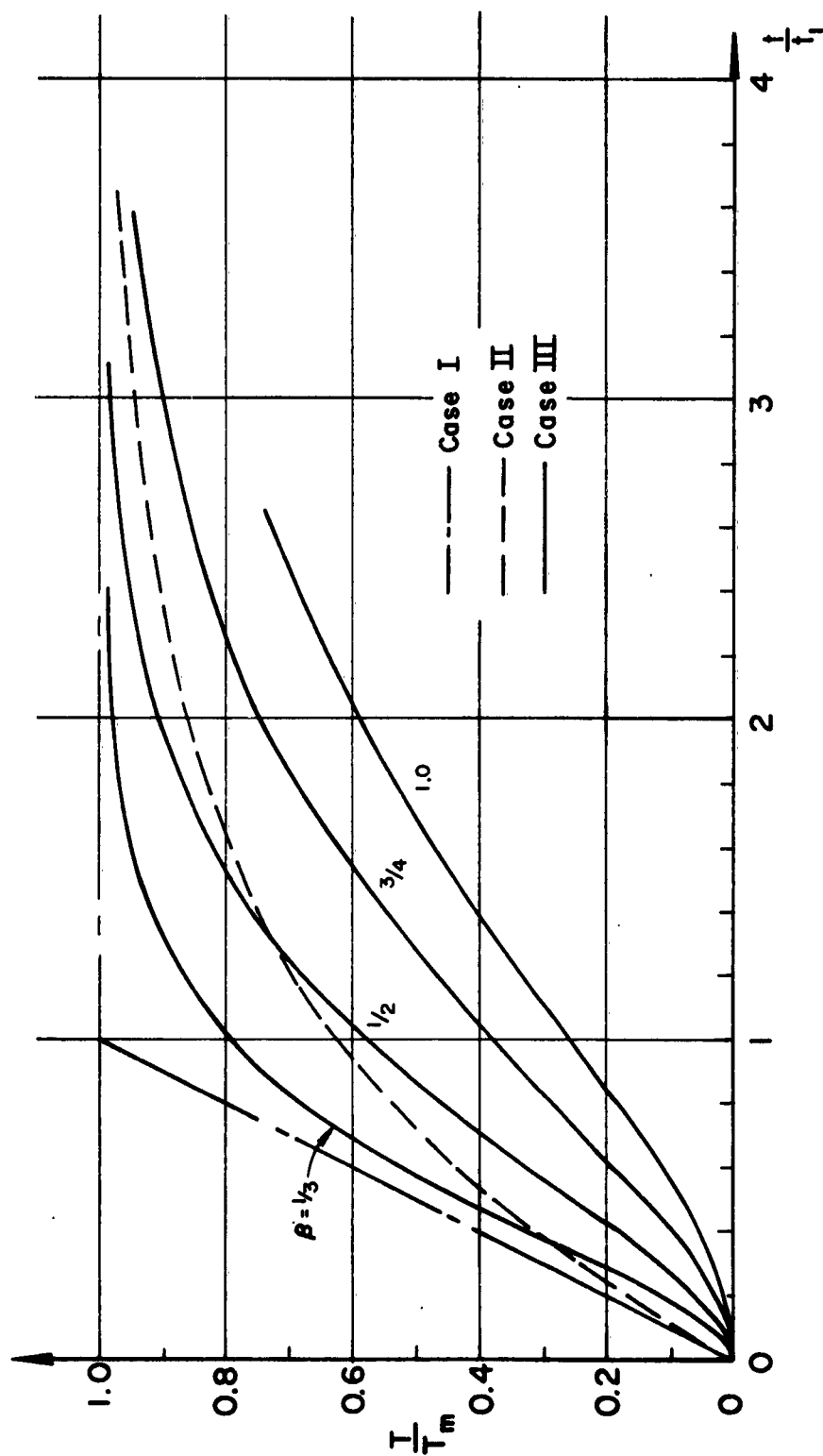


FIG. 9. COMPARISON OF INDUCED TEMPERATURE VARIATIONS

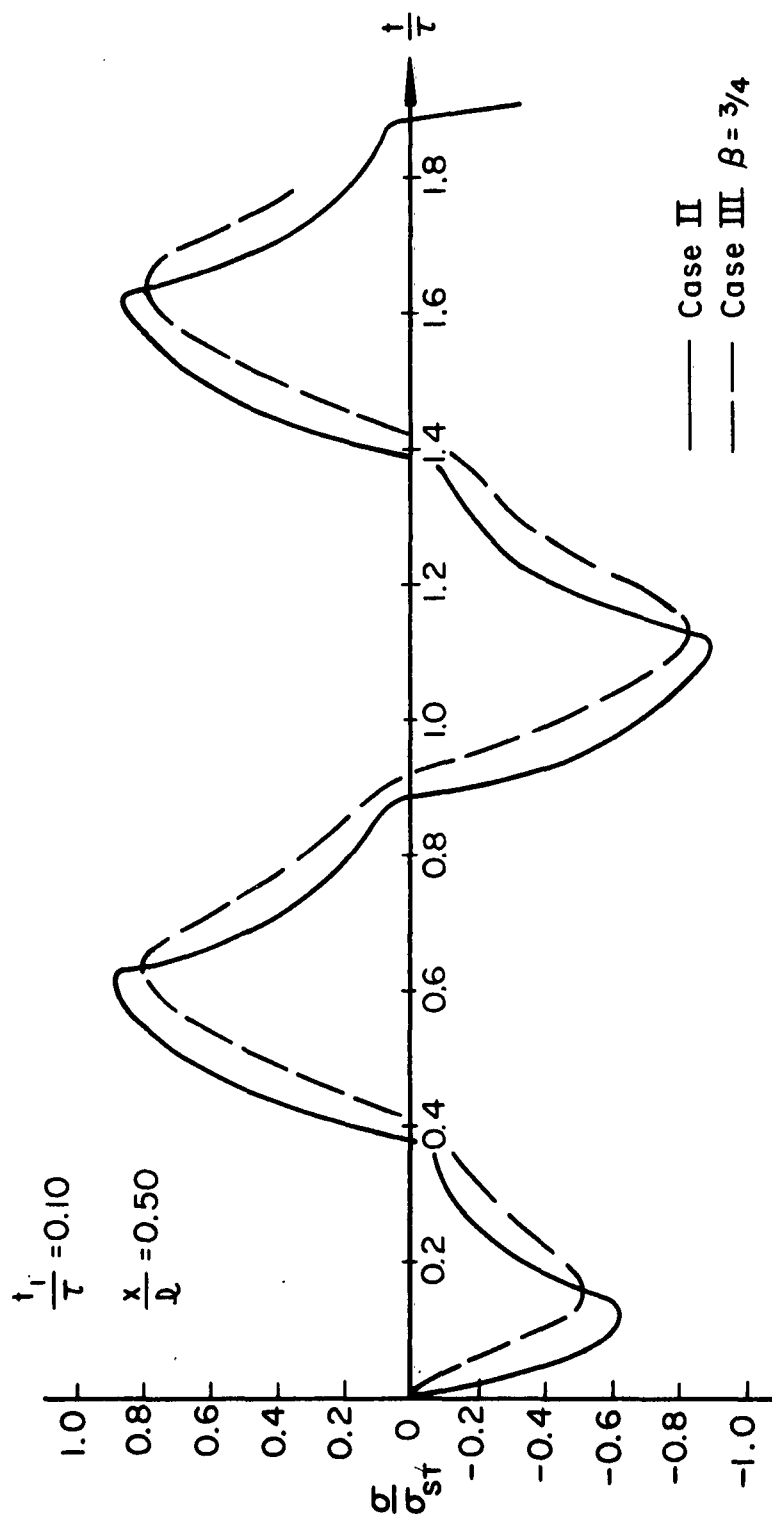


FIG. 10. COMPARISON OF STRESS HISTORIES PRODUCED BY CASE II AND CASE III HEATING

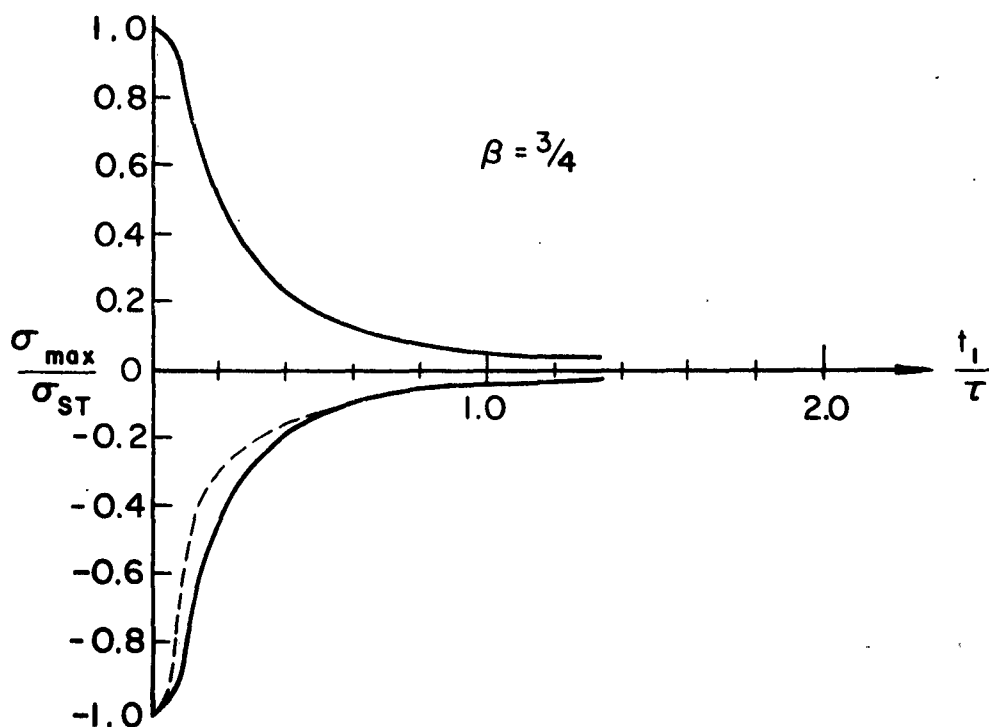
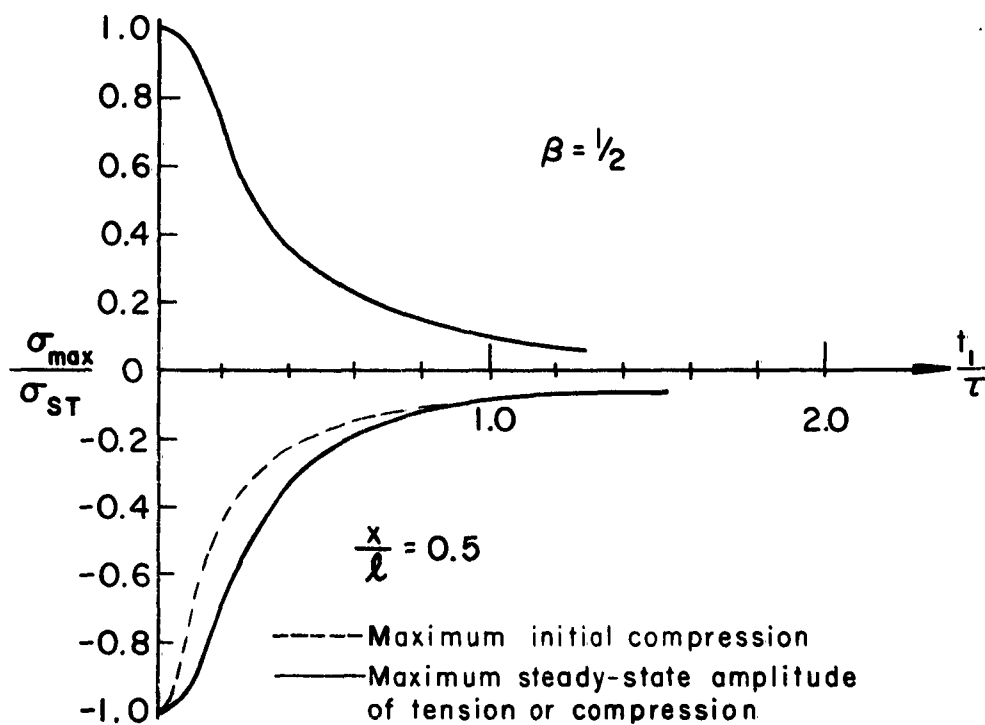


FIG. 11. VARIATION OF STRESS AMPLITUDES WITH RATIO OF EXCITING PERIOD TO FUNDAMENTAL PERIOD (CASE III)

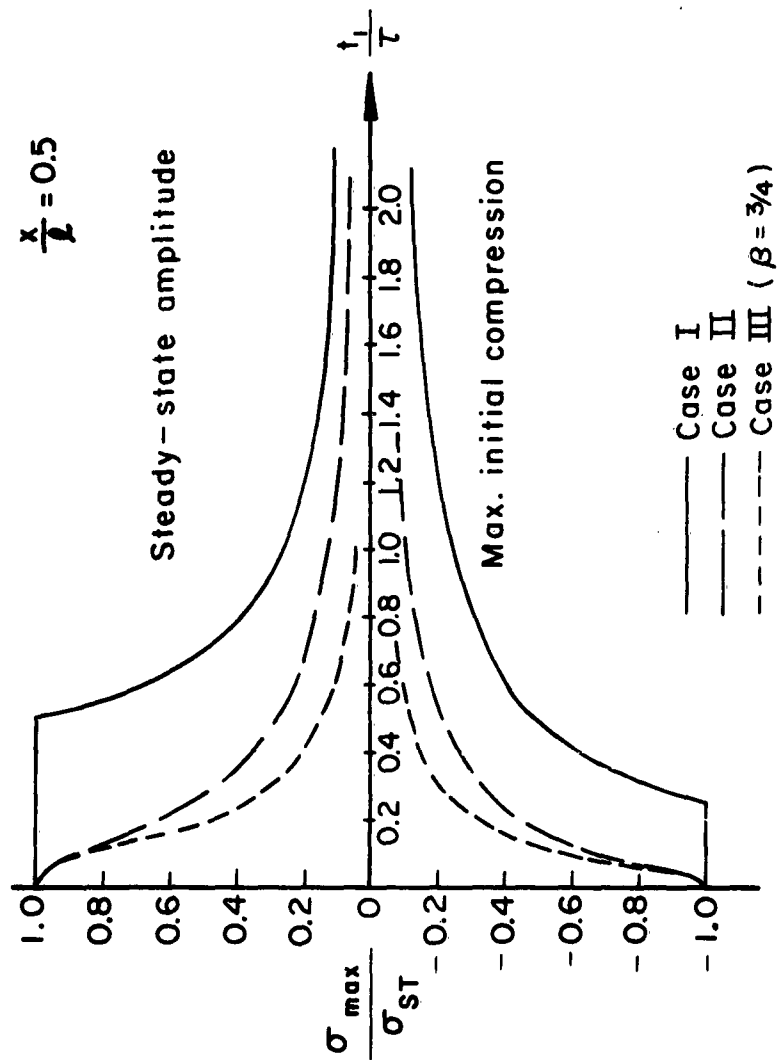


FIG. 12. THE EFFECT OF TYPE OF HEATING ON STRESS AMPLITUDE VARIATION

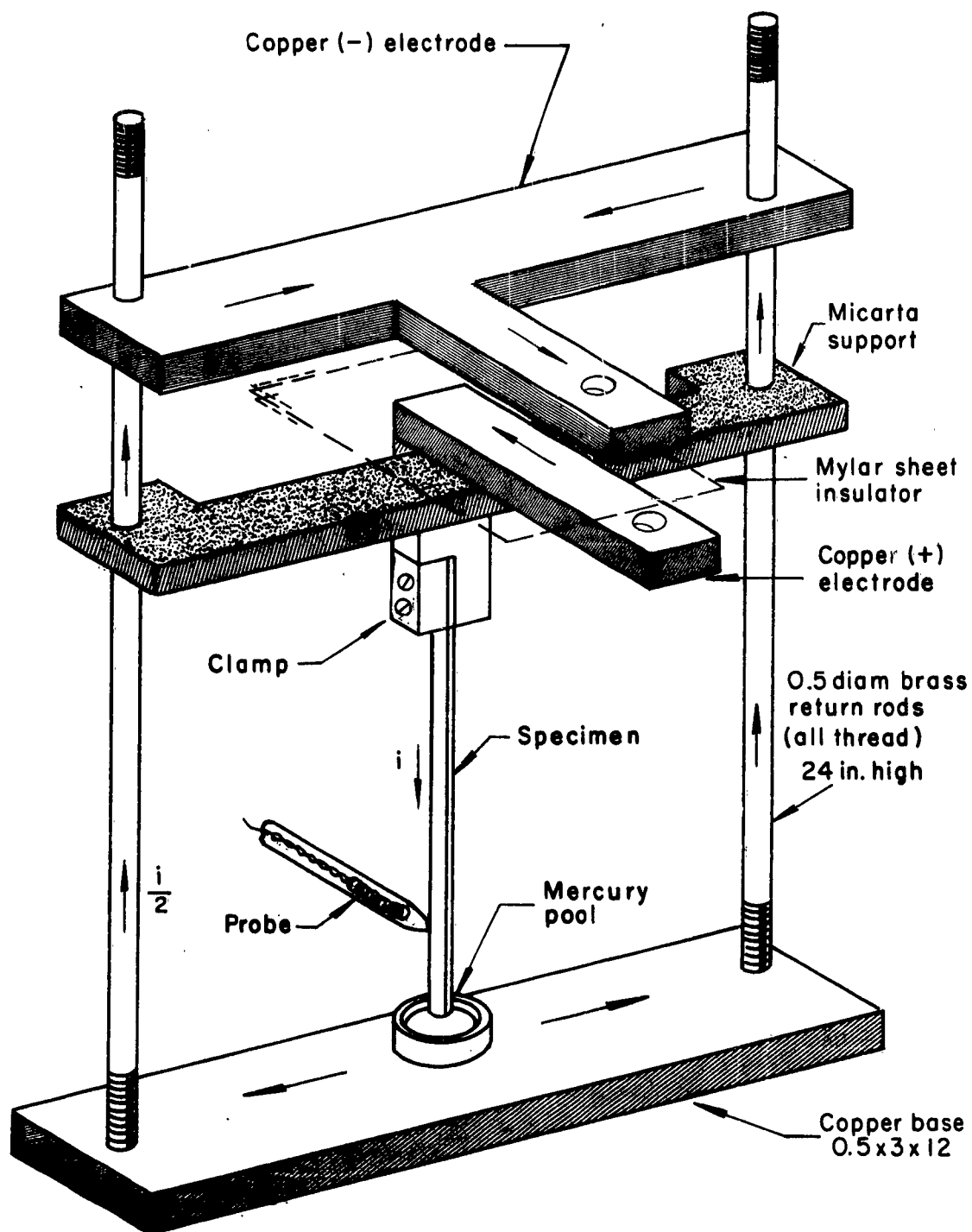


FIG. 13. HEATING JIG

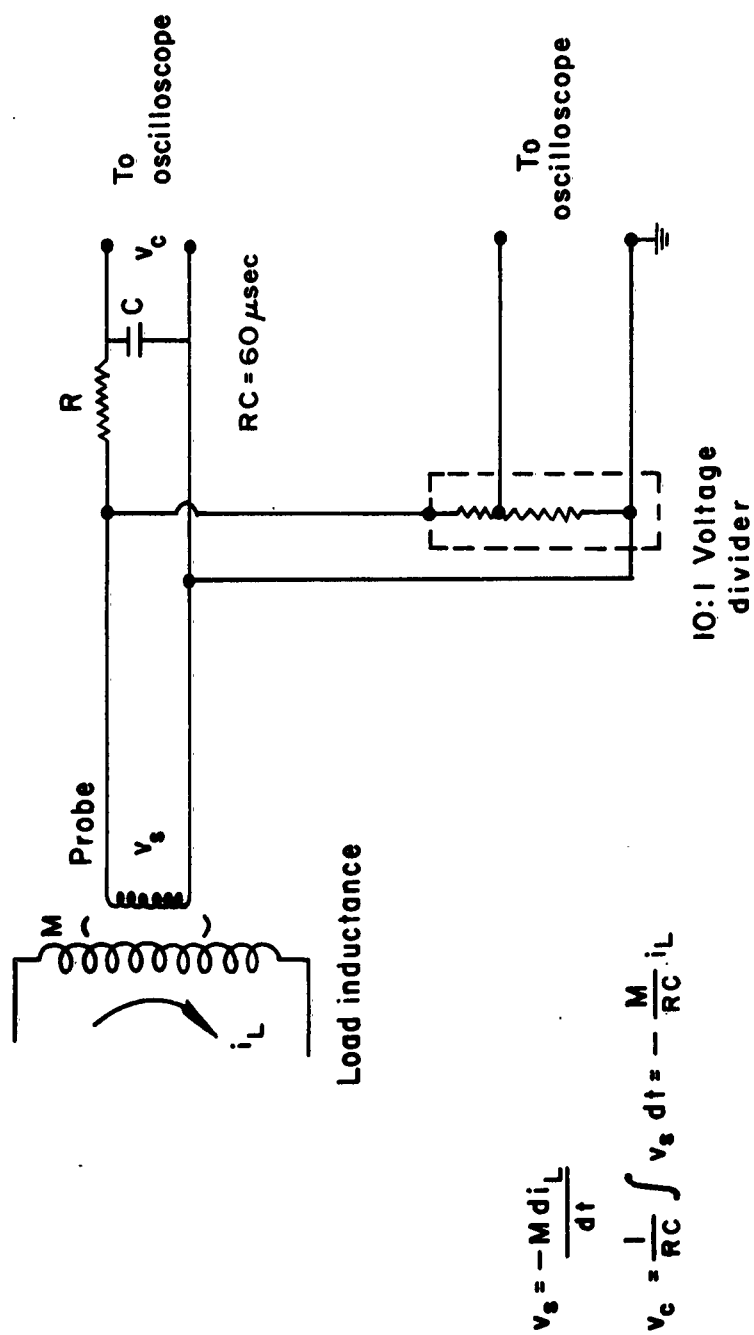


FIG. 14. INDUCTIVE PROBE CIRCUITRY

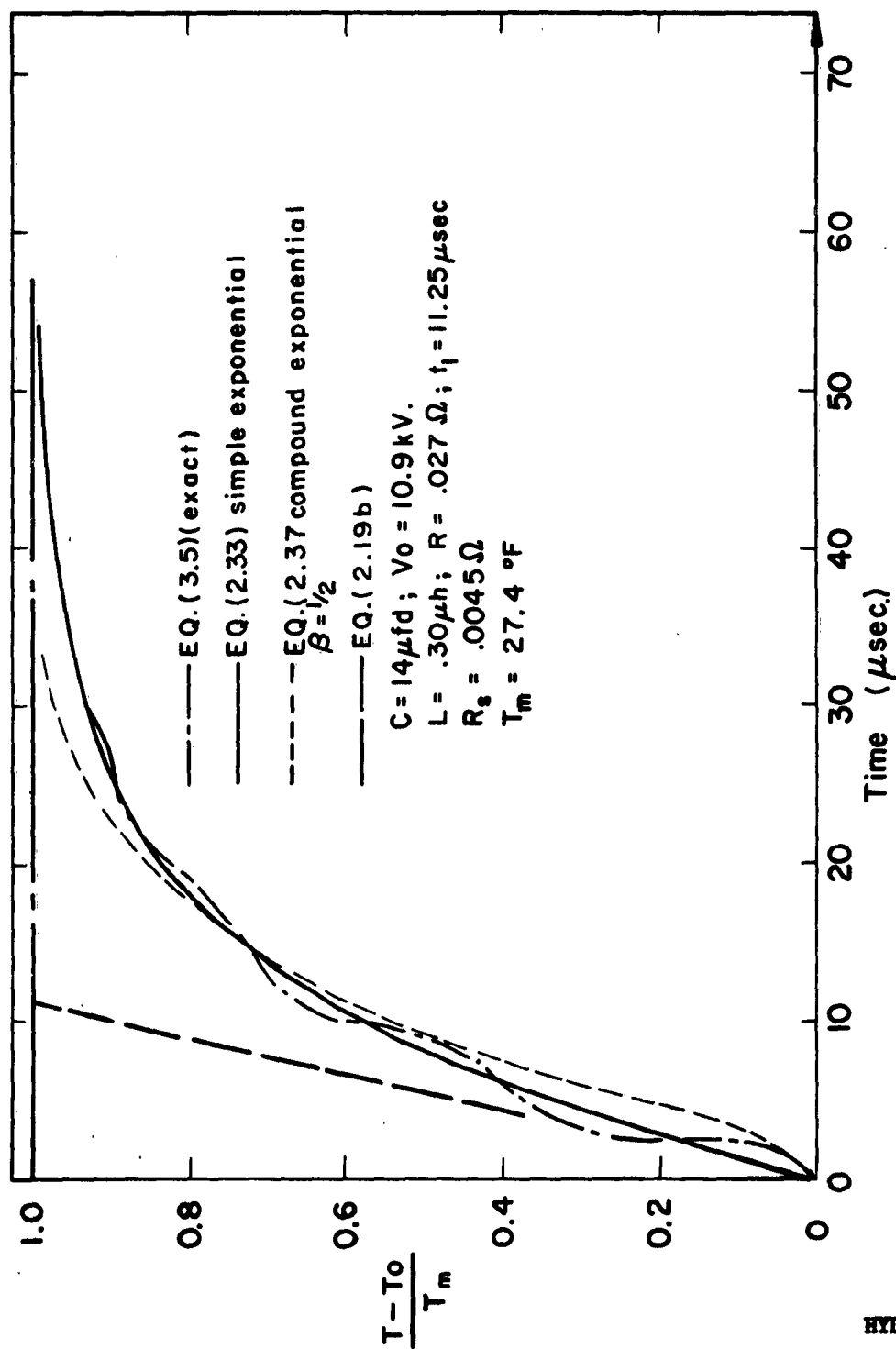


FIG. 15. COMPARISON OF EXACT TEMPERATURE VARIATION WITH CASE II

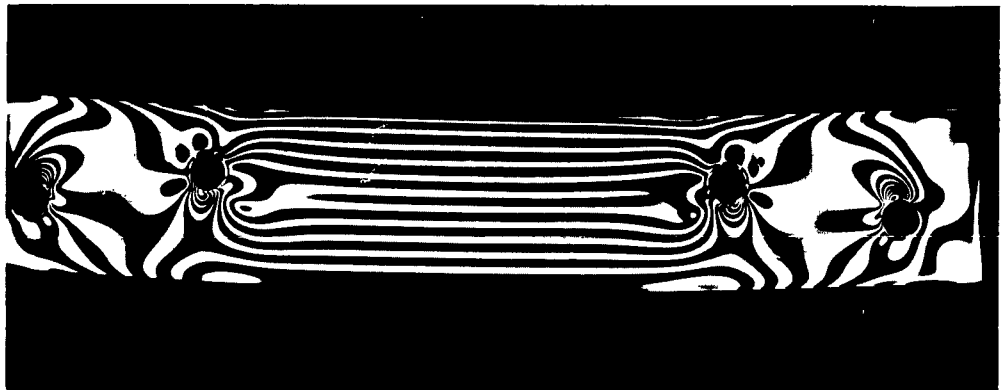


FIG. 16. FRINGE PATTERN IN PRESTRESSED BEAM

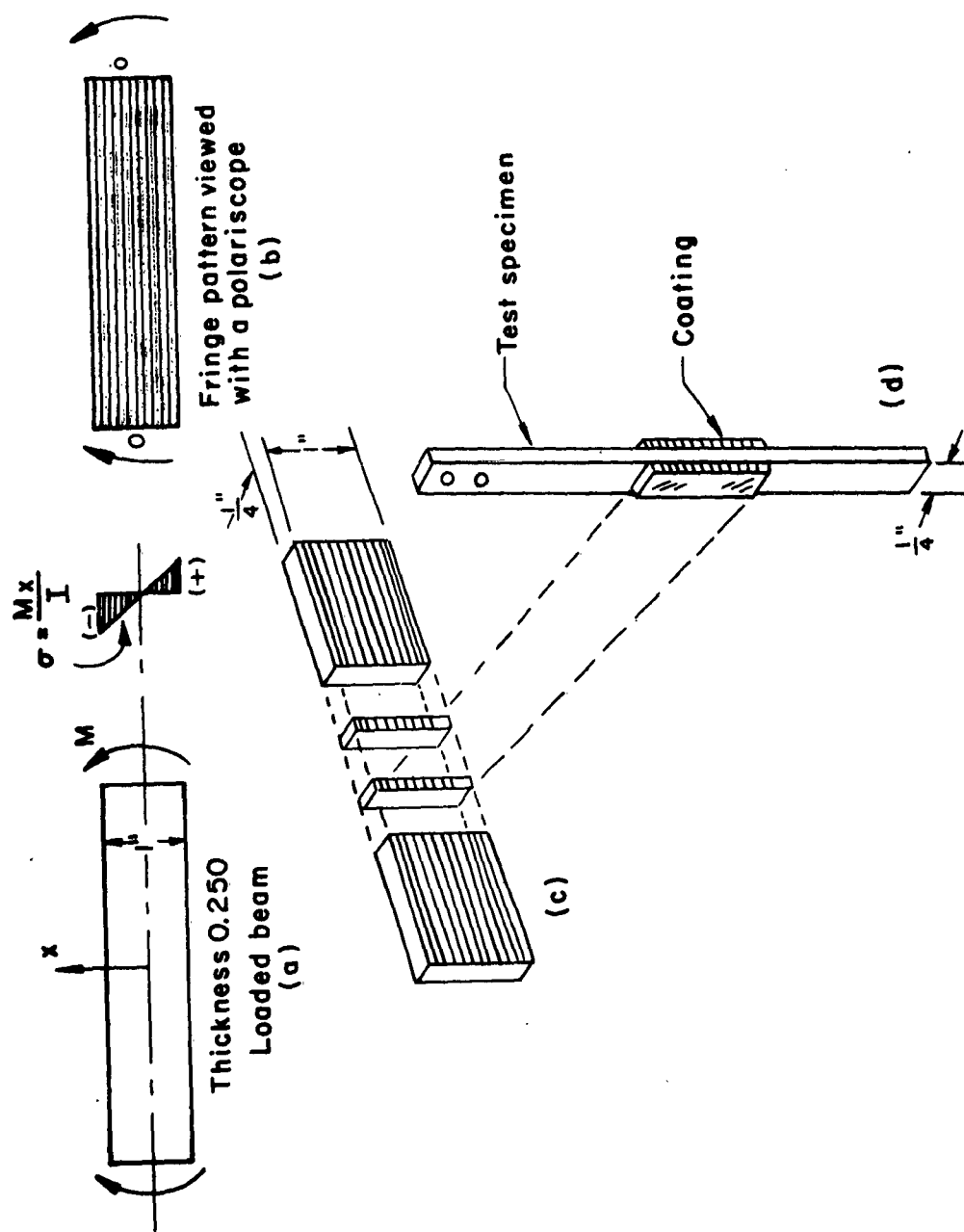


FIG. 17. SPECIMEN PREPARATION

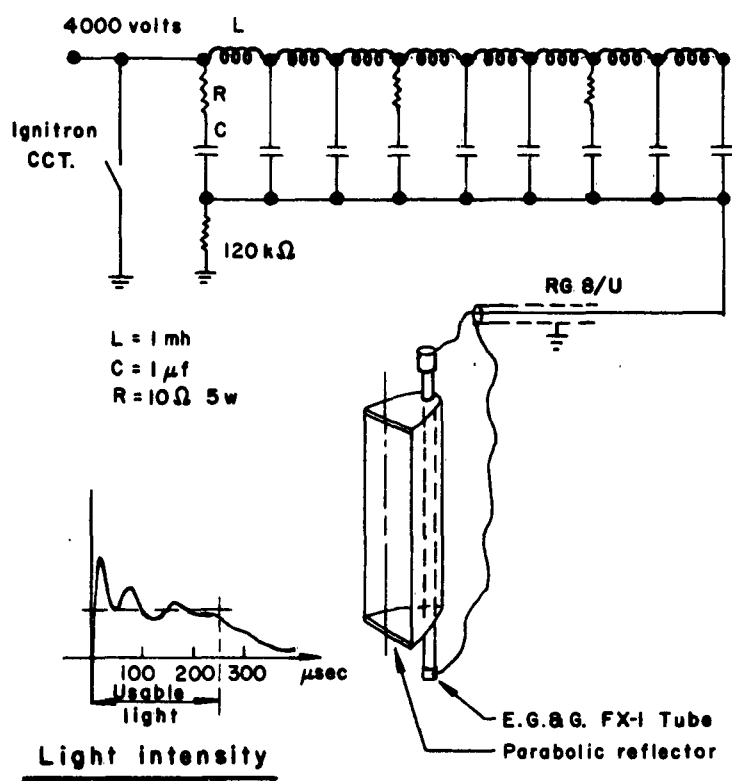


FIG. 18. LIGHT SOURCE CIRCUITRY

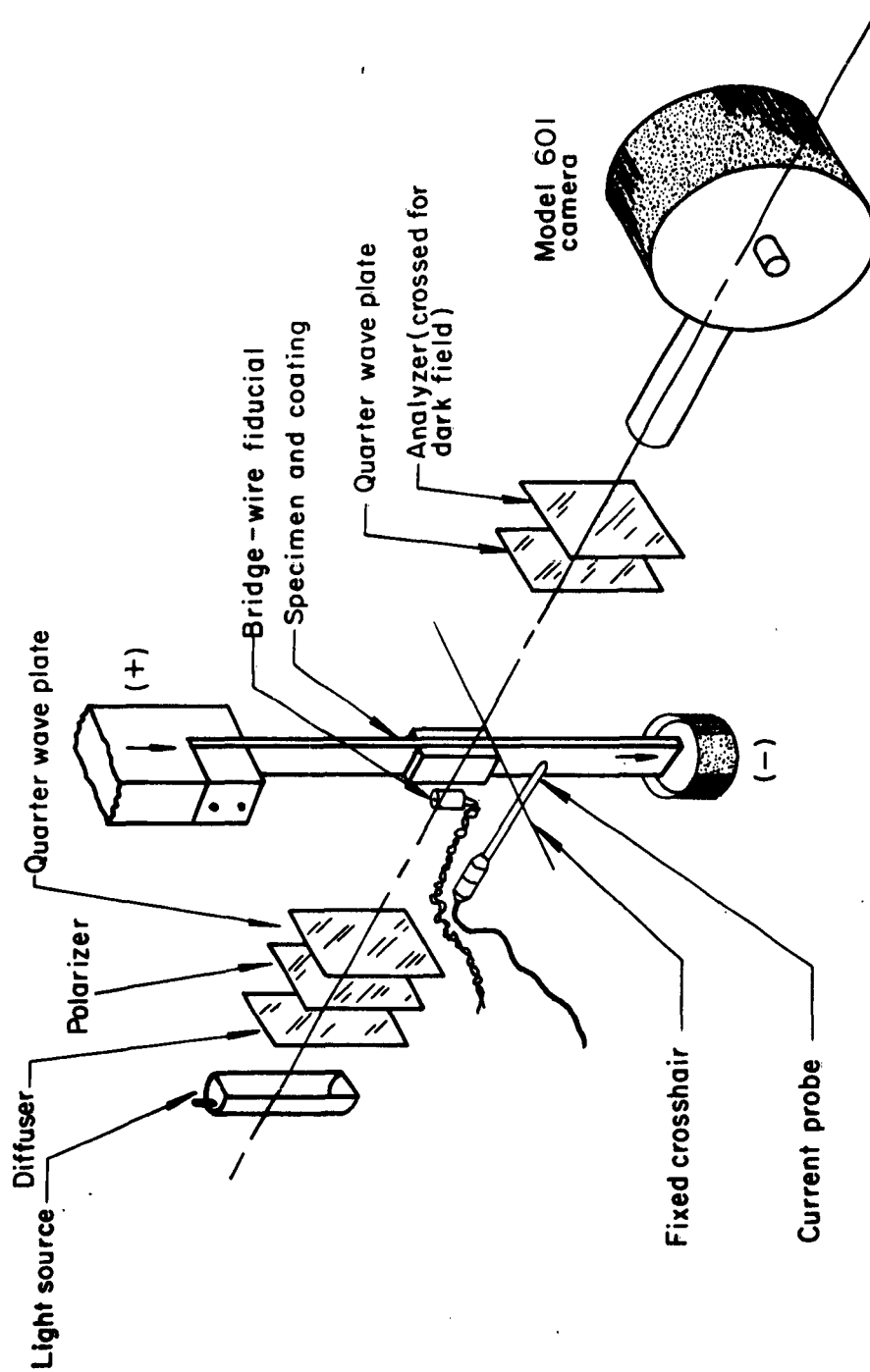


FIG. 19. EXPERIMENTAL APPARATUS

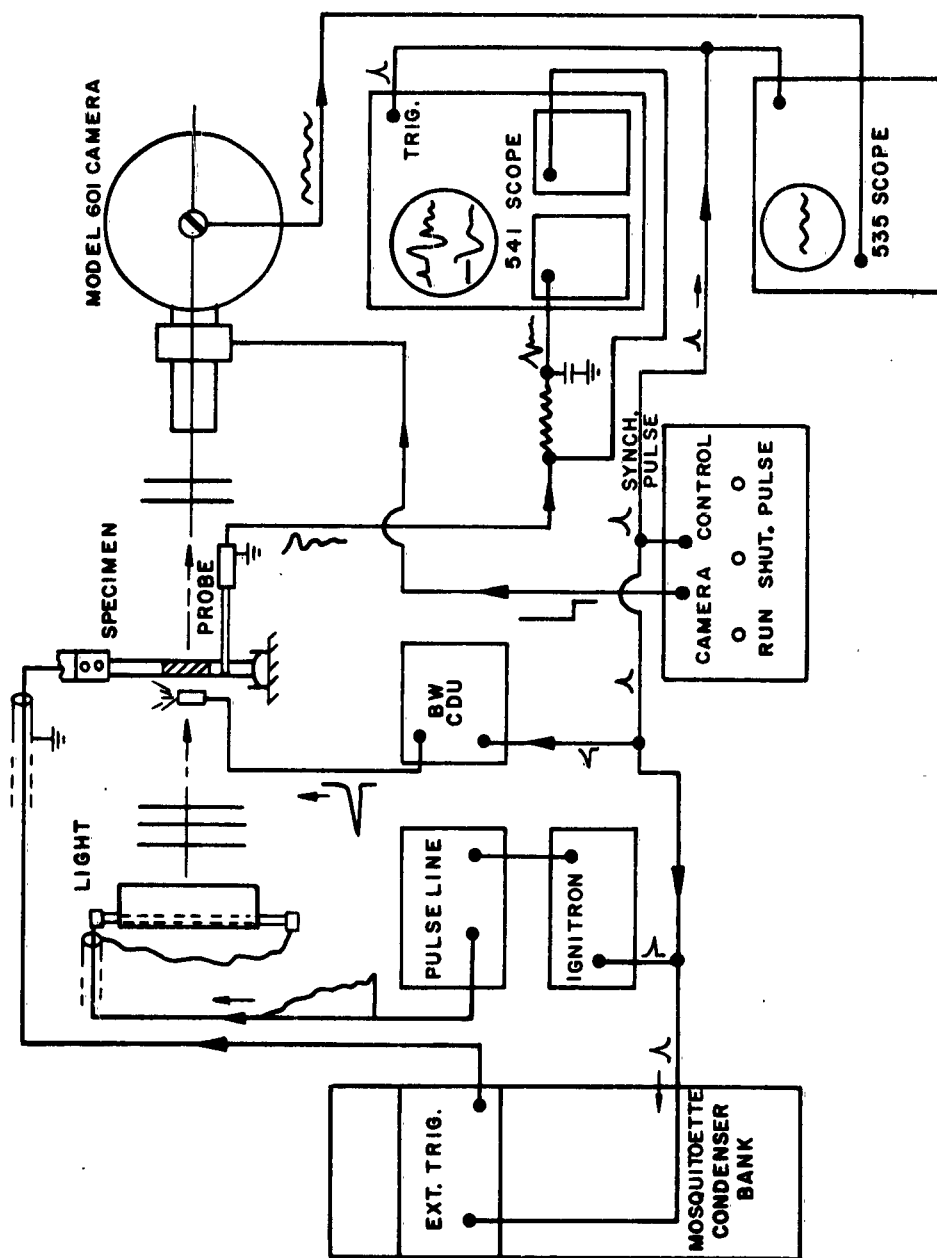


FIG. 20. BLOCK DIAGRAM

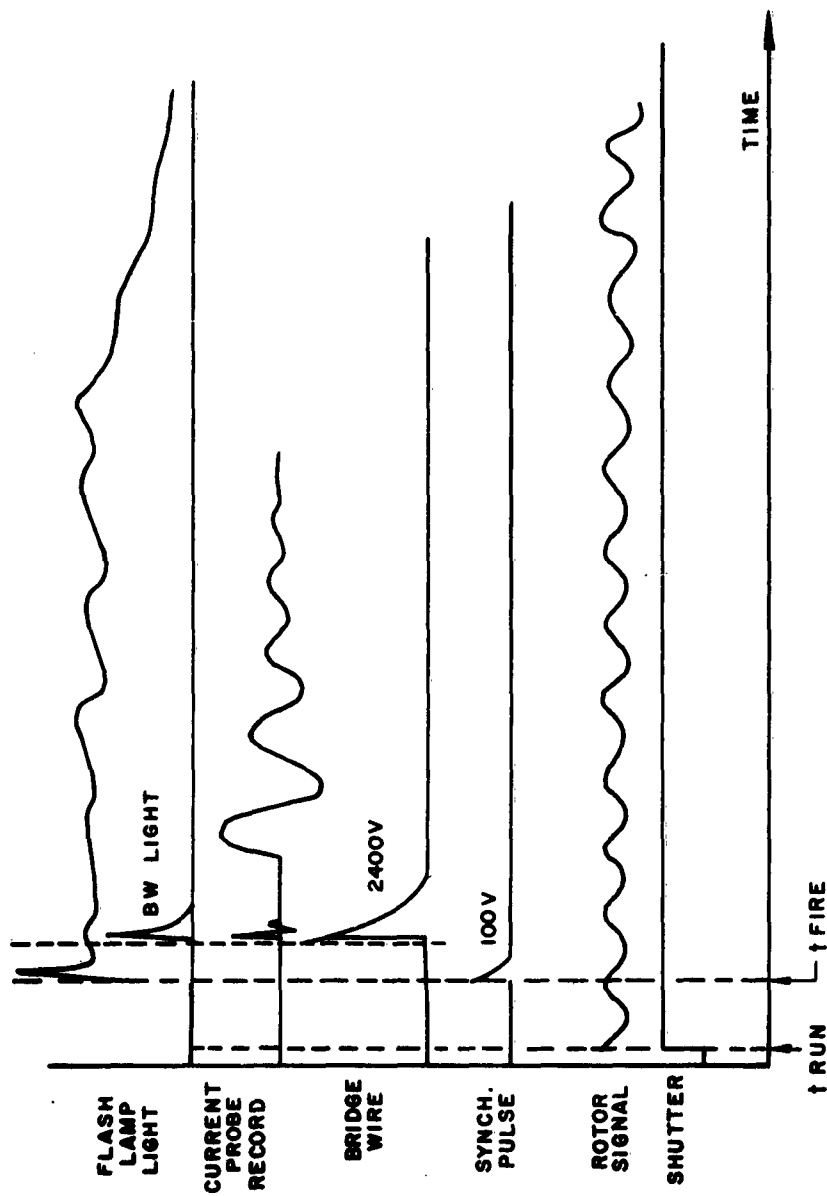
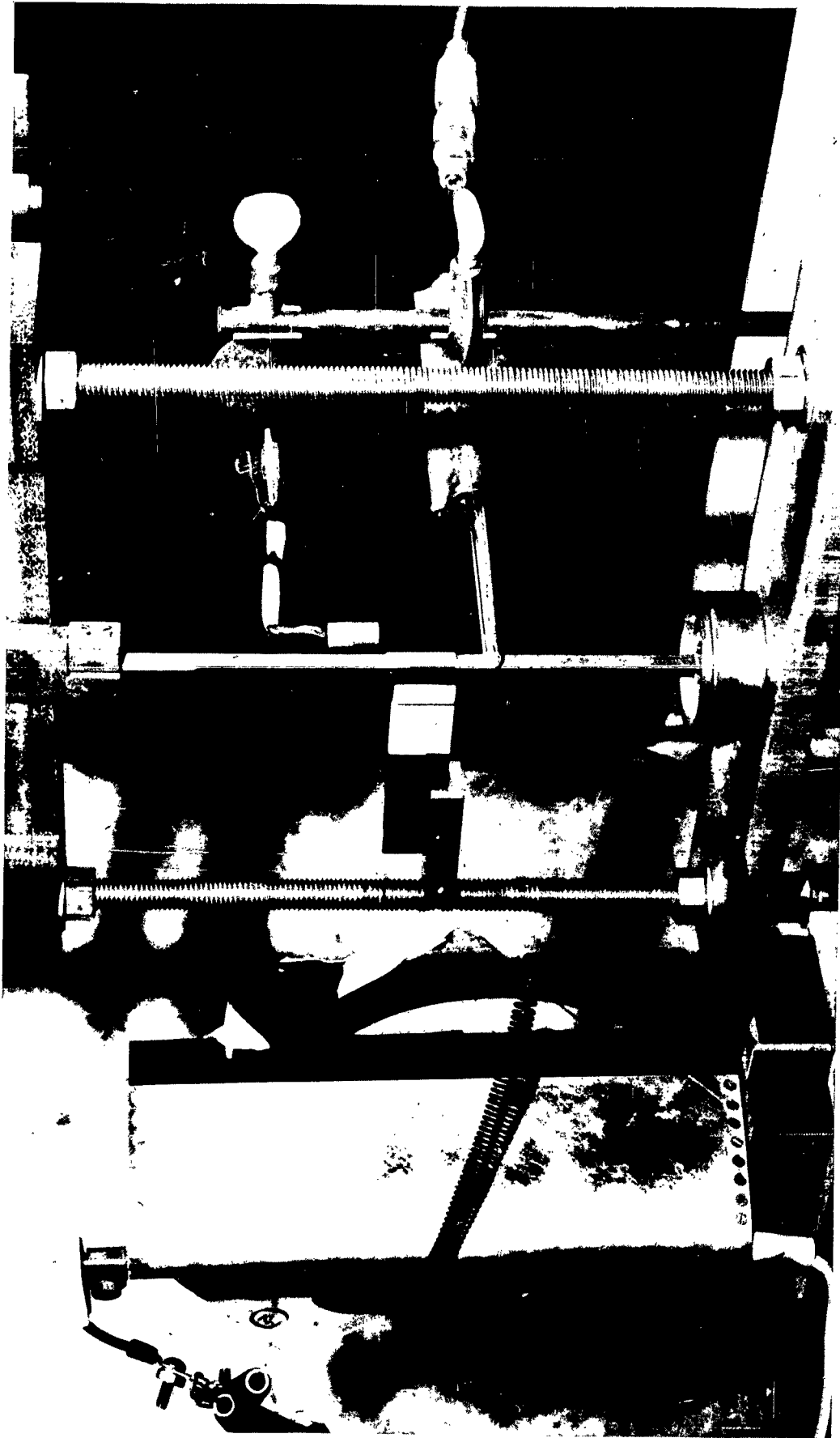


FIG. 21. FUNCTION DIAGRAM OF SEQUENCE OF EVENTS



82.

FIG. 22. HEATING JIG ASSEMBLY



FIG. 23. SPECIMENS

Run 1. 304 st. steel bar (fixed-free)
 0.125 x 0.250 x 12.0
 $T_m = 35^\circ F$ $\sigma_{ST} = 9400 \text{ psi}$

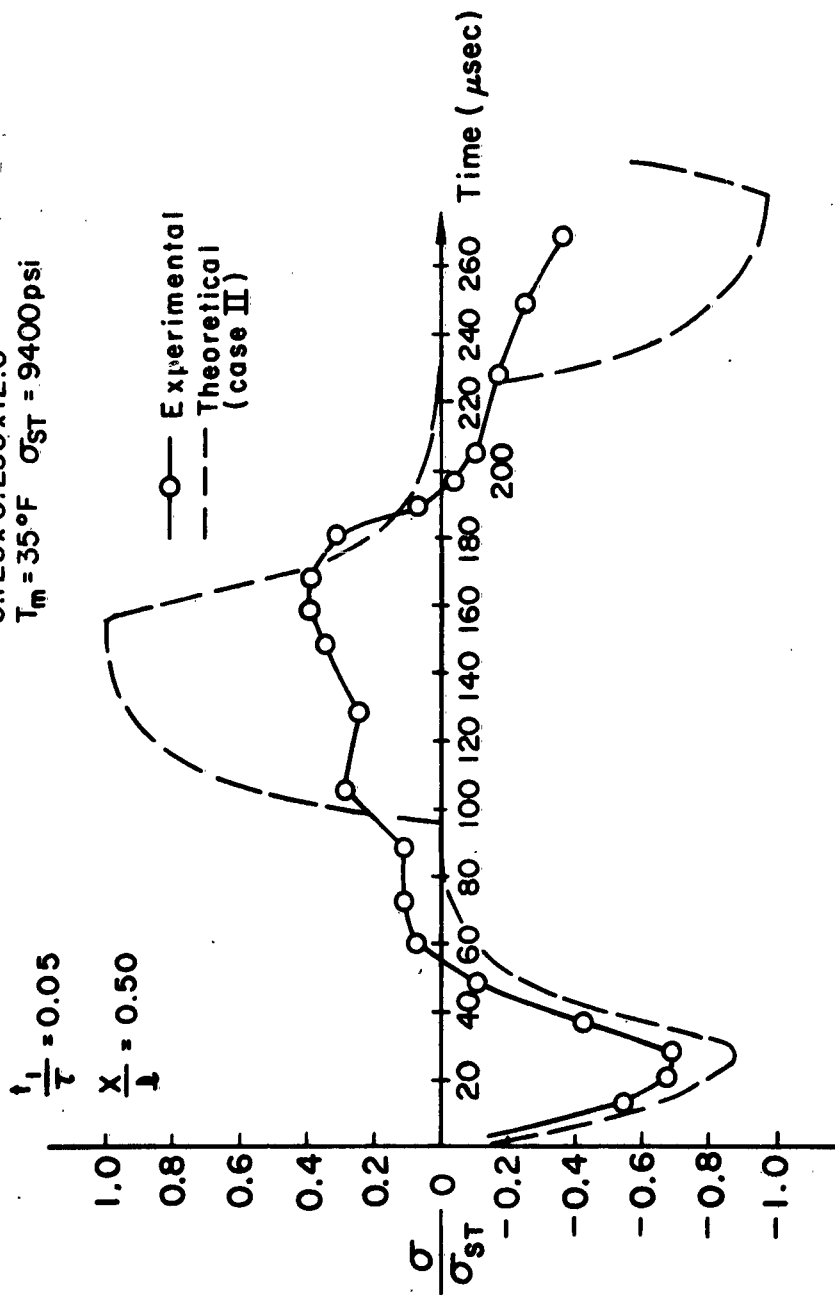


FIG. 24. STRESS HISTORY AT A POINT

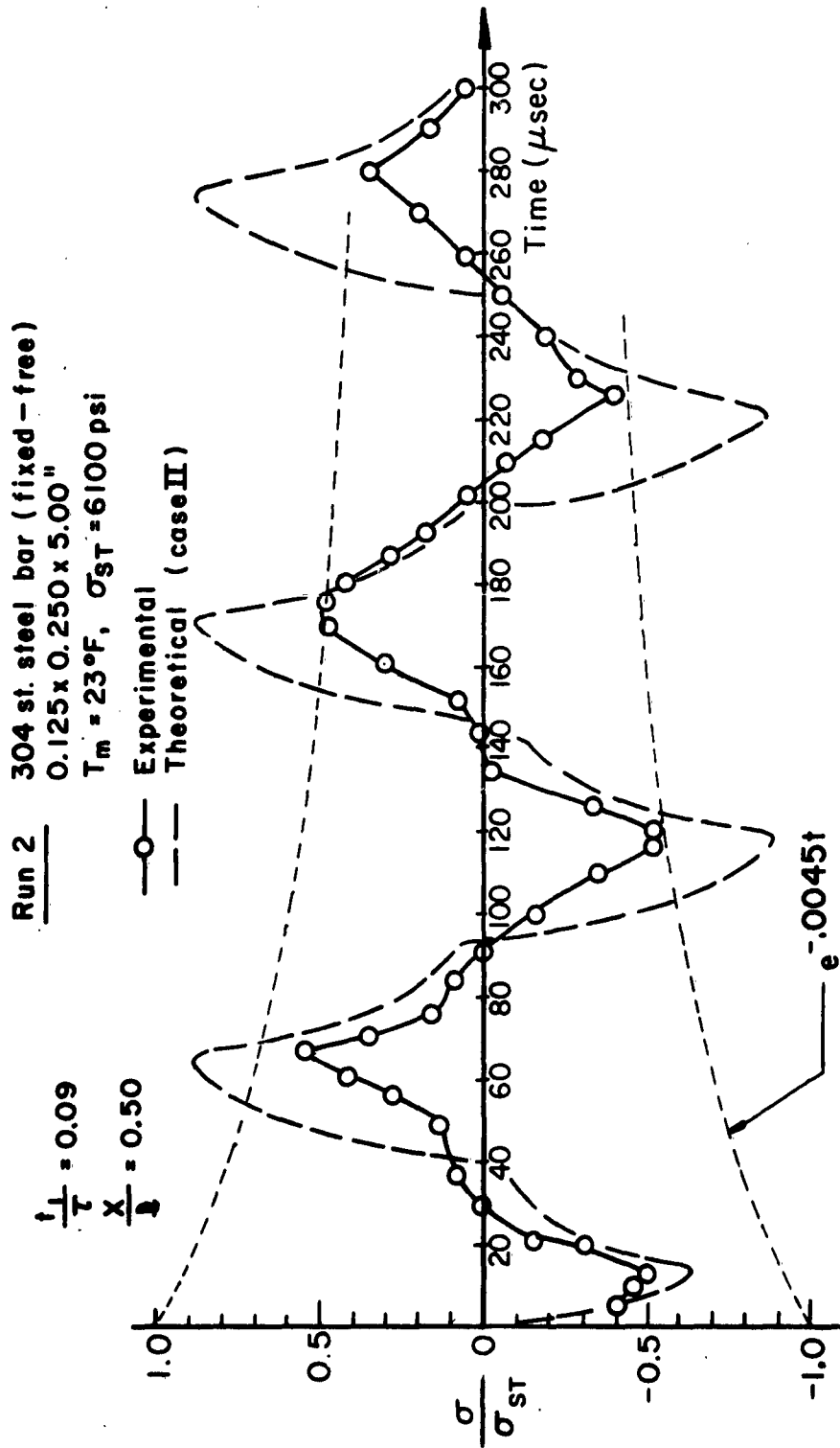
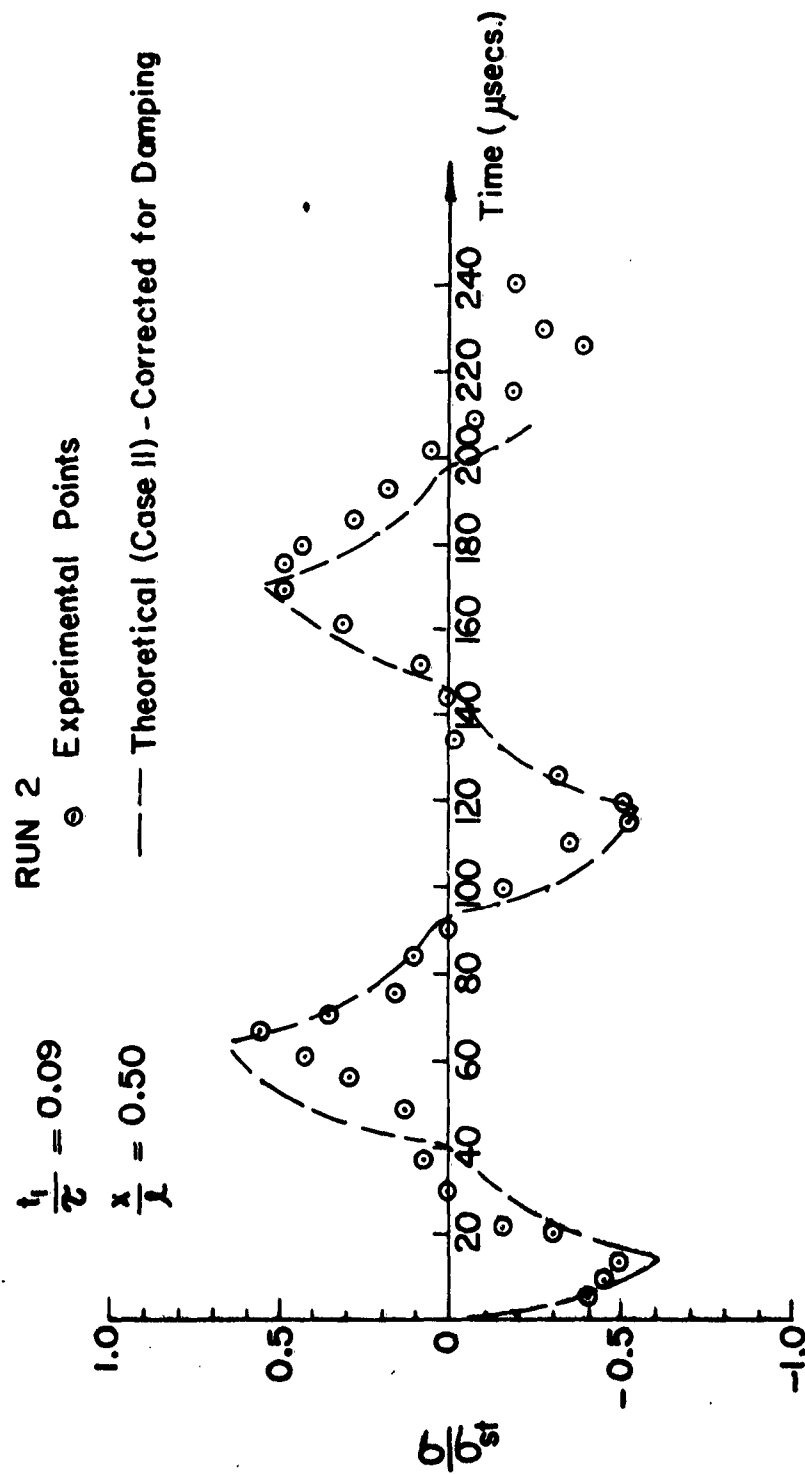


FIG. 25a. STRESS HISTORY AT A POINT



HYD 7981

FIG. 25b. STRESS HISTORY AT A POINT -
CORRECTED FOR DAMPING

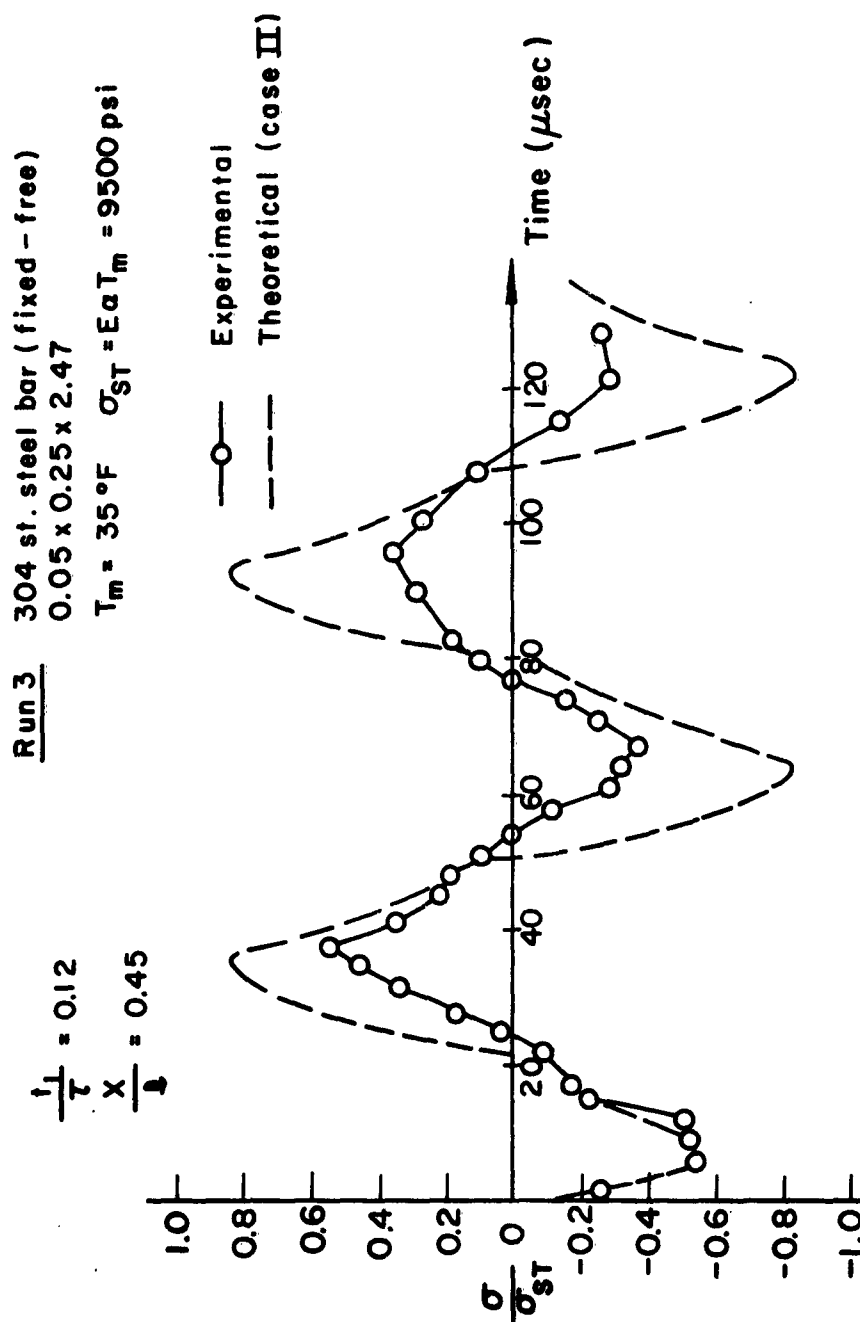


FIG. 26. STRESS HISTORY AT A POINT

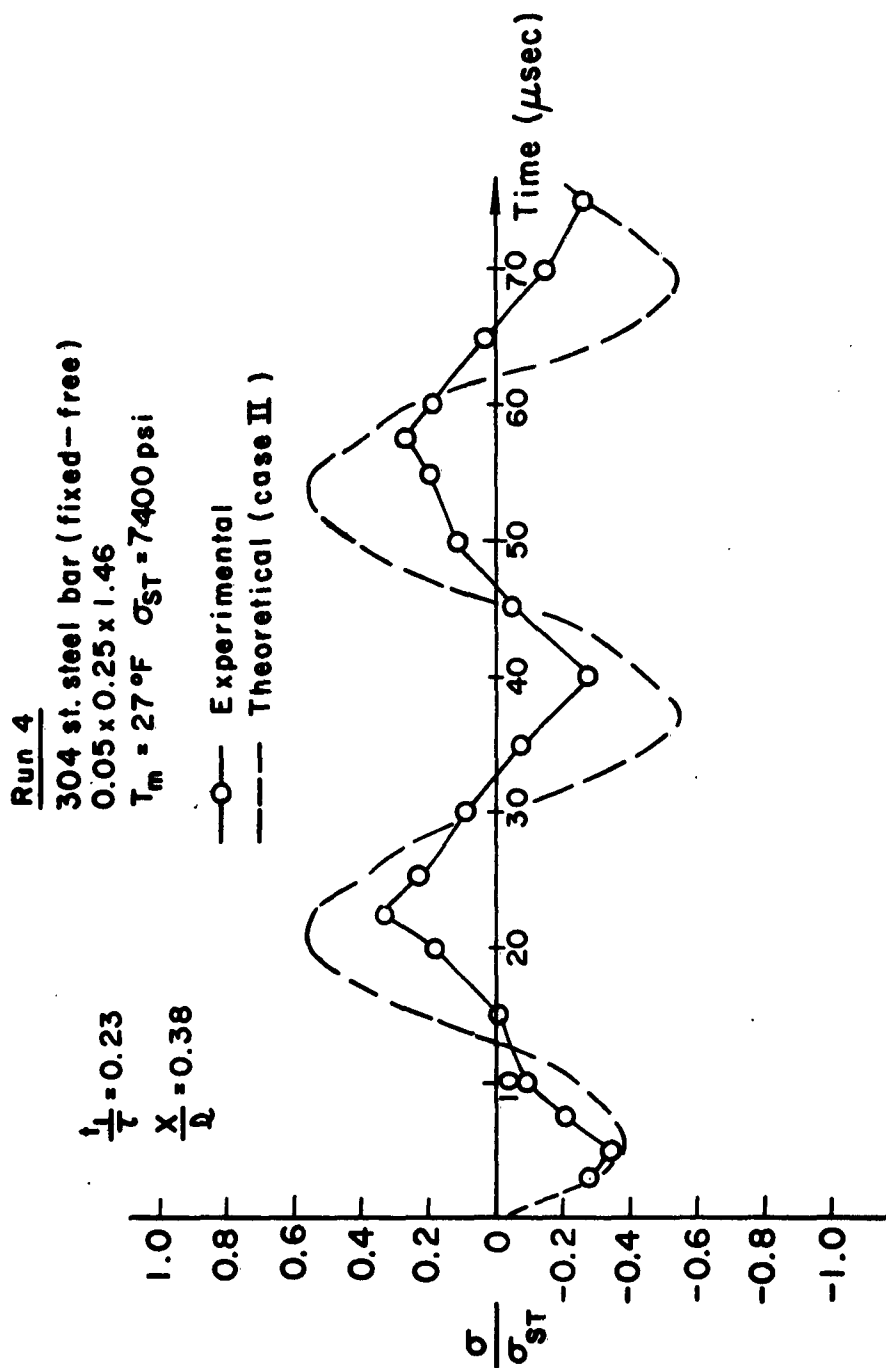


FIG. 27. STRESS HISTORY AT A POINT

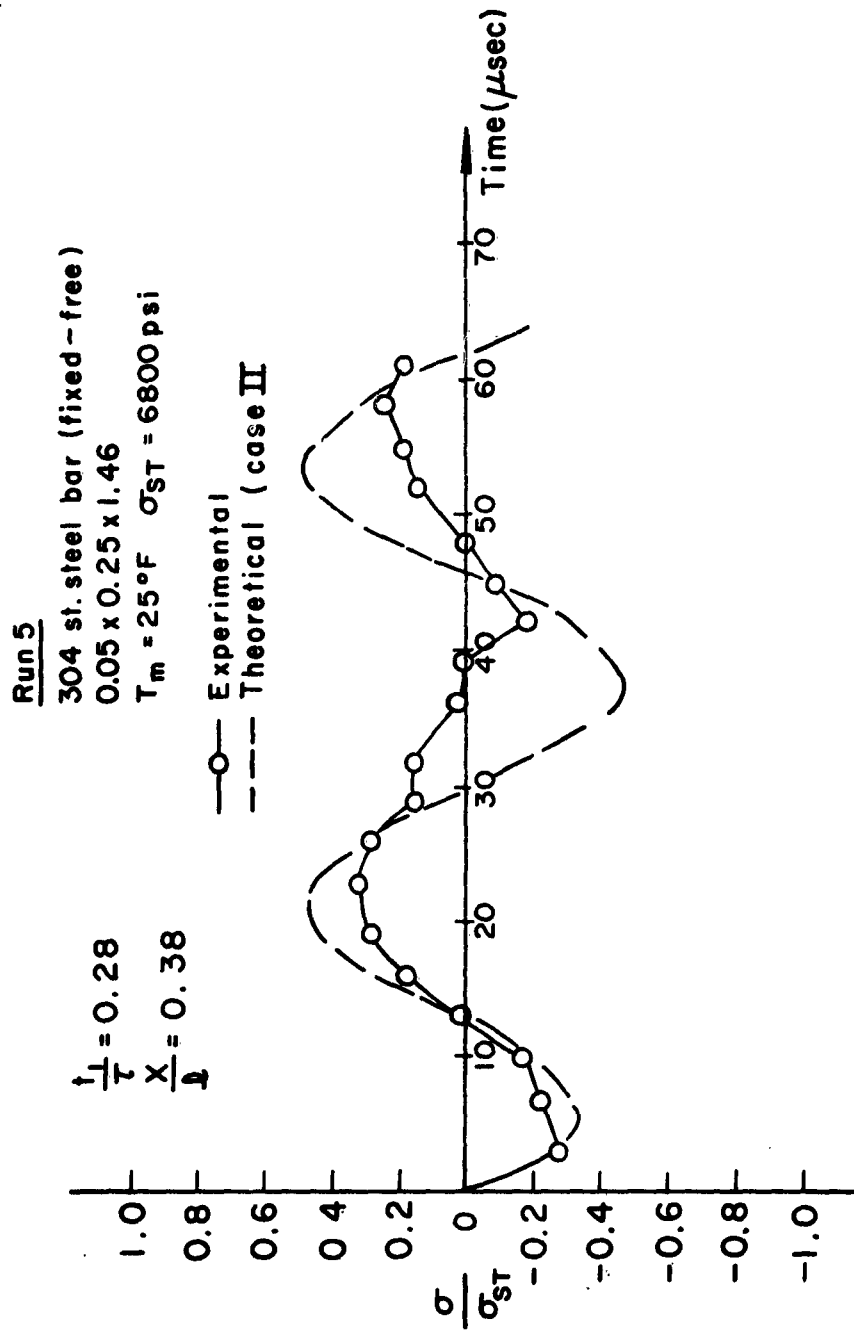


FIG. 28. STRESS HISTORY AT A POINT

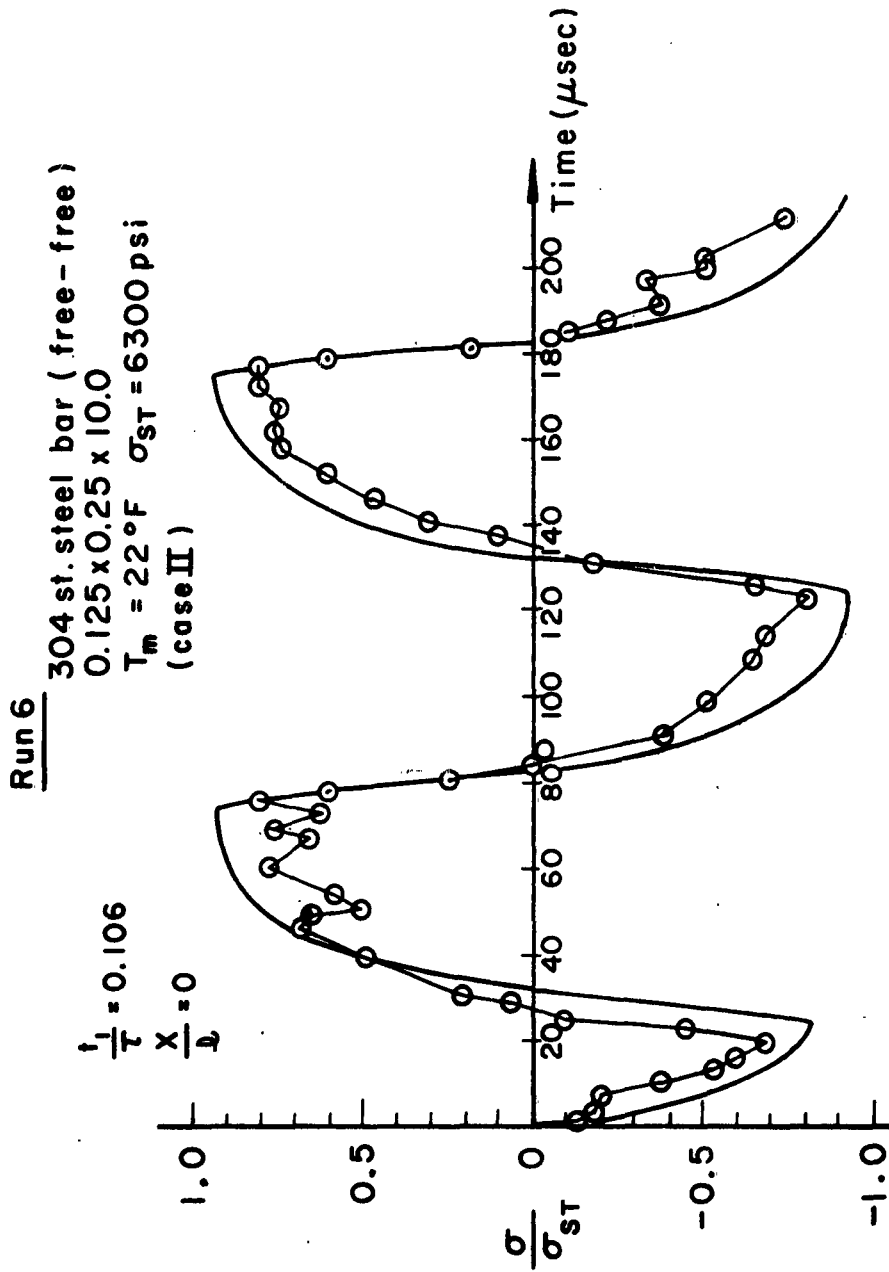


FIG. 29. STRESS HISTORY AT A POINT

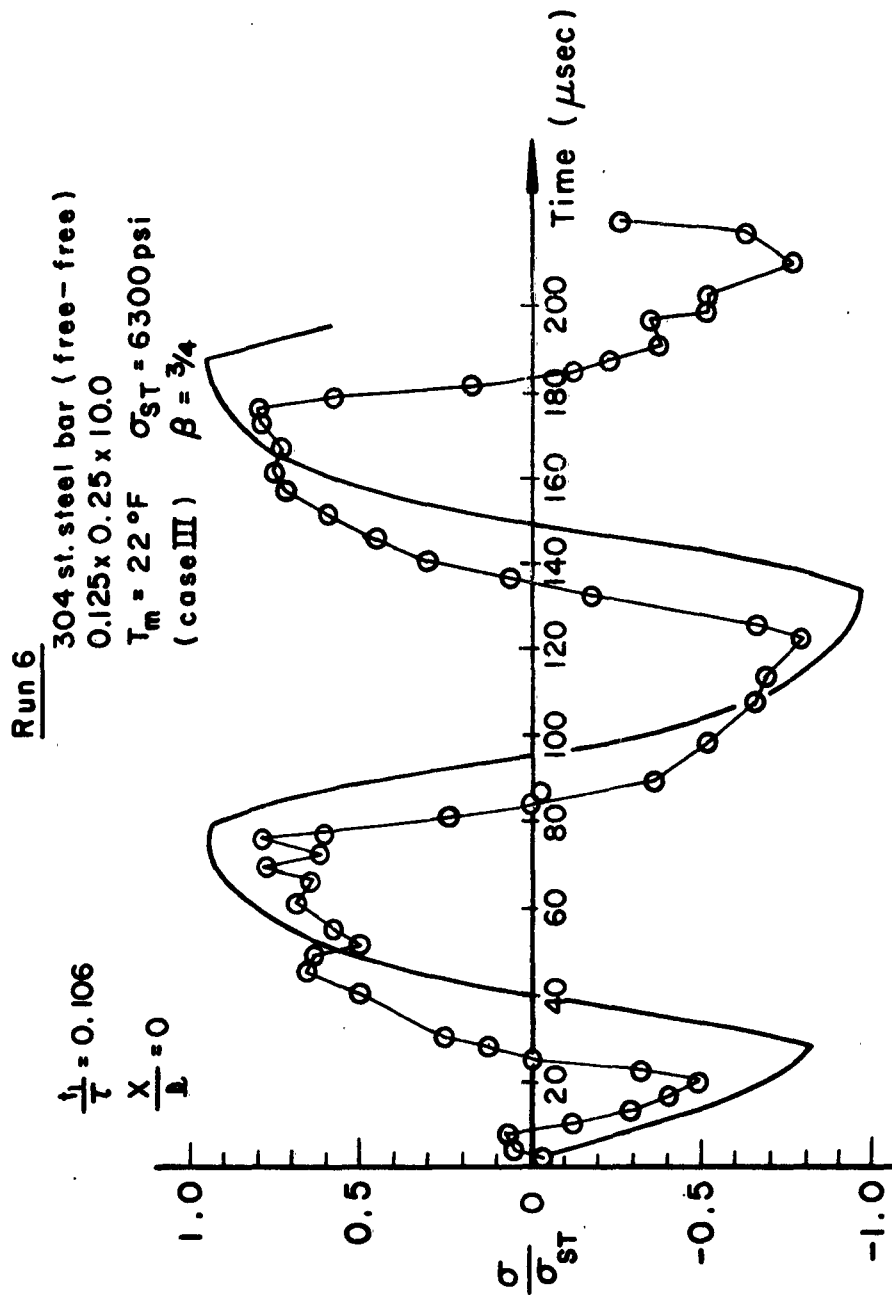


FIG. 30. STRESS HISTORY AT A POINT

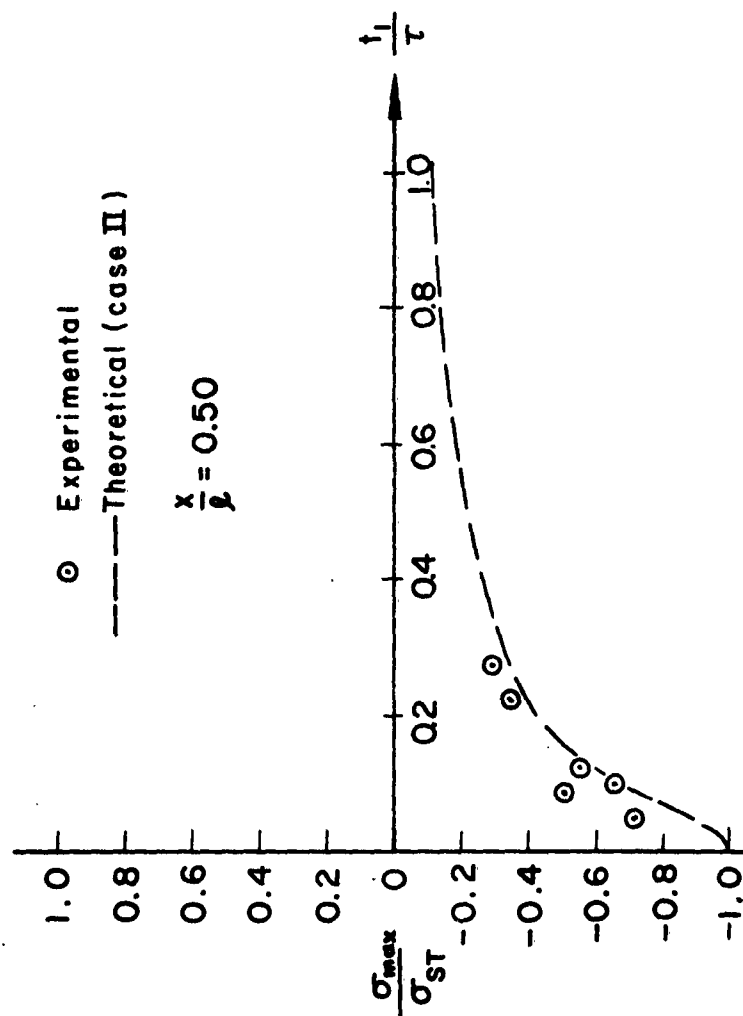
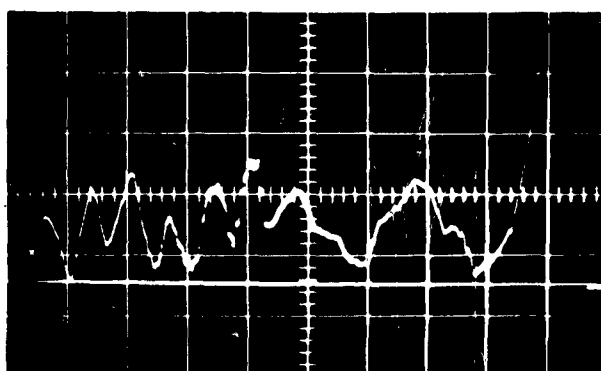
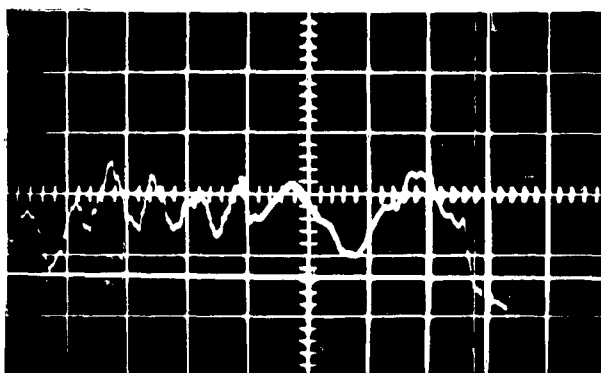


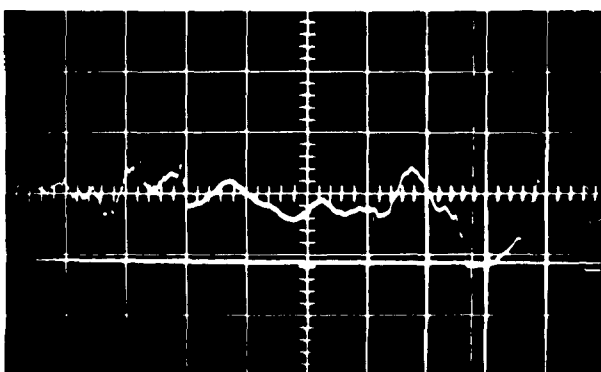
FIG. 31. VARIATION OF INITIAL COMPRESSION AMPLITUDE WITH THE RATIO OF HEATING PERIOD TO FUNDAMENTAL PERIOD



(a) MAXIMUM BOLT TENSION



(b) MEDIUM BOLT TENSION



50 usecs → | | ← t ← 0

(c) MINIMUM BOLT TENSION

FIG. 32. STRAIN GAGE SIGNALS

APPENDIX

1. Sample Data and Calculations

Tests on two different specimens were selected as representative. Hence the data reduction on a "fixed free" test (Run 2) and the "free-free" test (Run 6) are chosen for inclusion here. Figs. 1A and 2A illustrate the oscilloscope records of the output of the inductive probe and the camera rotor signal, respectively. The fringe movements are plotted, as shown in Figs. 3A and 4A. The fringe order at any given time is then calculated graphically by the construction shown in Fig. 5A. Once the fringe order is known, Eq. (3.21) is used to calculate σ/σ_{St} . The calculations of parameters are shown in the following.

Run 2

The camera interframe time is obtained from the oscilloscope record in Fig. 2A where it is shown that the period of oscillation is 500 μ secs. Since the rotor speed is half the signal frequency, the rotor turns at 1000 rps. From camera geometry, the interframe time is 2.95 μ secs. From Eq. (3.4) and the inductive probe record

$$R/2L = (1/\tau_c) \log(i_1/i_2) = (10^6/13.1) \log(2.015) = 0.0534 \times 10^6$$

From Eq. (3.3)

$$L = 0.275 \text{ uh.} \quad ; \quad R = 2(0.275)(0.0534) = 0.0294$$

For 304 stainless steel,

$$R_s = \eta L/A = (31 \times 10^{-6})(5)/(0.125)(0.250) = 0.005$$

Hence, from (3.6),

$$\begin{aligned} (CV^2/2)(J/Wc)(R_s/R) &= T_m \\ &= \frac{(14 \times 10^{-6})(10.3 \times 10^3)(9.48 \times 10^{-4})(0.005)}{2(0.28)(5)(0.125)(0.250)(0.12)(0.0294)} = 22.6^\circ\text{F} \end{aligned}$$

$$\sigma_{St} = E\alpha T_m = (30 \times 10^6)(9 \times 10^{-6})(22.6) = 6100 \text{ psi.}$$

$$t_1 = L/R = 10^{-6}/(2)(0.0534) = 9.36 \text{ } \mu\text{secs.}$$

$$\tau = 4L/a = 4(5)/0.20 = 100 \text{ } \mu\text{secs.}$$

$$m = \frac{1 + (A_c/A_s)(\rho_c/\rho_s)}{1 - (A_c/A_s)(E_c/E_s)} = \frac{1 + (0.06/0.125)(0.045/0.28)}{1 - (0.06/0.125)(0.5/30)} = 1.088$$

$$\tau' = \sqrt{m} \tau = \sqrt{1.088} (100) = 105 \text{ } \mu\text{secs.}$$

and

$$t_1/\tau' = 0.09$$

From the fringe data in Fig. 4A, $N_{\text{Avg}} = 0.55$.

$$\sigma/\sigma_{St} = \frac{N}{0.55} - (1 - e^{-t/9.36})$$

Hence, a calculation of N as a function of time will give σ/σ_{St} as a function of time.

Run 6

$$\text{Interframe time} = 2.95 \text{ } \mu\text{secs.}$$

$$R/2L = (10^6/16.7)\log(2.12) = 0.0451 \times 10^6$$

$$L = 0.50 \text{ uh. ; } R = 2(0.5)(0.0451) = 0.0451$$

$$R_s = (31 \times 10^{-6})(10)/(0.125)(0.25) = 0.010$$

$$T_m = \frac{(14)(12.56)^2(9.48 \times 10^{-4})(0.010)}{2(0.28)(10)(0.125)(0.250)(0.12)(0.045)} = 22.1^\circ\text{F}$$

$$\sigma_{St} = E\alpha T_m = (30)(9)(22.1) = 6300 \text{ psi.}$$

$$t_1 = L/R = 11.1 \text{ } \mu\text{secs.} \quad \tau = 2L/A = 100 \text{ } \mu\text{secs.}$$

$$m = 1.10, \quad \tau' = \sqrt{m} \tau = 108 \text{ } \mu\text{secs. ; } t_1/\tau' = 0.016$$

$$\sigma/\sigma_{St} = \frac{N}{0.55} - (1 - e^{-t/11.1})$$

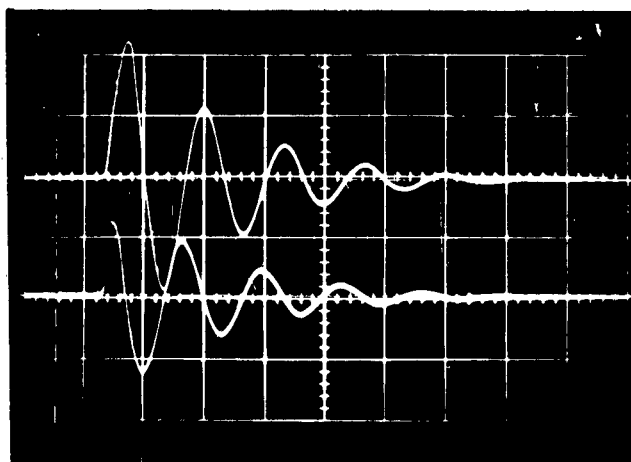
RUN 2

Current

0.5 volt/cm. —

Voltage

2 volts/cm. —

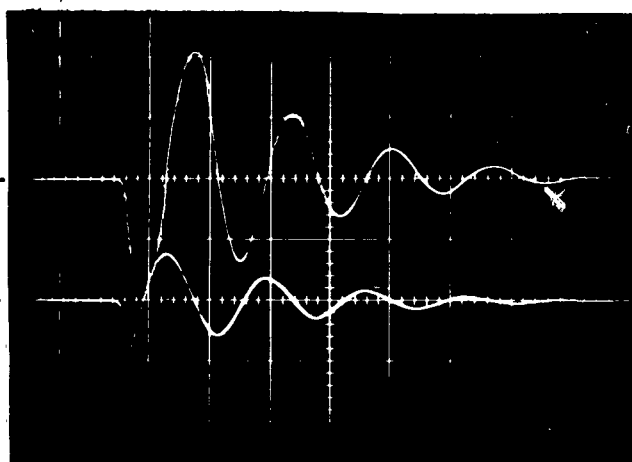
10 μ secs.RUN 6

Current

0.5 volt/cm. —

Voltage

2 volts/cm. —



Bridge wire Fiducial

FIG. 1A. OUTPUT OF THE INDUCTIVE PROBE

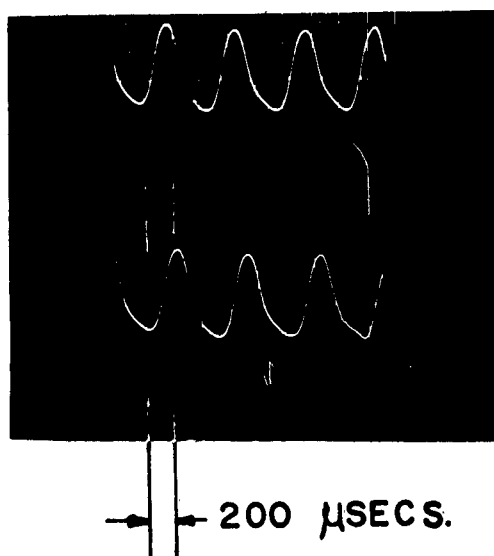
RUN 2RUN 6

FIG. 2A. CAMERA ROTOR SIGNAL

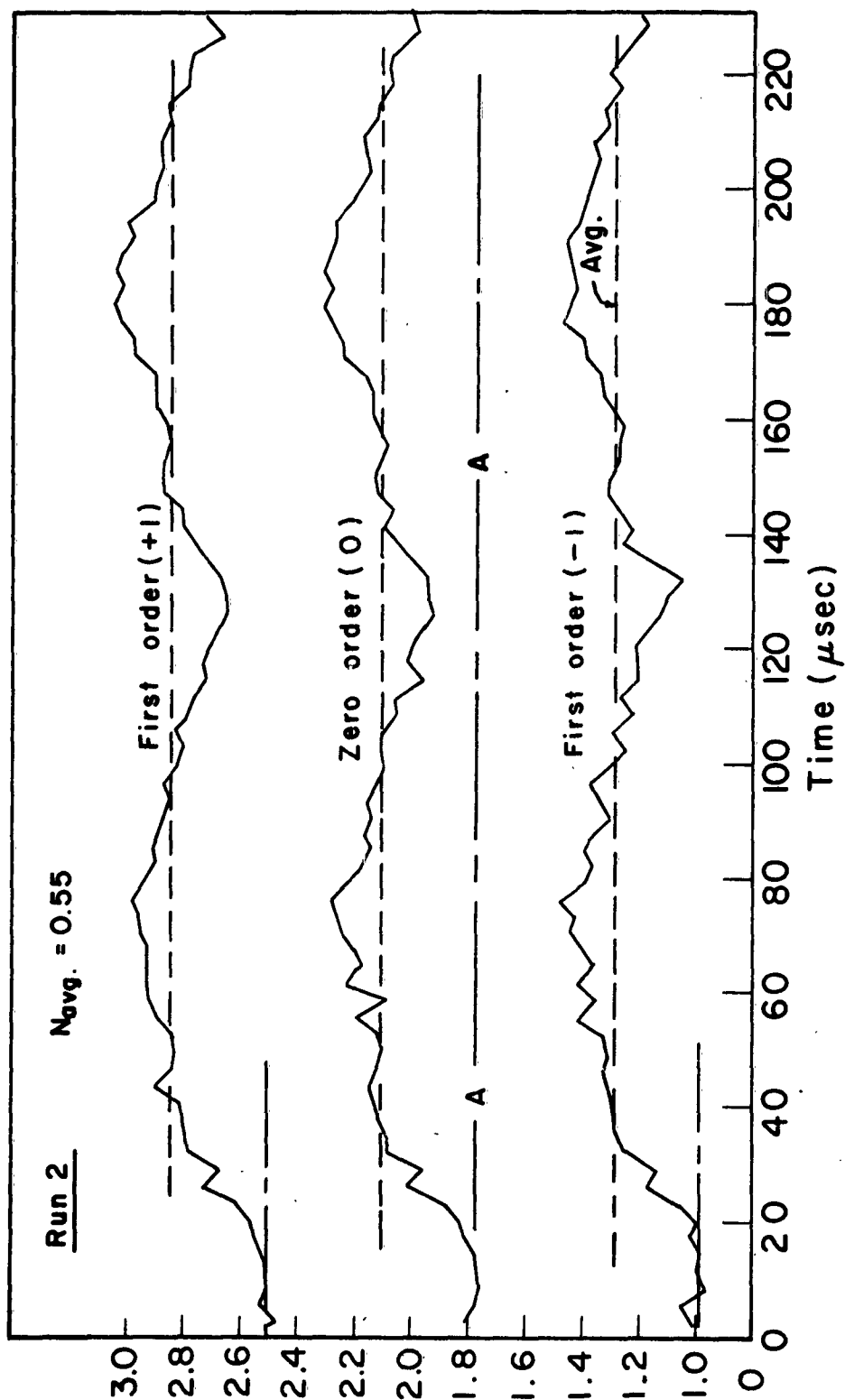


FIG. 3A. OBSERVED FRINGE MOVEMENTS

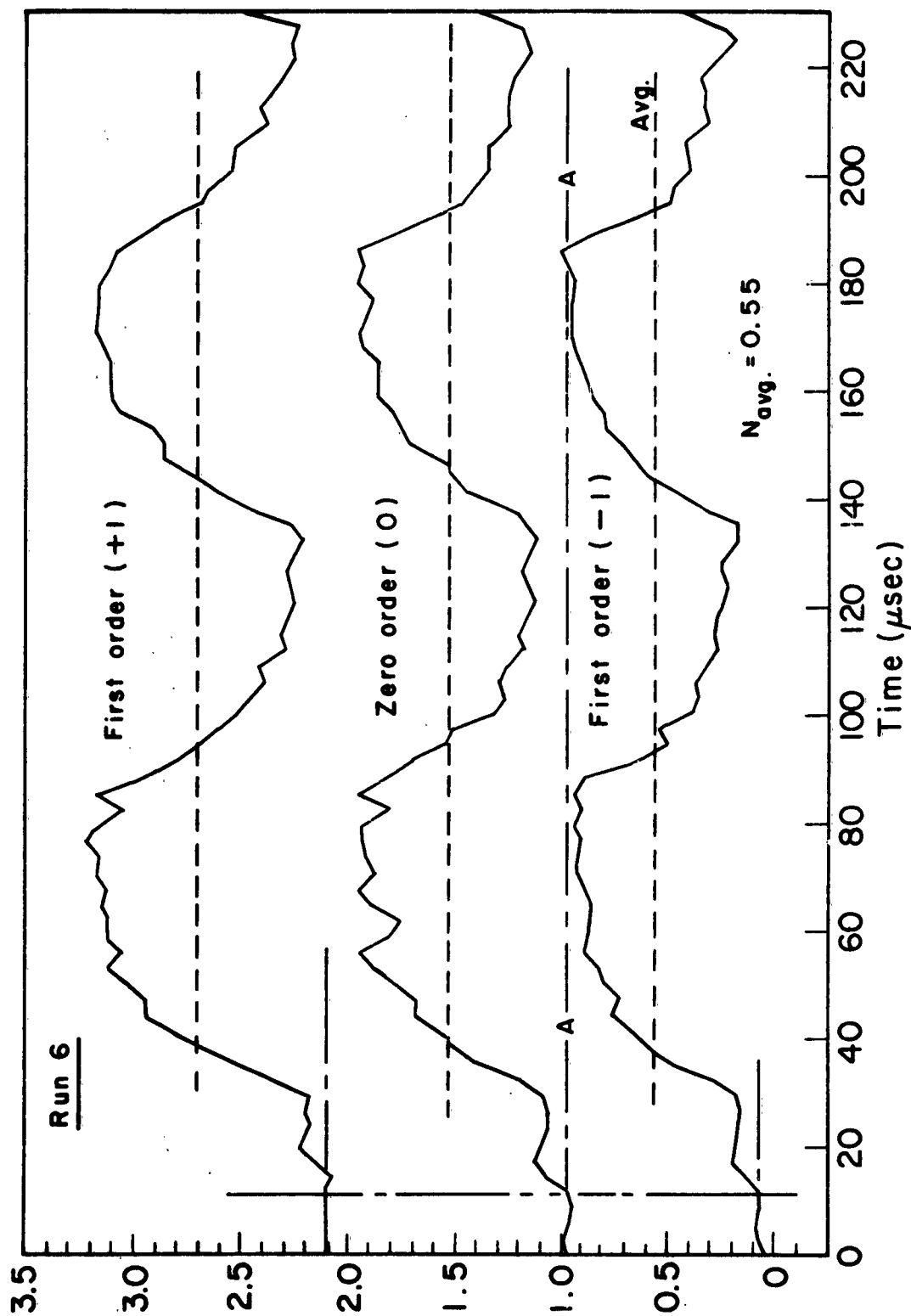


FIG. 4A. OBSERVED FRINGE MOVEMENTS

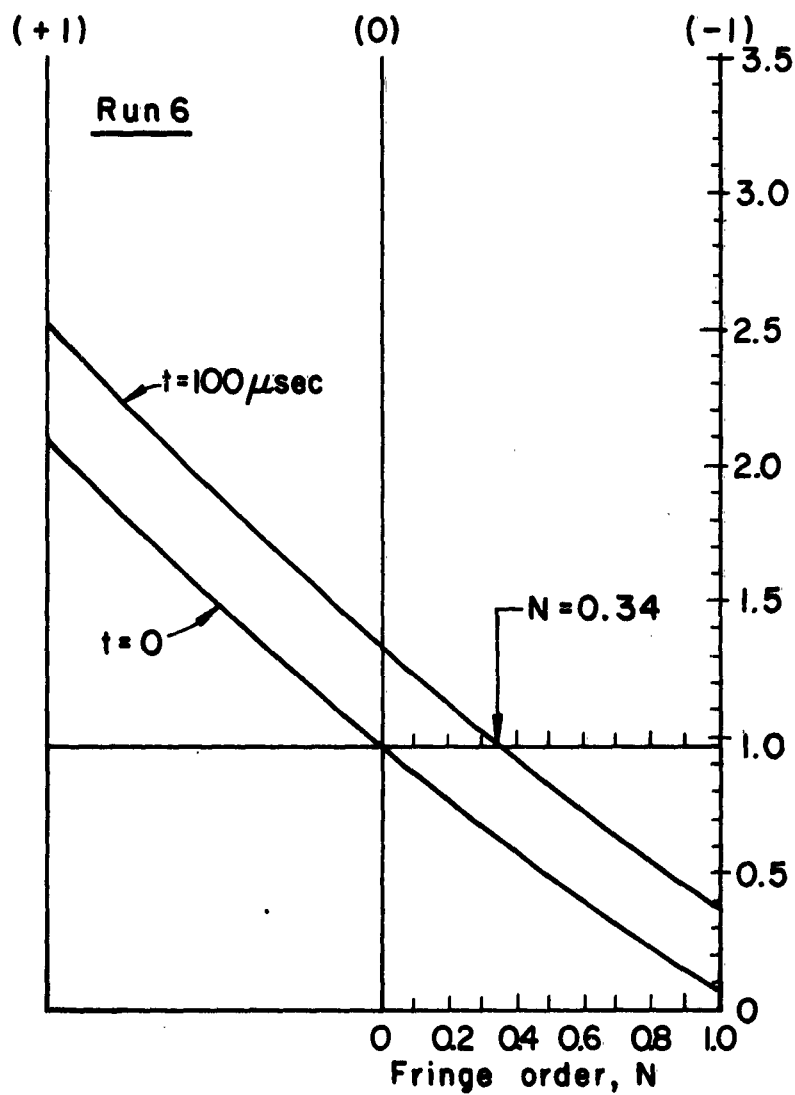


FIG. 5A. GRAPHICAL PROCEDURE FOR CALIBRATION OF FRINGE ORDER

2. Temperature Distribution in the Heated Specimen

In order to determine the time for significant temperature drop due to conduction out the ends of the bar, consider a rod of length l and thermal diffusivity D with lateral surfaces insulated, and the ends held at zero temperature. If the bar is initially at a uniform temperature T_m , the temperature in the bar for $t > 0$ is given by¹

$$T(x,t) = \frac{4T_m}{\pi} \sum_{n=1,3,5,\dots}^{\infty} \frac{1}{n} \sin\left(\frac{n\pi x}{l}\right) e^{-\frac{h^2 \pi^2 D t}{l^2}} \quad (1)$$

if $x = l/2$, then the temperature at the midpoint is

$$\frac{T}{T_m} = \frac{4}{\pi} \sum_{n=1,3,5,\dots}^{\infty} \frac{(-1)^{\frac{n-1}{2}}}{n} e^{-\frac{h^2 \pi^2 D t}{l^2}} \quad (2)$$

The properties of 304 stainless steel are

$$k = 9.4 \text{ BTU/hr/ft}^2/\text{°F/ft}$$

$$w = 485 \text{ lb/ft}^3$$

$$c = 0.12 \text{ BTU/lb°F}$$

$$D = k/wc = 0.16 \text{ ft}^2/\text{hr} = 44.5 \text{ ft}^2/\mu\text{sec.}$$

For the shortest specimen, let $l = 1.5$ inches, Hence

$$\frac{T}{T_m} = \frac{4}{\pi} \sum_{n=1,3,5,\dots}^{\infty} \frac{(-1)^{\frac{n-1}{2}}}{n} e^{-4n^2 t} \quad (3)$$

where t is in units of seconds.

¹R. V. Churchill, Operational Mathematics, McGraw-Hill, 1958, 2nd Ed., p. 218.

The results of this calculation give the temperature history at the center of a 1.5 inch bar as

t(secs.)	0.010	0.100	0.500	1.000
$\frac{T}{T_M}$	0.98	0.840	0.20	0.02

Since all measurements are made within the first 300 μ secs. after bank discharge, it can be concluded that the temperature of the bar remains constant at T_m . This result was calculated for the shortest possible specimen; hence, the time for significant temperature drop will generally be greater than 0.50 secs.

3. The Temperature History of the Photoelastic Coating

Consider a thin slab, infinite in extent, of the photoelastic material of thickness l subjected to a temperature T_m maintained constant for $t > 0$ at one surface ($x = 0$) and insulated at the other ($x = l$). This represents the worst heating condition possible since the heat at $x = l$ will actually be transferred away by radiation and convection to the surrounds. The conduction of heat through the slab is governed by the well known equation

$$\frac{k}{wc} \frac{\partial^2 T}{\partial x^2} = \frac{\partial T}{\partial t} \quad (1)$$

The boundary conditions are

$$T(0, t) = T_m \quad (2)$$

$$\frac{\partial T}{\partial x}(l, t) = 0 \quad (3)$$

Equation (1) can be easily solved by Laplace Transform techniques. Hence, defining $D = k/wc =$ thermal diffusivity, Eq. (1) in the transform $\bar{T}(x, s)$ becomes

$$D \frac{d^2 \bar{T}}{dx^2} = s \bar{T}$$

which has the solution

$$\bar{T}(x, s) = A e^{-\sqrt{s/D} x} + B e^{\sqrt{s/D} x} \quad (4)$$

The transformed boundary conditions are

$$\bar{T}(0, s) = \frac{T_m}{s} \quad (5)$$

$$\frac{dT}{dx}(l, s) = 0 \quad (6)$$

Substitution of (5) and (6) into (4) yields two simultaneous equations which can be readily solved for the arbitrary constants A and B.

With A and B known the solution is

$$\frac{\bar{T}(x, s)}{T_m} = \frac{1}{s} \frac{\cosh \sqrt{s/D} (l-x)}{\cosh \sqrt{s/D} l} \quad (7)$$

For inversion purposes, express the hyperbolic functions in the exponential form, and expand in a series by the binomial theorem.

Hence (7) gives

$$\begin{aligned} \frac{\bar{T}}{T_m} &= \frac{1}{s} \frac{e^{-\sqrt{s/D} x} + e^{-\sqrt{s/D} (2l-x)}}{1 + e^{-2\sqrt{s/D} l}} \\ &= \frac{1}{s} \left[e^{-\sqrt{s/D} x} + e^{-\sqrt{s/D} (2l-x)} \right] \sum_{n=0}^{\infty} (-1)^n e^{-2n\sqrt{s/D} l} \end{aligned}$$

Hence

$$\frac{\bar{T}}{T_m} = \frac{1}{s} \sum_{n=0}^{\infty} (-1)^n e^{-\sqrt{s/D} (2nl+x)} + \frac{1}{s} \sum_{n=0}^{\infty} (-1)^n e^{-\sqrt{s/D} [(2n+2)l - x]} \quad (8)$$

This can readily be inverted since from ref. 32

$$\mathcal{L}^{-1} \left[\frac{1}{s} e^{-\sqrt{s/D} x} \right] = \operatorname{erfc} \frac{x}{2\sqrt{Dt}} \quad (9)$$

The notation (erfc) is given by

$$\operatorname{erfc} x = 1 - \operatorname{erf} x$$

where (erf) is the error function. The inversion of (8) is readily obtained by the use of (9), and hence the solution for the temperature

in the coating is

$$\frac{T(x,t)}{T_m} = \sum_{n=0}^{\infty} (-1)^n \operatorname{erfc} \frac{2n\ell + x}{2\sqrt{Dt}} + \sum_{n=0}^{\infty} (-1)^n \operatorname{erfc} \frac{2(n+1)\ell - x}{2\sqrt{Dt}} \quad (10)$$

This solution converges quickly, and in order to illustrate the time scales for the coating to experience a significant temperature rise it will be necessary to evaluate (10) for some specific times and distances. The properties of the coating are as follows.

$$k = 0.00057 \text{ cal/cm sec } ^\circ\text{C}$$

$$\gamma = 1.239 \text{ gms/cc}$$

$$c = 0.27 \text{ cal/gm } ^\circ\text{C}$$

$$D = \frac{k}{\gamma c} = \frac{0.00057}{(1.289)(0.27)} = 0.0017 \text{ cm}^2/\text{sec.}$$

$$= 0.030 \text{ inches} = 0.076 \text{ cm.}$$

$$\frac{D}{\ell^2} = 0.294/\text{sec.}$$

At $x = 0$, obviously $T = T_m$, since the coating is separated by a glue interface of the same properties as the coating. We will assume the glue to be 0.005 inches thick and calculate the temperature history of $x/\ell = 0.167$ from

$$\frac{T}{T_m} = \sum_{n=0}^{\infty} (-1)^n \operatorname{erfc} \frac{n + 0.084}{0.54\sqrt{t}} + \sum_{n=0}^{\infty} (-1)^n \operatorname{erfc} \frac{n + 0.92}{0.54\sqrt{t}}$$

This calculation results in the following temperature history at $x = 0.005$ inches.

t(secs.)	0	0.010	0.050	0.100	0.500	1.000
$\frac{T}{T_m}$	0	0.038	0.32	0.48	0.77	0.84

As a result of this calculation, it can be concluded that the coating remains at substantially its initial temperature during the first ten milliseconds after bank discharge. The significance of this result lies in the fact that the optical properties of the coating remain constant, with the exception of possible dynamic effects, since all observations were made within about the first 300 μ secs. In order to verify the validity of this solution, a literature search revealed that this result is identical with that previously obtained by Carslaw and Jaeger^{*} for a very similar problem. These results are conservative since it was assumed that the coating was insulated over its outer surface and that the temperature of the bar remained constant. This latter assumption has been investigated in the previous section, where it was shown that the temperature remains nearly constant with respect to a millisecond time scale.

^{*}H. S. Carslaw and J. C. Jaeger, Conduction of Heat in Solids, Oxford Press, 1959, 2nd Ed., pp 96-99. (Note Eq. 9, p. 97).

4. Evaluation of the Secondary Principal Stress

In order to simplify the calculation of the axial stress from the stress-optic law (3.11), the secondary principal stress was assumed to be negligible. This simplifying assumption is justified as follows. The secondary principal stress σ_y arises from the inertial loading of the coating which must be accelerated in the y-direction due to the lateral expansion and contraction of the bar. Hence, the inertial stress σ_y in the coating is (refer to Fig. 1)

$$\sigma_y = \frac{m_c}{hL} \ddot{y}$$

where m_c = mass of coating

\ddot{y} = lateral acceleration

h = coating thickness

L = length of coating

The lateral acceleration is given by

$$\ddot{y} = va \dot{\epsilon}_x$$

where a = the sonic velocity, and $\dot{\epsilon}_x$ = axial strain rate.

The axial strain rate can be determined from the theoretical solutions of Sec. 2. Hence, assuming Case II heating, Eq. (2.34) gives

$$\dot{\epsilon}_{x_{\max}} = 30 \text{ in/in/sec.}$$

and since

$$m_c = \rho_c n \delta L$$

the maximum stress is

$$\sigma_{y|_{\max}} = \rho_c \delta v_s a \dot{\epsilon}_x$$

Substituting some representative magnitudes,

$$\sigma_{y_{\max}} = \frac{(0.045)(0.050)(0.30)(0.2 \times 10^6)(30)}{386} = 11 \text{ psi}$$

Hence, σ_y is very small compared to the axial stress σ_x , and can, therefore, be neglected.

5. Reinforcing Effect of the Photoelastic Coating

In order to determine the reinforcing effect of the coating consider a rectangular bar of uniform section A_s and density to be coated uniformly on two of its sides with a material having mass density ρ_c and cross-sectional area A_c as shown in Fig. 6A. With the passage of a longitudinal wave along the bar, the elemental length PQ will be displaced to the new position P'Q'. If the coating thickness is small relative to the bar thickness, then we can assume that shear strains in the coating are negligible relative to the axial strain. Further, we will assume that the axial strain in the coating is equal to the uniaxial strain in the bar, i.e.

$$\epsilon_c = \epsilon_s \quad ; \quad \frac{\partial u_c}{\partial x} = \frac{\partial u_s}{\partial x} = \frac{\partial u}{\partial x} \quad (5.1)$$

The influence of the coating on the motion of the bar can be determined by considering the forces acting on the element P'Q'. A Force balance on these elements yields.

$$\text{Bar:} \quad -2F + A_s \frac{\partial \sigma_s}{\partial x} dx = A_s \rho_s dx \frac{\partial^2 u_s}{\partial t^2} \quad (5.2)$$

$$\text{Coating:} \quad F - A_c \frac{\partial \sigma_c}{\partial x} dx = A_c \rho_c dx \frac{\partial^2 u_c}{\partial t^2} \quad (5.3)$$

Eliminating F between Eqs. (5.2) and (5.3), and substituting (5.1) we get,

$$\frac{\partial \sigma_s}{\partial x} - \frac{A_c}{A_s} \frac{\partial \sigma_c}{\partial x} = \left(1 + \frac{A_c \rho_c}{A_s \rho_s} \right) \rho_s \frac{\partial^2 u}{\partial t^2} \quad (5.4)$$

Differentiation of (5.4) with respect to x yields

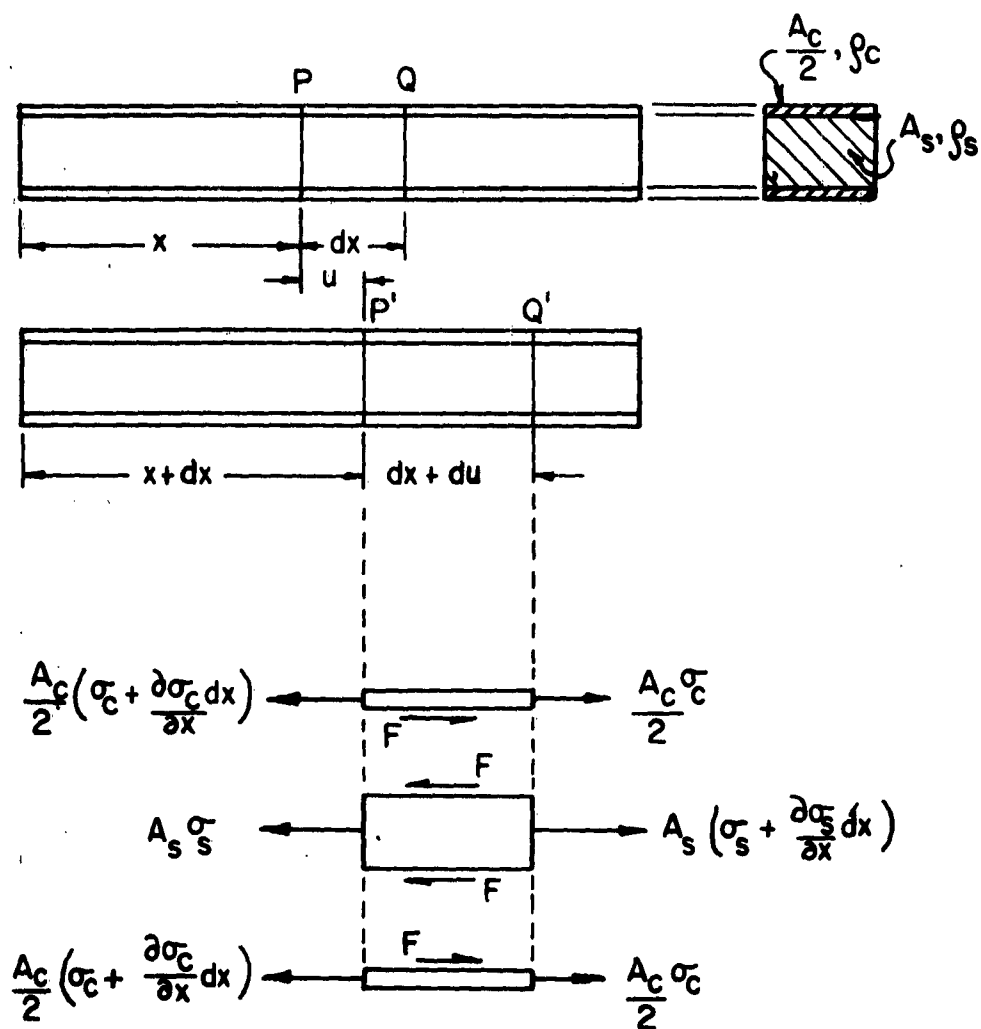


FIG. 6A. LONGITUDINAL MOTION OF THE COATED BAR

$$\frac{\partial^2 \sigma_s}{\partial x^2} - \frac{A_c}{A_s} \frac{\partial^2 \sigma_c}{\partial x^2} = \left(1 + \frac{A_c}{A_s} \frac{\rho_c}{\rho_s} \right) \rho_s \frac{\partial^2}{\partial t^2} \left(\frac{\partial u}{\partial x} \right) \quad (5.5)$$

The stress-strain relations are

$$\frac{\partial u}{\partial x} = \frac{\sigma_s}{E_s} + \alpha_s T(t) \quad (5.6)$$

$$\frac{\partial u}{\partial x} = \frac{\sigma_c}{E_c} \quad (5.7)$$

and

$$\frac{\partial^2 \sigma_c}{\partial x^2} = \frac{E_c}{E_s} \frac{\partial^2 \sigma_s}{\partial x^2} \quad (5.8)$$

Hence, substitution of (5.6) and (5.8) into (5.5) yields the equation

$$\frac{\partial^2 \sigma}{\partial x^2} = \frac{m}{a^2} \frac{\partial^2 \sigma}{\partial t^2} + m \rho_s \alpha_s \frac{\partial^2 T}{\partial t^2} \quad (5.9)$$

where

$$m = \frac{1 + \frac{A_c}{A_s} \frac{\rho_c}{\rho_s}}{1 - \frac{A_c}{A_s} \frac{E_c}{E_s}} \quad (5.10)$$

If we define

$$a' = \frac{a}{\sqrt{m}} ; \quad \tau' = \frac{4\ell}{a'} \quad (5.11)$$

then

$$\tau' = \sqrt{m} \tau \quad (5.12)$$

Hence, the corrected equation (2.8) is

$$\frac{\partial^2 \sigma}{\partial x'^2} = \frac{1}{a'^2} \frac{\partial^2 \sigma}{\partial t'^2} + m \rho \alpha \frac{\partial^2 T}{\partial t'^2}$$

which has the same solution given in Sec. 2 except that τ is exchanged for τ' . It should be noted that m appears in the terms multiplying the series solution but cancels out. For example, in Eq. (2.26)

$$\rho \propto a^2 T_m = m \rho \propto a'^2 T_m = m \rho \propto \frac{a^2}{m} = E \propto T_m = \sigma_{St}$$

Hence, only the period τ is affected. Consequently the stress amplitude is increased slightly due to the dependence upon the ratio t_1/τ which decreases as a result of the increase of τ to τ' by the factor \sqrt{m} .

This correction is not exact since the strain at the free surface of the coating is different from that at the interface and shear-strains are undoubtedly present. An exact solution of this problem would be extremely difficult to obtain, particularly in view of the fact that inertia effects must be included. The exact solution for static loading has been worked out by Duffy⁴⁰ who has shown that the birefringence observed perpendicular to the surface is significantly dependent upon the strain gradient and curvature at the metal surface. Since the birefringence is observed parallel to the surface in this work, these results do not directly apply here. This analysis illustrates nicely the nature of the required exact solution which would be further complicated by the addition of inertial terms.

While the correction factor (5.10) is not exact, it is considered sufficiently accurate for engineering purposes. Since the derivation is based on the assumption that the bar is coated over its entire length rather than only over a portion, this correction is undoubtedly conservative. This is apparent from an energy consideration since in most cases the total mass of the specimen is much lower than that of the coating. As pointed out in Sec. 5, two of the specimens were tested with different

coating lengths. It was observed that some coating effect on the response may have been present, but only when the coating and specimen volumes were nearly equal. Further, the period of oscillation measured experimentally is larger than the theoretical period τ by an amount very closely approximated by (5.12). Also, the physical nature of (5.10) is reasonable since it indicates that the inertia effect appears in the numerator while the stiffness appears in the denominator which is consistent with the definition of natural period of oscillation. Hence, it is evident that confidence in the validity of the correction factor as derived is justifiable.

6. Calibration of the Photoelastic Coating

In order to determine if the strain-optic coefficient of the coating is rate dependent, it was necessary to perform a dynamic calibration. Since there is no data available in the literature on the specific birefringent material used in this work, the calibration must be carried out at substantially the same loading rates experienced in the experiment. Also, the dynamic strain must be measured independently as well as simultaneously with the photoelastic method. Since the effects of rapidly heating an elastic rod are identical to the effects of heating a rod slowly, compressing it back to its original length, and then releasing it suddenly, it was apparent that an effective calibration could be performed in the following manner.

Rather than precompress a rod and design a complicated device to provide a sudden release, it was decided to prestretch a vertical rod clamped at its upper end, by loading it with a weight suspended from a thin wire fastened at the free end of the rod. Sudden release of the weight was accomplished by utilizing the capacitor band to explode the lower portion of the wire. Hence, the 0.125 x 0.250 x 5.00 inch specimen (run 2) was clamped in the heating jig as shown in Fig. 7A and preloaded with an 80 lb. weight suspended by a 0.016 inch diameter music wire approximately 15 inches long. Two 350 ohm semi-conductor strain gages were mounted on the uncoated sides of the bar at the same location as the coating. These gages were connected in series to cancel any effects due to lateral bending and insure measurement of only longitudinal strain. With the gages in a simple voltage divider circuit as shown, their output could be read directly on the 535 Tektronix oscilloscope. Since these gages have a gage factor of 123, small strains are easily measured

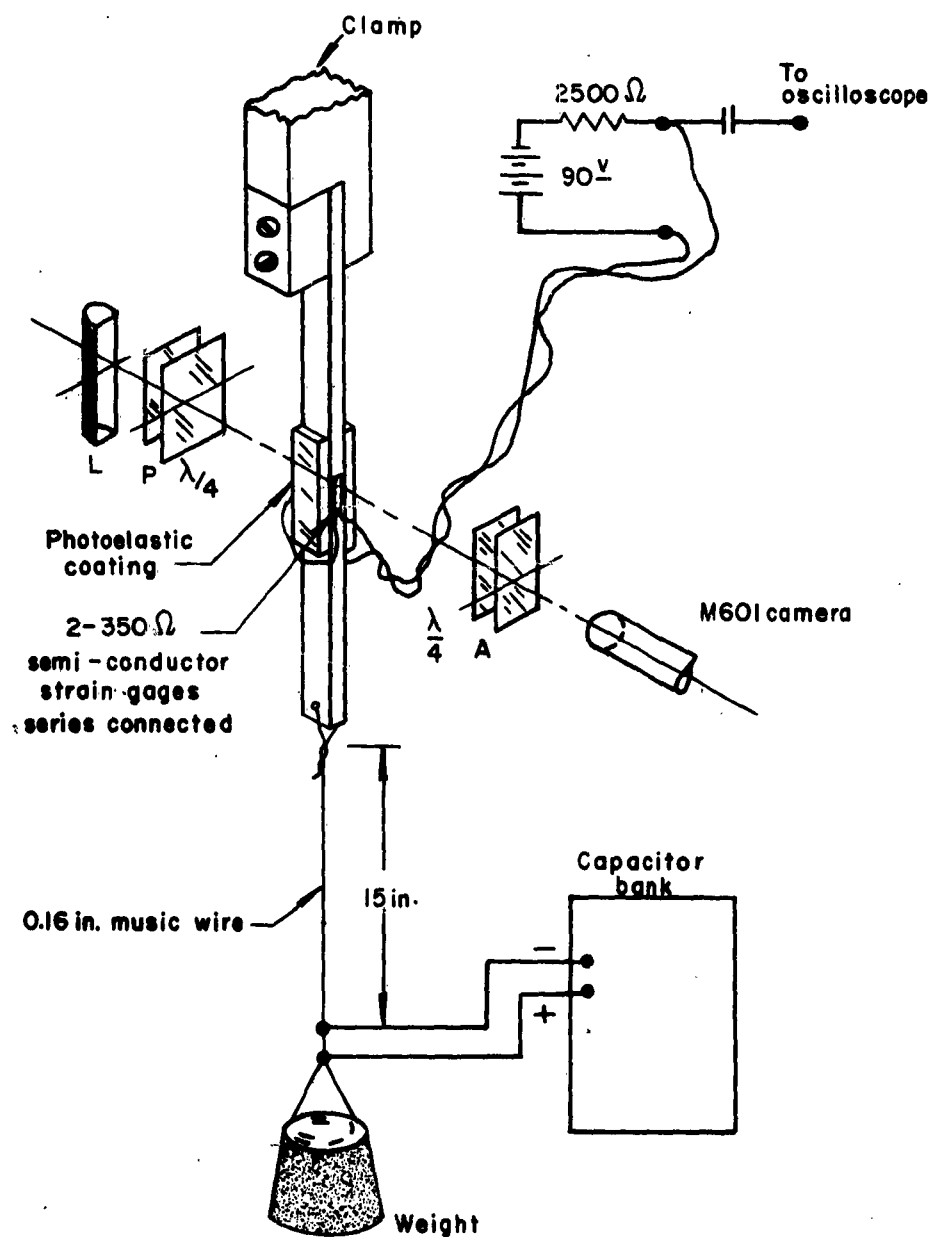


FIG. 7A. Dynamic calibration of photoelastic coating.

with little amplification. The strain was also measured independently with the photoelastic coating technique described in Sec. 3 by using all existing photographic equipment.

The sequence of events was very similar to the rapid heating tests. The room was darkened, camera brought up to speed, and with closure of the "fire" switch the synchronizing pulse triggered the oscilloscopes, discharged the capacitor bank to explode the wire, and after a suitable delay discharged the light source and bridge-wire. In this manner, the subsequent longitudinal oscillations of the rod were observed independently and simultaneously by electronic and photoelastic methods. The advantages of this method are that it was simple and provided a test at a representative frequency - in this case, 100 μ sec. period since the rod was 5 inches long. Also, sudden release was obtained as the mass of the wire is small relative to the bar mass. Since the unloading wave in the wire travels at the sonic velocity, the length of the wire was selected so that the transit time ($L/a = 75 \mu$ sec.) was greater than the discharge time of the capacitor bank. Hence, the strain gage output was obtained free of electromagnetic noise from the exploding wire. The light source delay was therefore selected to be approximately equal to this transit time.

The M601 film strip provided the fringe movements from which the fringe order was obtained at a point. In order to calculate strain, the static value of the strain-optic coefficient was obtained by loading the bar slowly in a standard tensile testing machine and observing the fringe movements with a telescope. Also, the output of the strain gages was observed. It was found that

$$\epsilon_1 = \frac{f_{\epsilon} N}{h} = 700 N \quad (6.1)$$

and

$$\epsilon_2 = 1.09 \epsilon_0 \quad (6.2)$$

where ϵ_0 is the output of the voltage divider in millivolts, ϵ is the strain in microinches/in., and h is the width of the coating (0.250 inches). Using (6.1), the dynamic strain was determined from the film record in the same manner as previously described. This result is compared with the strain gage record in Fig. 8A.

Since the static strain-optic coefficient was used, it is evident from Fig. 8A that good agreement exists and the dynamic strain-optic coefficient is not seriously reduced at this rate of loading. Hence, it can be concluded that the ratio of dynamic to static strain-optic coefficients can be taken as unity for this work and the simplified equation (3.18) used for data reduction.

This calibration technique is extremely useful since it can provide tests over a range of frequencies restricted only by the length of the rod. The only difficulty arises in selecting the weight. In order to provide enough space for the strain gage mounting, the cross-sectional area of the bar cannot be much less than the one used. Since the wire diameter should be small, the weight magnitude is limited, which in turn limits the initial axial strain present in the bar during the test. Consequently, the small fringe movements observed in the coating are sometimes difficult to measure visually. The data shown in Fig. 8A was obtained from measurement of fringe orders which did not exceed 0.14. Hence, there was a fair amount of scatter present, and it was necessary to pick those points which fell on the "best curve" drawn through all of the experimental points. However, this is not a serious compromise since

care was taken to select only those points which represented the average trend of the data so that there were as many points above, as well as below the strain gage record. The fact that the period of oscillation was also reproduced accurately provides sufficient evidence to conclude that dynamic optical effects can be neglected.

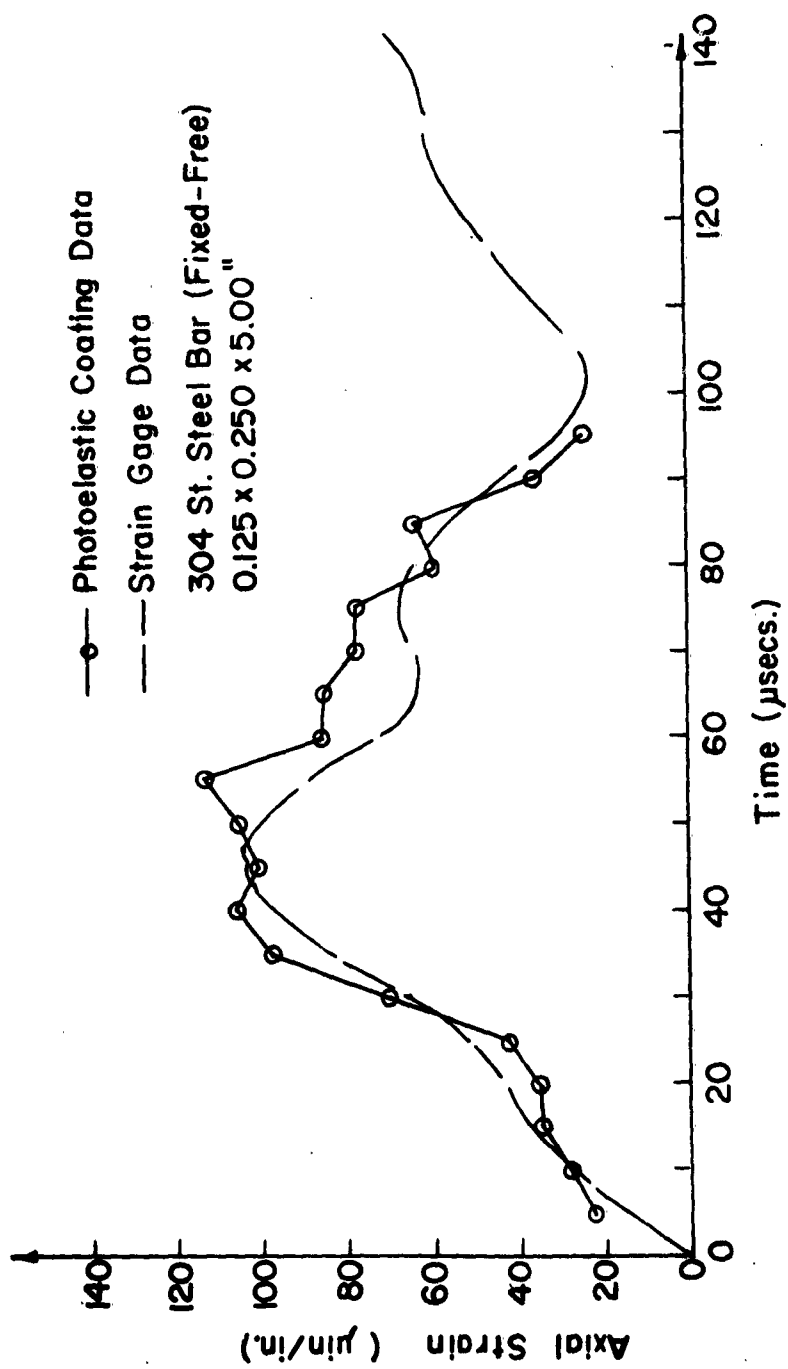


FIG. 8A. COMPARISON OF PHOTOELASTIC COATING DATA WITH STRAIN GAGE DATA